B.A.N. **17**, no. 6, 381–441

Communication from the Observatory at Leiden and the Netherlands Foundation for Radio Astronomy

THE NEUTRAL HYDROGEN IN THE CENTRAL REGION OF THE GALACTIC SYSTEM

G. W. ROUGOOR

Received May 21, 1964

Profiles of H I emission, spaced 0°.5 in galactic longitude and latitude have been taken from $l^{II} = -8°$ to $+22°$ ($R < 4$ kpc) with the 25-metre radio telescope in Dwingeloo (beam 0°.56). From $l^{II} = -2°$ to $+2°$ the spacing was 0°.25.

The gas in the central region of the Galaxy ($R < 4$ kpc) can, in part, be identified by its high velocity. The major portion of this gas appears to be moving away from the centre, having, however, at the same time a transverse rotational velocity.

The radial component (called "expansion") is 53 km/sec for the so-called 3-kpc arm where it crosses $l^{II} = 0°.0$ and about 135 km/sec for another arm situated beyond the centre.

The general rotational velocity is about 210 km/sec at $R = 4$ kpc, but may be as low as 50 km/sec around $R = 1$ kpc.

Inside 750 pc there is a rapidly rotating "nuclear disk" with a velocity of rotation of about 200 km/sec, which decreases steeply within 100 pc from the nucleus, which is formed by the complex radiosource Sagittarius A. This disk has a very sharp outer boundary; there is no evidence that it is expanding.

The thickness of the gas layer of the nuclear disk varies from 70 pc close to the nucleus to 250 pc at $R = 600$ pc. For $R > 750$ pc the thickness is everywhere about 260 pc.

The maximum of the H I emission is generally within 0°.1 of $b^{II} = 0°.0$. Only a few features at a distance of 5° from the centre are located about 0°.7 from the plane.

The 3-kpc arm (part III) is a regular feature, in front of the nucleus, which can be followed from $l^{II} = -22°$ to $+6°$. Its H I content is at least 2×10^7 solar masses. There are internal systematic motions in the arm, up to about 10 km/sec; these motions follow a rather regular pattern. The halfwidths in velocity form an equally regular pattern. At the core of the arm the halfwidth of the profile is about 15 km/sec. At larger distances from the plane values from 30 to 50 km/sec occur.

The absorption of the radiation from Sgr A gives a profile that is considerably narrower than the emission profiles. It is conceivable that the difference is due to the fact that a considerable part of the radiation of the Sagittarius source comes from a very concentrated component. The kinetic temperature of the hydrogen in the arm must be between 60 and 125 °K.

The gas behind the nucleus may be mainly concentrated in two arms (figure 1), although they do not come up to the 3-kpc arm in regularity and intensity. However, the total amount of H I emission at negative and positive velocities (which correspond to negative and positive longitudes, respectively) is equal to within 0.2 per cent.

The nuclear disk (part IV) stands out clearly in the high negative velocities between $l^{II} = -5°$ and $l^{II} = 0°$. At positive velocities it is to some extent intermingled with the expanding gas at a larger distance from the centre. Evidence can nevertheless be given that the disk must be roughly symmetrical. The mass of H I in the disk can be estimated to be between 10^6 and 10^7 solar masses. The total amount of gas is likely to be several times higher, because most of the hydrogen may be in molecular form, as indicated by the recent observations of OH at Parkes. From the rotational velocity the total mass of stars and gas within 750 pc from the centre is estimated to be about 10^{10} solar masses. From the highest velocities in the disk an estimate can be made of the centre of rotation, with an uncertainty of about 0°.1. This precision is, however, not sufficient to decide whether the displaced absorption of both H I and OH, which has been observed in front of the concentrated component of the Sagittarius source, is due to rotation or to an inflow of gas.

PART I

PROGRAMME AND OBSERVATIONS

1. Introduction

1.1. *Data before 1956*

21-cm line observations of the central region of the Galactic System were started in Dwingeloo in October 1956 with the just completed radio telescope. This instrument was then the largest steerable telescope in the world. The observations of the central region were given a high priority. A few years before, faint long wings of the 21-cm emission profiles had been discovered at high positive and negative velocities with the 7.5-metre Kootwijk radio telescope (KWEE, MULLER and WESTERHOUT, 1954). It was thought at that time that highly turbulent motion of the gas in the inner part of the Galactic

System caused these wings, a hypothesis which had to be abandoned when the results with higher resolution became available. There were other reasons to measure the 21-cm line emission in this region as early as possible. McCLAIN (1955) had taken some 21-cm line profiles on Sagittarius A, and concluded that the source was at a distance of about 3 kpc from the Sun. Others considered it to be the nucleus itself, at a distance of about 8 kpc, the co-ordinates being within the limits of accuracy the same as found from optical data. Although the galactic nucleus itself has not been observed optically, it can be located fairly well from objects in its vicinity. BAADE (1951) has observed RR Lyrae variables in a "window" which is relatively clear of absorption, 4° from the galactic centre. He found a very strong concentration of these variables at a distance of about 8 kpc. MINKOWSKI (1951) concluded from the number of planetary nebulae as a function of galactic longitude that the nucleus must be at $l^{\mathrm{I}} = 328° \pm 1°$ ($l^{\mathrm{II}} = +0°.3$), in accordance with the result of other authors (OORT, 1952). A position $l^{\mathrm{I}} = 328°.0$, $b^{\mathrm{I}} = -1°.5$ was obtained from 21-cm line measurements of the Kootwijk survey (VAN DE HULST, MULLER and OORT, 1954).

As regards the position of Sgr A, the mean result before 1956 was $l^{\mathrm{I}} = 327°.7$, $b^{\mathrm{I}} = -1°.4$, ($l^{\mathrm{II}} = 0°.0$, $b^{\mathrm{II}} = 0°.0$). In many extra-galactic nebulae very small condensed nuclei occur. This strongly supported the theory that the Sgr A source is actually the nucleus of the Galactic System. BAADE (1955) determined the size of the nucleus of M 31. From short-exposure plates of the nebula he found $2''.5 \times 1''.5$ (8×5 pc). This size was of the same order as could be estimated for Sgr A. These were the main data, radio and optical, which were known about the inner part of the Galactic System at the start of the observations to be described here.

1.2. *Preliminary observations*

Dr H. van Woerden started the programme by taking about 150 drift curves (B_x measurements, see section 2.2), in order to find out how far in galactic latitude and to how high a velocity the H I radiation occurred. The bandwidth was large, 140 kc/s, as this programme was to be done as quickly as possible. It was found that the layer was very thin, about 1°.0 to 1°.5 in galactic latitude. The maximum intensity was reached at about $b^{\mathrm{II}} = 0°.0$. The maximum velocity at which emission was found, was about 270 km/sec. These first observations were finished in January 1957. The results will not be published in detail. They will be used only in section 5.7. During these preliminary measurements the absorption of the Sgr A source by the cool H I of the 3-kpc arm and the remarkable expanding motion of this arm were discovered (VAN WOERDEN, ROUGOOR and OORT, 1957).

1.3. *Framework*

The measured profiles will be represented in tabular form and in two kinds of isophote charts:

a) With co-ordinates b and V, for various longitudes. These lend themselves in particular for studying the thickness of the gas layer.

b) With co-ordinates l and V, for various latitudes. Here we can follow spiral arms and other features in galactic longitude. At the right side of figure 1 such a chart is shown very schematically. It contains features found at various galactic latitudes. Below the line "Dwingeloo horizon" the isophotes have been constructed from observations made at the Department of Terrestrial Magnetism of the Carnegie Institution of Washington (to be referred to as D.T.M.), which were kindly put at our disposal by Dr B. F. Burke (see section 3.3 for a more detailed chart). The chart indicates the three parts into which this article is divided: the general survey (part II), the 3-kpc arm (part III), and the nuclear disk (part IV). The principal contents are summarized below.

Part II. Chapter 3 describes the central region as visible from Dwingeloo from $l^{\mathrm{II}} = -7°.7$ to $l^{\mathrm{II}} = +22°.7$. Most of the measurements were made during 1957 and 1958. These measurements will be given in the form of tables and of l–V diagrams like the diagram at the right in figure 1. The discussion (chapter 4) will include also data down to $l^{\mathrm{II}} = -23°$.

Part III. In the l–V diagram of figure 1 a long thin feature can be followed from $l^{\mathrm{II}} = -23°$ to $+5°$, which is indicated as "3-kpc arm". This name is now commonly used, and we shall retain it, although the choice of the name is rather arbitrary as the distance is derived only from the fact that the arm first appears at $l^{\mathrm{II}} = -22°$. Chapter 5 gives the profiles of this arm in more detail than was done in part II; it gives also an extension in galactic latitude. In chapters 6, 7 and 8 a discussion is given and some characteristics of the arm are derived. In the left-hand side of figure 1 a possible

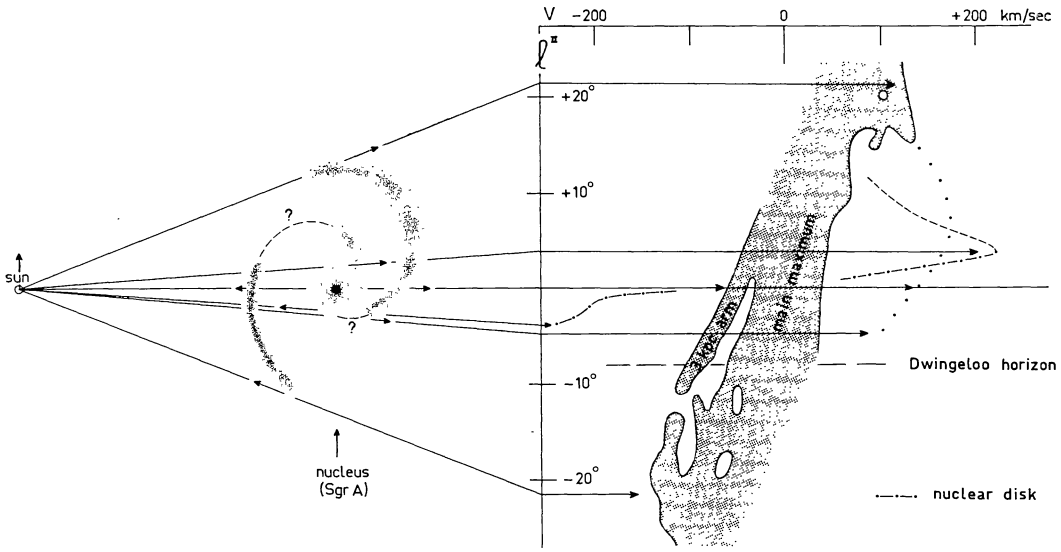

Figure 1. Sketch of possible distribution and motion of hydrogen in the central part of the Galactic System. Arrows in the left half indicate radial velocities as observed from the Sun. The right-hand part shows the relation with various features in the *l*–*V* chart; south of the line marked "Dwingeloo horizon" this is based on observations at D.T.M. (section 3.3). More elaborate *l*–*V* charts may be found in figures 7–13. The present chart shows clearly the separation between the 3-kpc arm with an expanding velocity of -53 km/sec and the main maximum. The dots at positive velocities indicate the arm with an expansion velocity of $+135$ km/sec, while the dashes show part of the "connecting arm" (section 4.1). The rapidly rotating nuclear disk is indicated by dash-dot curves.

distribution of the gas in the galactic plane is sketched. An essentially similar drawing has already been described in a previous article (ROUGOOR and OORT, 1960).

The 3-kpc arm is drawn between the Sun and the nucleus because it appears in absorption when observed in the direction of the nucleus (VAN WOERDEN, ROUGOOR and OORT, 1957). The expanding arm* at the other side of the nucleus is described in part II. In deriving figure 1 the assumption was made that the expansion velocity increases towards the nucleus; on this basis the latter arm has been drawn closer to the centre than the 3-kpc arm.

Part IV. Very close to the nucleus the *l*–*V* diagrams (e.g. figures 10 and 11) indicate large extensions to about $+270$ and -270 km/sec. At the negative side this feature stands quite apart from the other emission. The feature is of relatively low intensity and is therefore not completely shown in the schematic chart of figure 1. Chapter 9 gives the results of the observations of this feature, which was called the "nuclear disk" (ROUGOOR and OORT, 1960), and which has been also drawn at the left in figure 1. Many profiles of it were obtained during 1959 from $l^{II} = -2°$ to $+2°$ and $b^{II} = -1°$ to $+1°$. A discussion will be given in chapter 10.

1.4. *Execution of the programme*

The observations described in this article were started October 11, 1956. We finished March 16, 1963. The total observing time involved was 2 100 hours. The number of observers was about 25, mostly students from Leiden and Groningen, who worked each for a fortnight in Dwingeloo under the guidance of the chief-observer Mr S. Drenth.

The receiver has been kept in an excellent working condition by Professor C. A. Muller and his assistent Mr A. C. Hin. Mr R. J. van 't Land maintained the mechanical part of the telescope.

About 20 persons have co-operated in the computations, card-punching, preparation of the figures etc. In the beginning a ruler was used to read the measurements. Later on a reading machine was constructed (see section 2.3). Most of the "survey" profiles were reduced with this machine. From 1960 on an electronic

* Throughout this article we shall use the term "expansion" and "expanding arms" to indicate large-scale structures which have motions directed away from the galactic nucleus. The "expansion" studied in the present article is not necessarily associated with a real expansion of the gas in these structures.

computer (Electrologica X 1) accelerated the reduction greatly. A standard reduction programme was used, made by Messrs J. Hirsch, T. Hoekema and E. Raimond.

1.5. *Optical and radio data after 1956*

After the start of this programme many other investigations on the central region of the Galactic System or nuclei of other galaxies have been published in both the optical and radio continuum domain.

Fernie has made a critical review of the globular clusters to derive the distance to the centre (FERNIE, 1962). It has been recently recommended to use a standard value of 10 kpc for the reduction of 21-cm observations (cf. *I.A.U. Information Bull.* No. 11, 11, 1963). The source Sgr A has not yet been found optically, although Courtès, by a new observing technique, has discovered H II regions, which probably form part of the nuclear disk surrounding Sgr A (COURTÈS and CRUVELLIER, 1960a, b).

In the future X ray observations of the central region might become very important. The present observations are too incomplete to allow decisive conclusions (GURSKY *et al.*, 1963).

A very surprising discovery was the multiple structure of Sgr A at a wavelength of 3 cm (DRAKE, 1959a, b, c), which was later confirmed at a wavelength of 10 cm by Cooper and Price (cf. KERR, 1962). The structure of Sgr A will be discussed in detail in section 7.1.

In some extra-galactic nebulae phenomena have been found similar to those in our own Galaxy. A large mass concentration was found in M 31 and M 32 with the electronic camera of LALLEMAND, DUCHESNE and WALKER (1960; WALKER, 1962).

MÜNCH (1960) found expansion in M 31 by observation of the doublet line of O II ($\lambda = 3\,727$ Å). HUGH M. JOHNSON (1961) has reported new determinations of the size of the nucleus of M 31.

21-cm line observations were made at C.S.I.R.O., Sydney (KERR, 1962), at D.T.M. (BURKE and TUVE, 1962), and at the California Institute of Technology (CLARK, RADHAKRISHNAN and WILSON, 1962). The latter used an interferometer technique. The D.T.M. measurements will be described in section 3.3.

At the end of 1962 new observations were started with the 210-ft Parkes telescope, the results of which will be published early in 1965.

Surprising 18-cm line observations were made with the same telescope (ROBINSON *et al.*, 1964).

During the last two years a number of articles have been published about so-called massive or condensed objects, with masses between 10^6 and 10^8 times the mass of the Sun. These articles will not be discussed here, but we should remember that these objects may be closely related to nuclei of normal galaxies.

2. Measurements and reductions

2.1. *Introduction*

Most of this chapter consists of a description of the methods of measurements and reduction, which are different from those normally used. The normal procedure will be published later in the *B.A.N.* Most of it is covered in the following articles.

C. A. MULLER, *Philips Technical Review* **74**, 305 and 351, 1956: Description of the Kootwijk receiver, which is the prototype of the receiver used in the present investigation.

C. A. MULLER and G. WESTERHOUT, *B.A.N.* **13**, 151, 1957: This article contains a short description of the receiver and a full discussion of the standard reduction procedure.

H. C. VAN DE HULST, E. RAIMOND and H. VAN WOERDEN, *B.A.N.* **14**, 1, 1957: The antenna pattern of the Dwingeloo disk at a wavelength of 21 cm is given, both as a table and as a diagram.

G. WESTERHOUT, *B.A.N.* **14**, 215, 1958: The calibration of the pilot, the optical calibration and the determination of the radio axis of the Dwingeloo telescope.

H. VAN WOERDEN, K. TAKAKUBO and L. L. E. BRAES, *B.A.N.* **16**, 321, 1962: Stray radiation from remote sidelobes is discussed.

E. RAIMOND, *Sitzgsber. Akad. Heidelberg* **2**, 91, 1962/1963: A short but complete summary of the reduction, especially since the beginning of 1961, when the automatic reduction was started.

During the period covered by our measurements the receiver has been greatly improved by its designer Professor C. A. Muller. The main changes were:

a) A rematching of the mixer circuits in October 1957. This resulted in a considerable reduction of the frequency dependence of the zero level.

b) New intermediate-frequency filters permitting

simultaneous measurements in eight channels. They were installed in June 1958.

c) Since 1961 the output of the receiver is punched on paper tape for reduction by an electronic computer.

d) A special matched intermediate-frequency amplifier was built in 1961.

2.2. *Receiver characteristics*

a) *Bandwidth.* The available settings for bandwidth were 5, 10, 20, 40, 140 and 600 kc/s*. A bandwidth of 140 kc/s was used for the first observations in the autumn of 1956 (see section 1.2). This bandwidth is too broad for nearly all the features. 40 kc/s bandwidth is adequate for most profiles except the 3-kpc arm. (The main maximum of the profiles was not observed; this part of the profile would have required a bandwidth of 10 kc/s or less.) During the summer of 1957 the 3-kpc arm was measured with a bandwidth of 20 kc/s. In the autumn of 1957 we started the "general survey" with 40 kc/s bandwidth. This was used until the summer of 1958, when the eight-channel receiver came into operation. This latter has only bandwidths of 5, 10 and 20 kc/s, hence we continued the "general survey" with 20 kc/s. In table 4 the bandwidth which has been used for each profile is indicated by 20 or 40. For the absorption profile at negative velocities in the direction of Sgr A and for some other profiles a bandwidth of 10 kc/s was used.

b) *Tracking in α, δ (or l, b) and f (frequency).* The three variables can be changed independently. We use the following notation for the four possible different kinds of measurements:

TABLE 1

α	δ	l	b	f	Notation
c	c	c	c	v	A measurement
c	v	—	—	c	B_δ measurement
v	c	—	—	c	B_α measurement
c	c	c	c	c	C measurement

c = constant, v = variable.

During the preliminary observations in 1956, B_α measurements ("drift curves") were recorded. They were very useful for a first survey, in particular to get a rough impression about the distribution in latitude. B_α measurements have the advantage that the telescope does not move. But they are difficult to interpret, because the (α, δ) co-ordinates make an angle of 60° with the (l, b) co-ordinates in this region. Hence a drift curve cannot be regarded to be at a constant galactic longitude.

It is possible to change both α and δ in such a way that one gets tracks along lines of constant galactic longitude or latitude. We did not choose this type of measurements either, for two reasons. The observer is obliged to run both α and δ servomotors of the analogue computer at different rates after having started them at the right moment. Mistakes are easily made. In the second place the telescope has to move over a large angle during this procedure. The reduction would have been complicated even more since the elevation of the telescope was of the order of 1° to 20°.

For most observations A measurements were made. In principle C measurements do not differ much from A measurements. They have been used principally for cases where the intensities are low and long integration times are required to obtain sufficient accuracy. For the "general survey" and the "3-kpc arm" we made A measurements; for the "nuclear disk" C measurements proved rather suitable.

c) *Positions and position intervals.* In general we shall give throughout this article galactic co-ordinates in the new system. (If we use the old system, the values in the new system are in parentheses.) We started to make the observations at full, half and quarter degrees in the old galactic co-ordinate system. As the refraction correction had been sufficiently determined in October 1956 and January 1957, the positions could be corrected for refraction beforehand.

The thickness of the H I layer is rather small. In the "general survey" programme only galactic latitudes $b^{\mathrm{I}} = -0°.5, -1°.0, -1°.5$ and $-2°.0$ ($b^{\mathrm{II}} = +0°.9, +0°.4, -0°.1$ and $-0°.6$) were observed, the spacing in longitude being 0°.5 or 1°.0. In the beginning of 1963 new measurements were made at higher latitudes around $l^{\mathrm{I}} = 325°$ ($l^{\mathrm{II}} = -2°.7$). For the "3-kpc arm" an extension was made during 1961 at latitudes $b^{\mathrm{I}} = 0°.5, 0°.0, -2°.5$ and $-3°.0$ ($b^{\mathrm{II}} = +1°.9, +1°.4, -1°.1$ and $-1°.6$). For the "nuclear disk" we used a co-ordinate system with Sgr A as origin, because this disk is so strongly connected with the source. This co-ordinate

* In a later issue of the *B.A.N.* a description will be given of the filters.

system is not quite the same as the new galactic coordinate system, the difference being 0°.06 in galactic latitude. The spacing in this last programme was 0°.25, which is small compared to the beamwidth of 0°.56.

d) *Velocity intervals.* From the preliminary observations we had obtained some idea how far the "long wings" extend in velocity. Close to the nucleus the H I radiation appears from about − 270 km/sec to + 270 km/sec. In the receiver two comparison frequencies can be used simultaneously, one 1440 kc/s = 304 km/sec below the signal frequency, the other 1440 kc/s above it (MULLER, 1956). Hence we must switch off one of these comparison channels when 21-cm emission occurs at its frequency. When the profile really runs from − 270 to + 270 km/sec, only the lower comparison channel can be used for velocities from − 270 to − 34 km/sec, and the other comparison channel for velocities from + 34 to + 270 km/sec. Only in the small band from − 34 km/sec to + 34 km/sec can both comparison channels be used.

In switching off one of the comparison channels, only half of the time is used to get actual information. In the same time interval the noise fluctuations increase by a factor $\sqrt{2}$. In order to get the same noise fluctuation, we had therefore to observe twice as long.

The example discussed here is the worst case. Most of the 3-kpc arm observations and the measurements from $l^{I} = 337°$ to 350° ($l^{II} = +9°.3$ to 22°.3) have been made with two comparison channels.

2.3. *The reduction*

The recorded output u of the receiver can be split into two parts, j_{HI} being due to the radiation of the neutral hydrogen, and u_0 coming from the instrument. To get the actual value for the brightness temperature a number of corrections has to be applied which will be described in detail in a forthcoming publication. Throughout this article the brightness temperature will be given in "units". This unit has been defined in 1959 as a standard unit of temperature for the Dwingeloo measurements. It was meant to be as close to 1 °K as the accuracy of the observations permitted.

The principal corrections to be applied to j_{HI} are for

a) variations of the sensitivity of the receiver with time and air temperature;

b) alinearity of the receiver, for which the detector circuit is mainly responsible;

c) atmospheric extinction.

The last correction is almost exclusively a function of the elevation. In this programme the corrections for extinction are important only for longitudes around $l^{II} = -7°$. For higher longitudes they are generally small.

The variation of the instrumental output u_0 with time is generally called drift. This drift has been the most serious difficulty in our programme. During most of the measurements, which were possible for about three or four hours per day, the zero level was checked about four times by a C measurement (see table 1) of 15 minutes at high positive or negative galactic latitude. For the measurement of the nuclear disk (part IV) these checks were made at the same elevation ($\approx 8°$) as the measurement of the nuclear region itself. For the period February 24 to April 17, 1959, in which most of the disk measurements at negative velocities were made, the checks of the zero level for one frequency have been averaged for each day. A curve of the variation of this average during this period is shown in

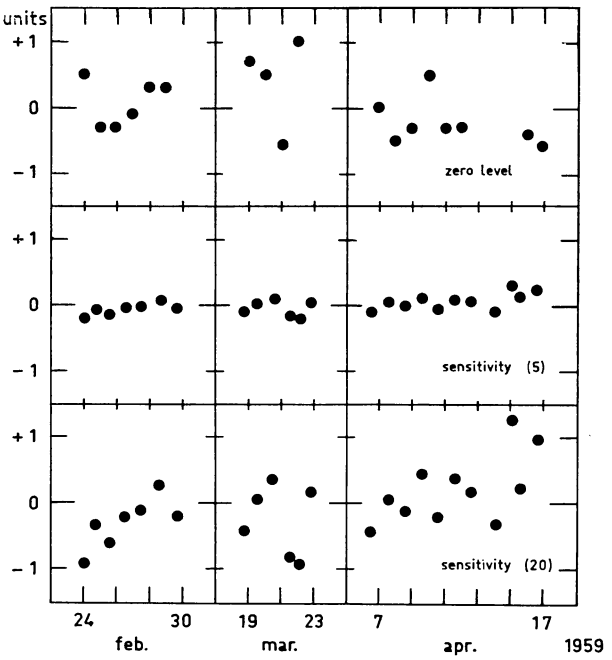

Figure 2. The variation of the zero level and of the sensitivity, during an interval of two months. The sensitivity variations are given for H I temperatures of 5 and 20 units ($\approx$ °K). The variation for a brightness temperature of 20 units shows nearly the same scatter as the variations in zero level. This demonstrates that the sensitivity variations are relatively unimportant for the low intensity emission measured during most of this programme.

TABLE 2

Calendar of the observations

Period		Programme	Bandwidth (kc/s)	Number of measurements	Hours	Days involved	Receiver (1 of 8 channels)	Spacing ℓ x b	Remarks
from	until								
October 11, 1956	November 4, 1956	preliminary observations	140	158	112	25	1	$\approx 2^\circ.5$	Also B_α measurements, absorption 3-kpc arm.
January 4, 1957	January 28, 1957	preliminary observations	40, 140	91	115	19	1	$\approx 2^\circ.5$	
June 22, 1957	September 29, 1957	3-kpc arm	20	498	563	84	1	$0^\circ.5 \times 0^\circ.25$	
November 26, 1957	February 19, 1958	survey	40	300	351	54	1	$0^\circ.5 \times 0^\circ.5$	
June 17, 1958	June 23, 1958	survey	40	14	22	6	1	$0^\circ.5 \times 0^\circ.5$	
July 17, 1958	August 4, 1958	preliminary observations	20	93	68	15	8	$0^\circ.5 \times 0^\circ.25$	Dense grid at $\ell^{I} \approx 335^\circ$, not described in this article.
September 11, 1958	September 24, 1958	3-kpc arm	10	66	53	13	8	-	Cross through galactic centre with spacings of $0^\circ.25$ in ℓ and b.
September 27, 1958	November 27, 1958	survey	10, 20	182	147	43	8	$0^\circ.5 \times 0^\circ.5$	
January 24, 1959	February 22, 1959	survey	20	117	121	26	8	$0^\circ.5 \times 0^\circ.5$	
February 24, 1959	July 25, 1959	disk	20	44	161	41	8	$0^\circ.25 \times 0^\circ.25$	C measurements, $-2^\circ < \ell^{II} < 2^\circ$.
October 6, 1959	November 14, 1959	disk	20	33	121	29	8	$0^\circ.25 \times 0^\circ.25$	
March 8, 1961	June 14, 1961	3-kpc arm	20	198	144	53	8	$0^\circ.5 \times 0^\circ.5$	Extension in latitude.
July 21, 1962	September 28, 1962	disk	20	162	110	45	8	$0^\circ.25 \times 0^\circ.25$	$-5^\circ < \ell^{II} < -2^\circ$, not described in this article.
February 18, 1963	March 1, 1963	disk	20	37	23	8	8	$0^\circ.25 \times 0^\circ.25$	
March 7, 1963	March 15, 1963	survey	20	14	15	8	8	-	Extension in latitude, not in a regular grid.
Total				2 007	2 126	469			

figure 2. The r.m.s. deviation of these points from the mean during this whole period is 0.5 unit. The noise of the receiver contributes 0.1 unit, if we assume a receiver noise of 1 200 units. So, the variation of the zero level as shown in figure 2 pictures the drift of the receiver rather than the noise variations. In the same figure the variation of the sensitivity is given for $j_{HI} = 5$ and 20 units, respectively. This diagram indicates the relative importance of the accuracy needed in determining j_{HI} and u_0 for small and large values of j_{HI}. At $j_{HI} = 20$ units the variations of the sensitivity and of the drift of the zero level are about equal.

Three measurements (figure 3) on the north pole show the variation of the zero level with frequency. (The hydrogen profile around 36.4 Mc/s has been left out.) Two of these measurements were made in 1957, one before the rematching of the mixer circuits, the other afterwards. A special matched i.f. amplifier yielded a practically constant zero level, which is clearly shown by the measurement of August 28, 1962.

In the examples shown, one of the comparison channels has been switched off, in order that no negative profile would occur at $f \approx 35.3$ Mc/s (figure 3). In this manner the positive velocities could be measured of which the range used for most of our measurements, has been indicated. Most of our measurements in this velocity range had a zero level like the one shown for November 25, 1957.

The zero level is very sensitive to an extra input of continuous radiation, such as is due, in part of the present programme, to Sgr A and its surroundings. Corrections for this background radiation have been obtained by measuring the profile of Cassiopeia A and comparing this with a part of the sky where no continuous radiation is present.

Examples of these corrections (for $b^{II} = -0°.06$, through Sgr A for the period between 1957 and 1961) are given in table 3. The corrections are expressed in units ($\approx$ °K). They are fairly constant over a large velocity range. The change of sign for negative and positive velocities is due to the different comparison channels which were used in the two cases.

TABLE 3
Corrections for background radiation (in units)

l^{II}	0°00	0°50	1°00	1°50	2°00
Negative velocities	+ 1.5	+ 0.7	+ 0.3	+ 0.3	+ 0.3
Positive velocities	− 3.0	− 1.5	− 0.7	− 0.5	− 0.5

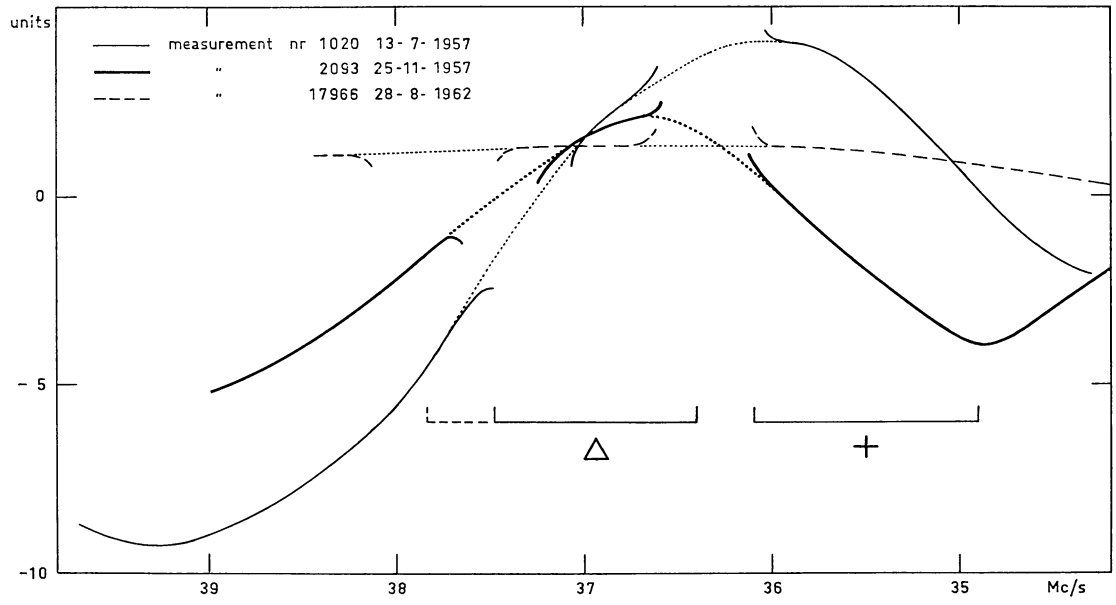

Figure 3. Three measurements of the north pole over an extended frequency range. The zero point of the ordinate is the zero level of the last stage of the receiver (the direct current amplifier). The actual H I profiles (at $f \approx 36.2$ and 37.3 Mc/s) has been left out. For measurements Nos 1 020 and 2 093 the distance Δ between signal and comparison channel was 1.080 Mc/s. For measurement No. 17 966, $\Delta = 1.440$ Mc/s. In the measurements plotted, only one comparison channel, viz. that on the low-frequency side, was used. The characteristic range for the observations of positive velocities is indicated by +.

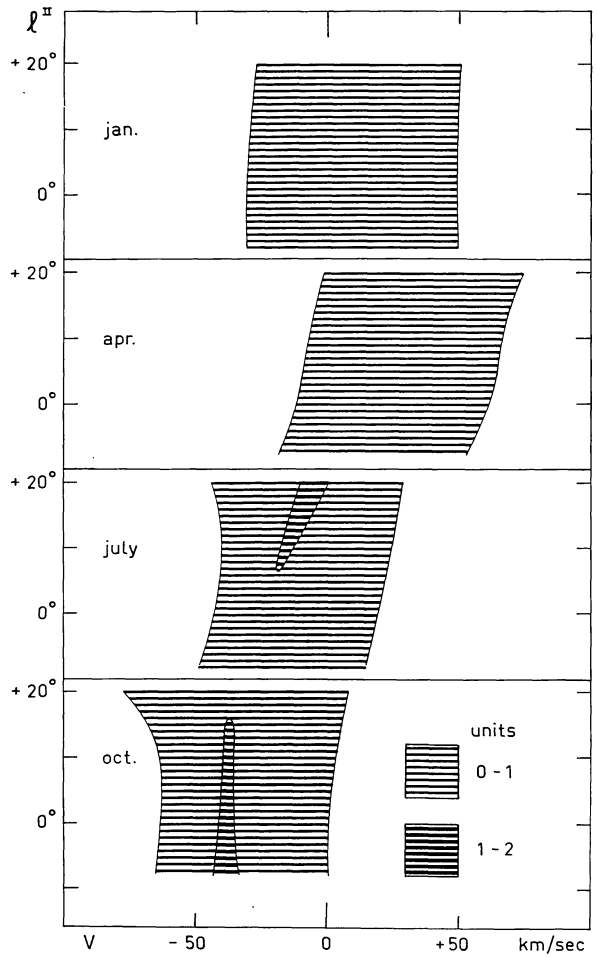

Figure 4. Stray radiation from the sidelobes of the antenna, computed for four different seasons for $b^{II} = 0°.0$.

No correction for stray radiation coming in from other parts of the sky through the sidelobes of the antenna pattern has been applied to any of our measurements. For determining this correction the distribution of the H I emission over the whole sky visible during the time of the measurement is needed, as well as the positions and intensities of the sidelobes of the antenna. In order to obtain a rough estimate of the influence of this stray radiation the Kootwijk catalogue of hydrogen profiles has been used (MULLER and WESTERHOUT, 1957). The far sidelobes of the antenna have been computed, but the results are quite uncertain. The resulting stray radiation for four different months is shown in figure 4 in the form of l–V charts. The maximum brightness is only 2 units (≈ 2 °K) in the velocity interval from 0 to -40 km/sec. Nowhere does the 1-unit isophote exceed ± 75 km/sec. Therefore we can trust that stray radiation has not affected the results very strongly.

After u_0 had been determined the resulting values of j_{HI} were reduced to brightness temperature in the manner illustrated in figure 5. The original recordings of the outputs of the eight channels have been indicated by different symbols, together with all the data the observer had to write down during the measurement.

The eight different zero levels u_0 were indicated on the recording by small lines. This is shown in figure 5 at the left and right sides. The recording was then measured by a reading machine which projected two movable light beams on the recording chart. One of the beams could be set at the zero level u_0, while the other could be made to follow the curve and read it at fixed frequency intervals (in our case 10 kc/s). The distance between the light beams which is proportional to j_{HI}, was read off by two helipots (variable resistors). In the amplification of the read-off signal the necessary factors for sensitivity and extinction could be included. In our case also a correction factor had to be applied for the extra continuous radiation from the galactic centre region (especially from Sgr A). This last factor was of the order of 1.03 throughout the central region; for the profile at Sgr A this factor was 1.30. After amplification the profile was recorded directly by the reading machine, with the correct scales for frequency and brightness temperature. The mean of three recordings obtained in this way is shown in figure 6.

PART II

THE GENERAL SURVEY

3. Tables and contour diagrams

3.1. *Introduction*

The profiles obtained according to the method described in chapter 2 were read off at each 5 km/sec in V for the four galactic latitudes $b^I = -0°.5$, $-1°.0$, $-1°.5$ and $-2°.0$ ($b^{II} = +0°.9$, $+0°.4$, $-0°.1$ and $-0°.6$). The numbers were written on a l–V chart

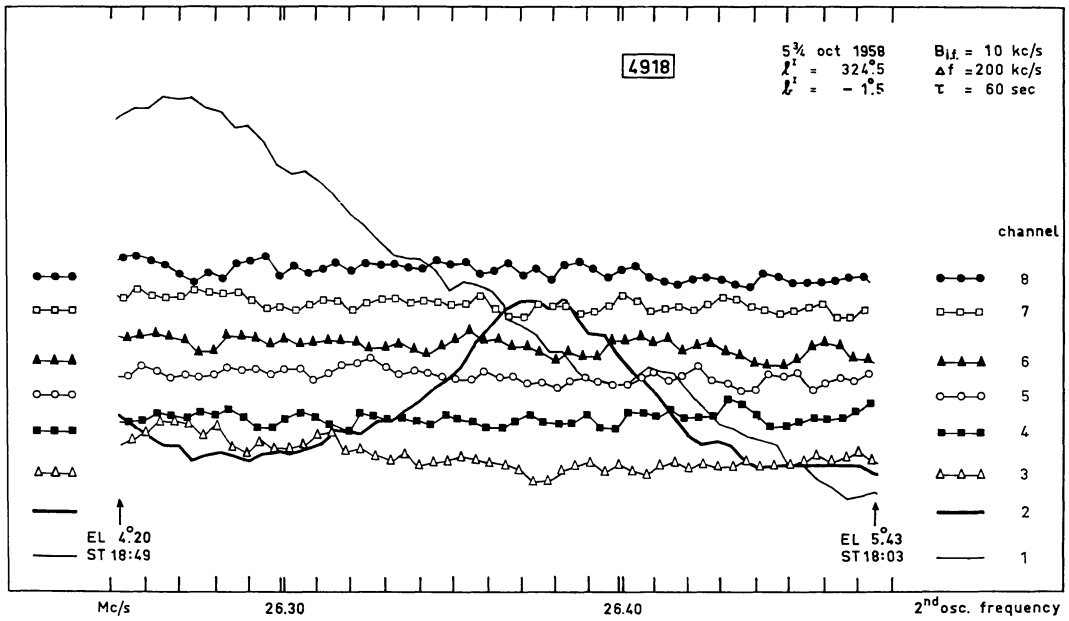

Figure 5. Measurement No. 4 918 (type A, duration 46 minutes) taken directly from the recorder sheet. A complete measurement is recorded in 48 seconds, with intervals of 6 seconds between the recordings of successive channels which are indicated by different symbols. The zero levels are shown at the left- and right-hand side of the recording. They have been determined from C measurements made some time before and after this measurement. The main maximum (channel 1) and the 3-kpc arm (channel 2) jump out at first sight. The emission of the disk can be distinguished at closer inspection. EL = elevation of the telescope, ST = sidereal time, Δf = the distance between channels, τ = time constant.

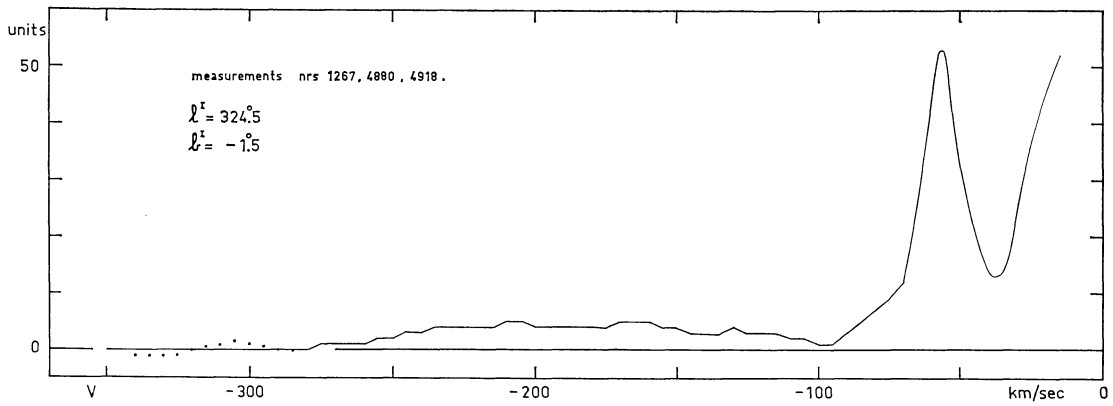

Figure 6. Mean profile from three measurements (one of which is shown in figure 5). The scatter of the points at the left-hand side gives an impression of the accuracy.

(like the right-hand side of figure 1) and smooth isophotes were drawn. The isophotes are at 2.5, 5, 10, 15, 20 and 25 units (≈ °K). The charts at $b^I = -0°.5$, $-1°.0$ and $-1°.5$ ($b^{II} = +0°.9$, $+0°.4$ and $-0°.1$) have been constructed from measurements with a spacing of 0°.5 in longitude. In this case there is, of course, some correlation between adjacent profiles. At positive velocities the l–V diagram at $b^I = -2°.0$ ($b^{II} = -0°.6$) has been constructed from profiles which were in general one degree apart in longitude. The greater spacings gave no difficulties at this latitude, because the distribution is much smoother. If it became clear that no

TABLE 4

ℓ^{I}	ℓ^{II}	B		- 30		- 40		- 50		- 60		- 70		- 80		- 90		-100		-110		-120		-130
$b^{I} = -0.5°$	$b^{II} = +0.9°$																							
320.0	352.3	20							11	07	08	09	11	13	16	19	24	22	14	08	05	04	04	03
320.5	352.8	20							12	12	11	11	10	10	12	19	21	15	08	04	03	03	04	04
321.0	353.3	20						14	10	09	10	10	10	12	16	21	19	12	04	01	00	01	01	01
321.5	353.8	20						08	05	08	11	14	16	13	15	16	11	05	01	00				
322.0	354.3	20						09	08	08	10	13	17	20	19	16	09	04	01	00				
322.5	354.8	20					19	10	06	06	09	12	16	21	20	14	08	02	00					
323.0	355.3	20					16	09	06	06	09	13	19	24	22	12	05	02	01	00				
323.5	355.8	20					12	06	05	06	13	19	26	24	17	07	03	01	00	00	00	00	00	00
324.0	356.3	20				18	09	06	05	08	15	22	25	23	15	07	03	02	01	01	01	02	02	03
324.5	356.8	20				15	08	04	04	06	11	18	17	12	07	04	02	02	02	01	01	01	01	01
325.0	357.3	20			15	09	04	03	03	07	11	13	10	07	04	03	02	02	03	04	05	05	05	05
325.5	357.8	20			10	07	04	03	04	07	08	08	06	03	02	01	01	01	01	01	01	01	02	03
326.0	358.3	20			09	06	05	05	05	06	07	05	03	02	01	01	00							
326.5	358.8	20	24	17	11	08	06	05	05	08	08	05	03	02	02	01	00							
327.0	359.3	20	29	18	11	08	08	08	08	09	08	06	04	02	01	00								
327.5	359.8	20	26	15	09	07	07	06	06	06	06	05	03	02	01	00								
327.7	000.0	10	27	16	11	09	07	07	07	07	06	05	03	02	01	00								
328.0	000.3	20	26	18	13	10	10	09	09	08	06	04	03	02	01	00								
328.5	000.8	20	31	21	13	09	10	10	09	07	04	03	01	00										
329.0	001.3	20	29	19	13	10	10	10	09	08	07	06	03	02	01	00								
329.5	001.8	20	24	18	14	13	13	13	11	09	07	05	02	01	00									
330.0	002.3	20	22	16	12	10	10	12	11	07	03	01	00											
330.5	002.8	20	19	14	10	08	09	11	11	05	01	00												
331.0	003.3	20	20	13	09	10	12	10	07	03	00													
331.5	003.8	20	22	15	15	16	12	06	03	02	00													
332.0	004.3	20	29	21	16	12	08	03	01	00														
332.5	004.8	20	38	22	15	08	04	01	00															
333.0	005.3	20	29	14	07	03	00																	
$b^{I} = -1.0°$	$b^{II} = +0.4°$																							
320.0	352.3	10						39	24	15	10	09	15	32	45	53	53	34	16	09	05	02	01	03
320.5	352.8	20						37	29	20	15	14	20	30	39	46	40	24	11	05	03	02	02	03
321.0	353.3	20						37	24	16	13	13	20	29	38	39	29	18	08	04	03	03	03	02
321.5	353.8	20						21	15	14	16	21	25	28	29	27	22	11	05	03	03	01	01	01
322.0	354.3	20						20	13	11	15	20	25	29	29	23	15	08	03	01	00			
322.5	354.8	20					25	16	11	10	11	15	27	33	25	17	13	08	03	00				
323.0	355.3	20					18	11	10	10	13	26	41	41	28	14	08	03	01	00	00	00	00	00
323.5	355.8	20					15	09	10	14	23	44	49	38	26	14	05	00	00	00	00	00	00	00
324.0	356.3	10				27	13	11	13	21	34	41	38	28	18	09	03	01	01	00	00	01	01	02
324.5	356.8	10				24	15	12	17	24	37	38	28	18	12	07	03	01	01	00	00	01	01	01
325.0	357.3	20			27	19	12	10	15	26	30	26	20	14	08	04	02	01	01	01	01	01	02	02
325.5	357.8	20			19	13	09	11	17	23	23	18	13	10	07	04	01	00	00	00	00	00	00	01
326.0	358.3	10			13	10	08	13	18	21	19	16	12	08	05	03	02	01	00	00	01	01	01	02
326.5	358.8	10	32	21	15	12	12	16	20	20	18	15	12	09	07	05	04	04	03	03	03	04	04	04
327.0	359.3	20	32	23	17	14	16	19	22	21	17	14	11	08	06	06	06	06	05	05	04	05	05	05
327.5	359.8	20	32	21	17	15	15	13	13	16	15	13	09	06	04	03	02	02	02	02	02	02	02	02
327.7	000.0	10	32	22	18	16	15	09	08	13	13	09	06	04	02	01	00							
328.0	000.3	10	35	25	21	17	15	14	14	13	10	07	04	03	02	01	00							
328.5	000.8	10	36	25	21	19	19	18	16	14	12	09	06	04	02	01	00							
329.0	001.3	20	40	26	22	23	22	19	14	10	08	06	04	02	00									
329.5	001.8	20	33	23	22	24	26	23	12	09	07	05	03	01	00									
330.0	002.3	20	28	23	22	23	23	18	12	08	05	02	01	00										
331.0	003.3	20	32	21	17	19	18	14	11	06	04	00												
331.5	003.8	20	37	26	24	24	18	11	05	01	00													
332.0	004.3	20	43	34	24	18	11	03	00															
332.5	004.8	20	52	35	21	15	05	00																
333.0	005.3	20	46	32	19	09	04	01	00															
333.5	005.8	20	48	31	17	08	03	01	00															

ℓ^{I}		-140		-150		-160		-170		-180		-190		-200		-210		-220		-230		-240		km/sec	
$b^{I} = -0.5°$																									
320.0	02	01	00	00	00	01	01	01	01	02	02	01	00												
320.5	04	02	02	01	01	01	02	03	03	03	03	01	00												
321.0	01	01	02	02	02	02	02	03	04	03	03	02	01	01	00										
323.5	00	00	00	00	00	00	01	01	01	01	02	02	02	02	02	03	04	04	04	04	02	01	01	01	01
324.0	03	03	03	03	03	03	04	04	04	04	04	04	04	04	04	03	03	03	03	02	01	00			
324.5	01	01	01	01	02	03	03	03	03	03	02	02	02	02	01	01	01	00							
325.0	05	05	05	05	05	04	03	03	03	03	03	04	04	04	03	03	02	01	00						
325.5	03	02	02	03	03	02	02	02	02	02	02	03	03	02	01	01	01	01	00						
$b^{I} = -1.0°$																									
320.0	04	04	04	03	01	00																			
320.5	03	02	00																						
321.0	02	02	02	01	00																				
321.5	01	00																							
323.0	00	00	00	00	00	00	00	00	00	00	00	00	00	00	00	00	00	01	02	03	03	02	01	00	
323.5	01	01	01	02	02	02	02	02	02	01	01	00	01	01	02	02	03	04	04	05	05	05	05	03	02
324.0	03	03	04	05	05	06	06	06	06	05	05	05	04	04	04	04	04	03	03	03	02	02	02	02	01
324.5	00	01	02	03	04	05	05	05	06	06	06	06	06	06	06	05	05	03	03	02	02	02	01	01	01
325.0	03	04	04	04	04	04	04	05	05	06	07	08	07	07	06	06	06	05	03	02	01	01	01	01	00
325.5	02	02	03	04	04	04	04	04	05	05	05	06	08	07	06	05	04	02	01	00					
326.0	02	02	02	02	02	02	03	04	04	04	05	05	06	06	05	04	03	02	01	00					
326.5	04	04	04	04	05	05	05	06	06	06	06	06	06	05	05	04	03	02	01	01	00				
327.0	06	06	07	07	07	07	07	07	06	05	05	04	04	03	02	02	01	00							
327.5	01	01	01	01	01	01	00																		

TABLE 4 (continued)

l^I	l^{II}	B		-30		-40		-50		-60		-70		-80		-90		-100		-110		-120		-130		-140		-150		-160		-170		-180		-190		-200		-210		-220		-230		-240			km/sec
$b^I = -1^{\circ}.5$ $b^{II} = -0^{\circ}.1$																																																	
320.0	352.3	20			50	39	44	48	39	23	14	08	11	29	49	48	35	19	10	05	03	02	03	04	04	04	04	03	02	01	01	00																	
320.5	352.8	20			49	45	49	50	38	23	13	12	24	37	43	33	21	13	07	04	03	02	01	00																									
321.0	353.3	20			49	48	49	44	28	16	12	16	28	45	44	26	15	10	07	05	04	02	01	01	00																								
321.5	353.8	20		59	44	38	31	23	16	12	10	12	23	44	38	16	06	04	04	03	02	01	00																										
322.0	354.3	20		56	49	43	34	20	14	09	08	13	24	33	26	10	04	02	02	01	01	01	00																										
322.5	354.8	20		50	44	42	30	16	09	06	11	19	32	29	16	07	04	01	00																														
323.0	355.3	20		50	41	34	21	13	10	13	24	39	42	31	18	08	04	02	01	00																													
323.5	355.8	20	59	44	36	28	13	09	11	16	34	51	47	32	19	09	05	03	02	02	02	02	02	01	00	00	00	00	00	00	00	00	00	00	00	00	00	00	00	00	00	01	01	02	03	03	03	02	02
324.0	356.3	10	52	45	38	25	13	11	16	22	37	46	35	22	13	08	05	04	03	03	03	03	03	04	04	04	04	04	04	04	05	05	05	05	04	03	03	02	02	02	03	03	04	05	05	06	05	04	04
324.5	356.8	20	52	46	37	23	14	14	21	34	52	45	24	12	09	07	05	03	01	01	02	02	03	03	03	04	03	03	03	04	04	05	05	05	05	04	04	04	04	04	04	05	05	04	04	03	03	02	01
325.0	357.3	20	41	32	25	16	10	13	22	38	43	26	12	08	07	05	03	01	00	00	00	00	00	01	01	02	02	02	02	02	03	03	04	04	04	04	05	05	04	03	02	02	01	01	00				
325.5	357.8	20	00	00	17	11	06	14	23	27	23	13	07	05	04																																		
326.0	358.3	10	40	27	16	10	09	18	25	28	23	16	12	10	08	06	05	04	04	03	03	03	03	04	04	04	04	04	04	04	04	04	04	04	05	06	08	09	10	09	08	06	04	03	02	00			
326.5	358.8	20	44	28	17	13	13	19	25	25	19	14	12	11	10	08	07	06	06	06	07	07	08	08	08	08	09	08	09	09	09	09	09	10	11	12	13	13	13	12	10	08	05	03	02	01	01	00	
327.0	359.3	10	40	27	21	17	19	21	24	22	17	12	10	09	07	06	06	06	06	08	09	11	12	13	13	14	14	14	14	13	13	13	13	12	11	10	09	08	06	04	03	02	00						
327.3	359.6	20	23	13	13	13	11	02	00	11	10	09	08	08	07	07	07	07	07	08	08	08	08	09	09	08	08	08	08	08	08	08	08	06	05	03	02	02	02	02	02	01	01	00					
327.5	359.8	10	19	04	09	09	07	-16	-15	05	08	06	05	05	05	05	05	05	05	05	05	06	06	06	05	05	05	05	06	05	05	05	04	03	02	02	02	00											
327.7	000.0	10	18	-08	04	03	-02	-33	-35	-04	04	03	02	03	04	04	03	03	03	03	04	03	03	02	01	01	01	01	01	01	00																		
328.0	000.3	10	20	03	07	03	00	-12	-13	03	07	05	04	03	03	03	03	03	03	03	04	03	02	02	01	01	01	00																					
328.5	000.8	10	30	22	18	10	14	19	17	15	15	12	09	06	05	04	03	03	03	02	02	02	02	01	00																								
329.0	001.3	20	43	29	24	24	27	24	18	12	10	08	05	02	01	00																																	
329.5	001.8	20	41	30	28	35	34	22	11	07	06	05	04	02	00																																		
330.0	002.3	20	31	24	29	37	33	19	08	05	05	04	03	02	01	00																																	
330.5	002.8	20	35	23	28	38	29	13	06	04	03	02	00																																				
331.0	003.3	20	38	27	31	29	19	10	06	05	03	02	01	00																																			
331.5	003.8	20	49	35	31	23	15	09	04	01	01	00																																					
332.0	004.3	20	42	40	30	14	06	02	01	00																																							
332.5	004.8	20	51	44	28	13	05	01	00																																								
333.5	005.8	20	54	35	17	07	04	02	00																																								
334.0	006.3	20	54	36	16	07	04	02	00																																								
$b^I = -2.0$ $b^{II} = -0.6$																																																	
320.0	352.3	10						17	15	08	04	04	08	16	25	24	16	07	04	02	01	01	02	02	02	01	00																						
321.0	353.3	20						09	08	06	05	07	17	31	38	24	10	05	02	02	02	02	02	01	01	00																							
321.5	353.8	20						07	06	05	05	11	20	29	20	09	03	01	01	01	01	00																											
322.0	354.3	20						05	03	03	06	11	19	19	11	03	01	00																															
322.5	354.8	20					11	06	03	01	02	05	10	09	03	01	00																																
323.0	355.3	20					09	04	04	05	08	14	16	09	04	03	02	00																															
323.5	355.8	20					07	04	04	07	12	15	15	10	07	05	03	03	03	03	02	02	02	01	01	01	01	01	00																				
324.0	356.3	20				10	05	04	06	09	13	15	13	09	05	03	03	02	02	02	03	03	03	02	02	02	02	02	02	02	01	00																	
324.5	356.8	20				09	06	05	08	16	25	20	13	06	03	02	02	02	02	02	01	01	01	02	02	01	01	01	03	04	04	04	04	04	04	04	03	03	02	02	02	02	01	01	01	01	01	01	01
325.0	357.3	20			16	10	06	06	13	21	24	17	06	02	02	02	02	01	01	01	00	00	00	00	00	00	00	01	01	02	02	03	04	04	04	03	02	02	01	01	01	01	00						
325.5	357.8	20			18	08	04	09	16	17	14	11	04	02	02	03	02	00	00	00	00	00	00	00	00	00	00	01	02	02	03	03	03	04	04	04	04	03	03	02	02	02	02	02	01	00			
326.0	358.3	20				08	06	12	19	21	17	12	09	07	05	00																																	
326.5	358.8	20	40	24	13	10	10	17	23	24	20	13	08	08	08	07	06	06	06	06	06	06	06	06	05	04	04	04	04	04	04	04	03	02	02	01	01	00											
327.0	359.3	20	33	20	14	10	13	18	21	19	14	07	04	04	04	03	03	03	04	05	05	06	06	06	06	06	06	06	06	05	05	04	03	02	02	02	01	01	01	01	01	00							
327.7	000.0	10	26	13	08	08	13	18	17	11	05	04	04	04	04	05	05	06	06	06	05	04	04	03	03	02	02	01	00																				
328.0	000.3	20	23	12	08	09	14	18	16	10	05	04	05	05	06	06	07	07	06	05	04	03	02	01	01	01	00																						
328.5	000.8	20	22	14	15	19	23	21	16	11	07	06	05	06	06	05	04	03	02	00																													
329.0	001.3	20	25	19	21	25	28	19	12	07	05	04	03	03	02	01	01	01	01	01	01	01	00																										
330.0	002.3	20	29	17	20	24	21	08	03	01	00																																						
331.0	003.3	20	32	21	20	16	06	01	00																																								
331.5	003.8	20	37	30	21	11	01	00																																									
332.0	004.3	20	39	34	24	08	04	02	00																																								
332.5	004.8	20	34	32	19	05	03	01	00																																								
333.0	005.3	20	42	34	18	06	03	03	01	00																																							
333.5	005.8	20	49	34	18	06	02	00	01	01	00																																						
334.0	006.3	20	48	32	17	08	02	00	01	01	00																																						
l^I	l^{II}	B		-30		-40		-50		-60		-70		-80		-90		-100		-110		-120		-130		-140		-150		-160		-170		-180		-190		-200		-210		-220		-230		-240			km/sec

TABLE 4 *(continued)*

l^I	l^{II}	B	+ 30	+ 40	+ 50	+ 60	+ 70	+ 80	+ 90	+100	+110	+120	+130	+140	+150	+160	+170	+180	+190	+200	+210	+220	+230	+240	km/sec
$b^I = -0.°5$		$b^{II} = +0.°9$																							
321.5	353.8	20	31	25	20	15	10	06	04	02	01	00													
322.0	354.3	20	35	26	21	15	11	08	05	04	02	01	00												
322.5	354.8	40					10	08	07	06	05	04	03	02	02	02	02	02	02	01	01	00							
323.0	355.3	40					13	11	09	08	07	06	06	06	06	06	05	05	05	04	03	02	01	01	00				
323.5	355.8	40						14	13	13	12	11	11	10	10	09	08	06	05	04	03	02	00						
324.0	356.3	40			19	14	11	11	11	12	12	12	12	11	10	10	10	10	09	08	05	03	02	01	01	01	00		
324.5	356.8	40				10	09	08	08	09	11	14	16	16	17	17	17	16	14	11	07	04	02	01	00				
325.0	357.3	20	39	28	17	10	06	05	04	03	03	05	06	08	10	12	14	16	16	15	13	09	05	02	00				
325.5	357.8	20	46	33	20	09	06	04	03	02	02	02	03	04	05	06	07	08	09	09	09	08	07	05	03	00			
326.0	358.3	40	44	34	22	15	10	05	05	04	03	04	05	05	07	08	08	07	07	07	07	08	09	09	07	05	03	01	00	
326.5	358.8	20	52	41	30	18	08	03	01	01	01	02	04	05	06	08	09	09	08	06	05	04	04	03	02	01	01	00		
327.0	359.3	40	40	32	25	16	09	06	05	05	04	05	05	06	06	06	06	06	05	04	04	03	03	02	02	01	01	00		
327.5	359.8	20	39	30	23	16	09	05	03	02	02	02	03	03	04	04	04	04	04	04	03	03	03	01	01	00				
328.0	000.3	40		22	14	09	06	04	02	01	01	01	02	02	03	04	04	05	04	04	04	03	02	02	02	01	01	01	01	01	00
328.5	000.8	20		28	20	13	05	03	01	01	02	02	03	04	04	05	05	05	04	04	04	03	02	01	01	00					
329.0	001.3	40	33	23	15	10	07	05	04	03	03	04	04	05	05	06	06	06	06	05	04	03	02	03	03	02	01	01	01	01	01	01	01	01	00
$b^I = -1.°0$		$b^{II} = +0.°4$																							
322.0	354.3	40					07	06	05	04	04	03	02	02	02	02	02	01	01	00									
322.5	354.8	40				14	11	09	09	08	08	08	08	08	09	10	10	09	07	05	03	02	01	00					
323.0	355.3	40					12	11	10	09	09	09	09	09	11	13	15	15	12	09	06	04	02	01	00				
323.5	355.8	40					12	10	10	09	10	10	10	11	11	11	10	09	06	04	02	00							
324.0	356.3	40					10	09	08	07	06	06	06					05	04	03	02	01	00							
324.5	356.8	40				15	09	08	08	09	09	10	11	12	12	13	13	14	14	13	09	07	05	04	02	01	00			
325.0	357.3	40			10	06	04	03	04	04	05	05	06	06	07	08	08	10	10	10	10	10	08	07	05	03	01	01	00		
325.5	357.8	40	51	31	16	08	05	04	03	04	04	04	04	05	07	08	10	11	13	14	14	13	11	09	06	04	02	00		
326.0	358.3	40	60	40	22	14	09	05	05	05	06	06	07	07	08	08	09	10	11	12	13	14	14	13	10	07	05	03	02	01	01	00			
326.5	358.8	20		49	27	15	09	05	04	05	07	08	08	07	07	07	08	08	09	10	10	10	09	07	05	04	03	02	01	00						
327.0	359.3	40	49	37	26	19	13	10	09	08	08	08	08	08	08	08	08	08	08	08	08	08	08	07	06	04	03	02	01	00						
327.5	359.8	20	54	40	29	21	13	07	05	04	05	06	06	06	06	06	06	07	07	08	09	10	10	10	09	08	07	06	05	05	04	02	02	01	01	01	00
328.0	000.3	40		27	19	14	10	07	06	05	05	06	06	07	07	08	09	09	10	10	11	11	12	12	12	12	11	10	09	08	07	06	05	04	02	02	01	01	00
328.5	000.8	20		31	19	13	09	07	06	06	07	07	08	09	10	10	10	10	10	10	10	10	10	10	11	12	13	13	12	11	10	09	08	06	05	05	04	03	02
329.0	001.3	40		31	21	17	13	11	10	12	13	14	15	15	15	15	14	14	13	13	12	11	11	10	11	12	13	13	12	11	10	10	09	08	08	07	06	06	05
329.5	001.8	20			18	13	09	05	04	04	04	05	06	07	07	06	06	06	06	05	05	05	05	06	06	07	07	08	09	09	09	09	08	08	07	06	05	05	04
330.0	002.3	40			13	08	05	05	05	05	05	05	05	05	05	05	04	04	03	02	02	03	03	04	05	05	06	07	07	07	06	05	04	03	02	02	01	01	01
330.5	002.8	20			12	06	04	04	04	05	05	06	06	06	07	07	09	08	06	05	04	04	04	04	05	05	06	08	10	10	08	06	04	03	02	02	01	00	
331.0	003.3	40			11	09	08	09	09	09	10	10	10	10	09	09	09	09	08	08	08	07	07	07	08	09	09	10	11	11	10	09	06	04	02	02	01	01	01
331.5	003.8	20			07	04	03	03	04	07	08	07	06	06	06	07	08	08	07	05	04	03	03	03	04	06	07	08	09	10	10	09	08	05	03	02	01	01	01
332.0	004.3	20				06	05	05	06	07	07	06	04	02	01	03	04	05	05	05	04	03	03	03	03	04	05	05	06	06	07	07	07	06	03	03	03	01	01
332.5	004.8	20				13	10	09	08	07	06	05	05	04	04	04	04	06	07	06	05	04	04	05	05	05	06	06	07	08	09	11	12	10	08	06	04	03	03
333.0	005.3	20				14	11	10	10	09	07	04	05	05	06	06	06	06	07	07	06	05	05	04	04	04	05	05	06	06	07	08	10	11	09	07	05	03	02
333.5	005.8	20					07	06	06	06	05	05	04	05	05	05	05	06	09	09	09	08	07	06	05	05	05	05	05	07	08	08	08	08	08	06	04	02	01
334.0	006.3	40					06	05	05	05	05	05	05	05	05	05	06	07	08	09	09	07	06	06	06	05	04	04	03	03	04	05	05	05	05.	03	02	01	01
334.5	006.8	20					10	08	07	06	06	07	09	09	09	08	08	11	14	14	11	08	07	07	05	04	03	03	04	05	07	09	09	07	04	02	01	01	00
335.0	007.3	40					09	07	06	05	05	05	05	05	04	02	02	02	03	04	05	05	05	05	03	03	02	02	02	02	03	05	06	07	06	04	03	01	01
335.5	007.8	40					08	05	03	03	04	04	06	06	06	05	03	03	05	07	09	11	11	09	08	05	05	04	04	04	05	05	07	08	07	05	03	01	00
336.0	008.3	40					06	04	03	05	05	05	05	05	04	04	04	05	09	12	14	13	10	06	04	03	02	02	03	04	06	07	07	06	04	03	01	00	
336.5	008.8	40					09	06	06	06	07	08	08	07	06	06	07	09	12	14	13	10	07	04	03	03	03	04	05	06	09	10	09	06	04	02	01	00	
337.0	009.3	40				12	10	08	07	06	06	05	05	04	04	05	07	09	10	08	06	04	02	02	02	03	05	07	09	10	09	07	04	01	00				
337.5	009.8	40					16	13	09	07	06	06	08	07	06	07	08	09	09	07	05	03	03	04	05	05	07	08	09	10	10	07	05	02	01	00			
338.0	010.3	40					17	14	11	09	08	07	07	07	07	06	05	05	05	03	03	03	03	03	03	04	04	06	07	07	06	04	02	00				
338.5	010.8	20					16	11	08	06	05	05	05	06	06	06	06	06	05	05	04	03	03	04	05	10	12	10	05	03	01	00						
339.0	011.3	40					13	09	06	03	02	02	02	02	03	03	04	04	05	04	04	03	02	02	03	04	05	05	05	04	03	02	01	00				
339.5	011.8	20						19	12	09	07	06	05	05	05	05	05	09	11	09	06	03	02	02	04	05	06	06	06	04	02	01	00						
340.0	012.3	40						15	10	08	08	09	08	07	08	10	12	14	11	06	04	04	05	05	06	06	07	04	01	00								
340.5	012.8	20					23	13	09	07	06	05	03	02	03	04	04	05	05	05	04	03	03	03	03	04	04	04	03	00								
341.0	013.3	40						11	09	07	05	05	05	05	05	04	04	03	03	04	05	07	08	08	06	05	03	02	01	00								
341.5	013.8	20							08	08	08	07	06	05	05	05	05	05	05	05	04	05	07	07	07	06	04	02	01	00								
l^I	l^{II}	B	+ 30	+ 40	+ 50	+ 60	+ 70	+ 80	+ 90	+100	+110	+120	+130	+140	+150	+160	+170	+180	+190	+200	+210	+220	+230	+240	km/sec

1964BAN....17..381R

TABLE 4 *(continued)*

l^I	l^{II}	B	+ 30	+ 40	+ 50	+ 60	+ 70	+ 80	+ 90	+100	+110	+120	+130	+140	+150	+160	+170	+180	+190	+200	+210	+220	+230	+240	km/sec
342.0	014.3	40						11	10	10	10	09	07	06	06	07	08	08	08	08	07	06	04	03	02	01	00									
342.5	014.8	20						09	10	11	10	07	04	03	03	05	08	10	10	10	09	08	06	03	01	00										
343.0	015.3	40						08	09	10	10	06	02	02	04	06	09	10	10	10	10	10	07	04	02	01	00									
343.5	015.8	20						06	07	10	09	07	06	06	08	12	14	14	13	13	12	09	05	02	00											
344.0	016.3	40						07	07	08	09	09	09	10	11	12	15	15	15	14	12	08	05	02	01	00										
344.5	016.8	20						11	10	12	12	12	14	18	19	17	17	20	18	12	07	04	02	01	00											
345.0	017.3	40						16	16	16	15	13	15	19	19	18	18	21	19	14	09	03	01	00												
345.5	017.8	20						12	17	19	14	11	09	14	17	18	20	20	16	10	03	01	00													
346.0	018.3	40							23	25	22	16	16	20	24	24	22	18	12	05	02	01	00													
346.5	018.8	20							30	27	21	18	20	28	35	32	26	16	07	03	00															
347.0	019.3	40								34	31	27	25	25	29	34	30	21	12	05	02	01	00													
347.5	019.8	20							46	41	29	21	20	24	28	31	29	18	10	04	02	00														
348.0	020.3	40								41	32	22	19	23	30	32	26	18	10	04	01	00														
348.5	020.8	40									30	24	21	24	30	29	21	12	06	02	00															
349.0	021.3	20									42	37	35	35	33	28	17	07	02	01	00															
349.5	021.8	40										55	55	53	44	30	16	06	02	01	00															
350.0	022.3	40												58	39	19	07	02	01	00															
b^I = - 1°5			b^{II} = - 0°1																																	
321.5	353.8	20	45	29	19	12	07	05	03	02	01	01	01	00																						
322.0	354.3	20	49	31	20	12	07	05	04	04	03	03	02	02	02	01	00																			
322.5	354.8	40			11	08	06	04	04	04	05	05	06	06	06	05	04	03	02	01	00														
323.0	355.3	40			13	09	06	04	02	01	01	02	03	05	06	07	06	05	03	02	01	00													
323.5	355.8	40			10	07	05	04	03	03	03	03	04	05	04	03	02	01	01	00															
324.0	356.3	20		36	23	12	07	02	00	00	00	00	01	01	01	00																			
324.5	356.8	20		34	19	10	05	04	02	02	01	02	03	03	02	02	01	01	01	01	00														
325.0	357.3	20		34	16	09	06	04	03	02	01	02	02	03	03	04	04	03	02	02	02	01	01	00											
325.5	357.8	20		39	19	12	08	06	05	02	02	02	02	02	03	04	04	04	05	05	04	02	00												
326.0	358.3	40			20	12	09	06	04	03	03	04	04	04	03	03	03	03	02	02	02	02	01	01	01	00										
326.5	358.8	40		50	29	15	11	10	09	09	09	10	10	09	08	07	06	06	07	07	07	07	07	07	06	05	04	03	02	02	01	01	00			
327.0	359.3	40			21	18	16	15	14	13	11	09	07	07	07	07	07	08	09	09	09	10	09	09	08	07	06	05	04	03	02	01	01	01	01	01	00	
327.5	359.8	40	34	27	20	14	11	09	09	09	10	11	11	11	10	10	10	11	11	12	12	12	13	13	13	12	10	09	08	07	06	06	07	08	08	07	06	06	07	07	06	05	04	03	02
327.7	000.0	40	25	19	13	08	04	03	04	07	09	10	10	10	10	10	10	11	11	12	13	13	13	13	12	12	11	10	09	09	08	08	07	05	04	03	01	01	00						
328.0	000.3	40			21	16	13	12	12	13	13	13	12	12	12	12	13	14	14	14	14	14	13	12	11	10	09	09	09	09	09	09	08	06	05	04	03	02	02	01	01	00				
328.5	000.8	40		34	26	20	16	14	12	12	12	13	14	14	13	13	12	12	11	11	12	12	12	12	13	12	12	11	10	09	08	07	06	06	06	06	06	05	04	03	02	01	01	00		
329.0	001.3	40			23	17	14	11	09	09	11	14	14	14	13	11	09	09	09	08	08	08	09	10	12	13	13	12	11	09	08	08	08	08	07	07	06	06	05	04	04	03	02	02	01	00	
329.5	001.8	40				14	11	09	08	08	10	11	10	09	07	06	06	07	07	08	10	12	13	14	14	14	13	12	10	09	08	07	06	06	07	08	08	07	06	06	07	07	06	05	04	03	02
330.0	002.3	40			20	15	12	10	08	07	06	06	07	07	06	05	04	04	04	05	07	08	10	12	13	14	14	13	12	10	09	08	06	05	05	05	05	05	06	06	07	07	08	08	07	06	05	04
330.5	002.8	40			21	15	12	10	09	07	07	07	09	09	08	07	06	06	05	06	06	06	07	08	08	09	10	11	11	10	09	07	05	04	04	04	04	04	05	06	06	05	05	05	04	04	04	
331.0	003.3	40			18	15	13	11	10	09	09	09	10	11	11	10	09	07	06	04	04	04	04	05	06	08	09	10	11	10	09	08	06	04	03	02	02	03	04	06	06	06	05	05	04	04	03	03
331.5	003.8	40			13	09	06	07	08	08	09	08	07	06	05	05	04	04	03	03	03	03	03	03	03	05	08	10	10	10	09	08	07	06	05	04	04	04	04	05	05	05	05	04	03	02	01	00
332.0	004.3	40				12	09	08	07	07	06	06	05	04	03	02	02	02	02	02	02	02	02	02	02	03	04	05	06	07	07	07	06	05	04	03	02	02	02	02	02	02	01	01	01	01
332.5	004.8	40			25	18	12	08	06	06	07	07	07	05	04	03	03	03	02	02	02	02	02	02	03	04	04	05	05	06	08	09	08	07	06	05	04	03	03	03	03	02	02	01	01	00	
333.0	005.3	40			22	16	12	09	09	09	10	12	13	10	06	04	04	04	05	05	05	05	04	04	04	04	05	05	06	07	08	09	10	09	08	06	05	03	02	02	01	01	01	01	00		
333.5	005.8	40							08	09	11	13	11	08	05	04	04	06	07	07	07	08	08	09	09	09	08	09	10	10	11	13	13	12	08	05	03	02	01	01	00					
334.0	006.3	40				09	06	05	05	07	10	13	13	10	07	05	06	07	07	07	08	09	12	13	11	10	11	12	12	12	13	13	12	10	07	05	03	02	01	00					
334.5	006.8	40				10	06	05	06	08	11	13	12	08	05	06	07	08	08	09	10	11	12	12	12	12	12	11	10	08	08	07	05	03	02	01	00								
335.0	007.3	40				15	10	08	08	09	10	12	11	07	05	05	06	07	08	09	10	11	12	14	15	15	13	10	07	05	04	04	04	03	02	01	00								
335.5	007.8	40				18	14	11	10	09	10	10	09	08	06	05	06	10	14	16	15	15	15	16	15	13	10	07	06	05	05	04	03	02	01	00									
336.0	008.3	40				19	14	11	11	11	11	10	07	05	05	07	12	17	17	15	12	09	07	06	06	06	05	05	05	05	05	04	02	01	01	00									
336.5	008.8	40				24	18	17	16	15	14	12	11	09	06	06	08	14	16	15	12	07	03	02	05	06	07	06	06	05	04	03	01	00											
337.0	009.3	40				28	25	23	20	18	15	13	11	09	07	06	05	08	10	11	09	05	03	03	05	07	08	07	05	03	02	02	01	00											
337.5	009.8	40					28	25	22	19	17	15	14	12	09	08	07	08	09	10	08	06	05	05	07	08	08	07	05	04	03	02	01	00											
338.0	010.3	40					36	35	29	21	14	14	16	15	11	08	07	09	10	09	07	05	05	07	10	11	09	06	04	03	02	01	00												
338.5	010.8	40							22	16	12	12	14	13	10	07	07	08	10	10	09	07	06	07	08	09	07	05	04	02	01	00													
339.0	011.3	40						20	15	10	08	10	14	14	10	08	08	13	15	13	10	09	08	09	09	08	05	04	02	00														
339.5	011.8	20						32	23	15	09	10	13	15	14	10	13	21	26	17	10	07	06	08	10	09	07	05	03	01	00													
340.0	012.3	40						27	20	16	15	15	14	13	14	17	21	21	16	10	08	07	09	10	08	06	04	02	00														
340.5	012.8	40						21	18	15	13	13	13	13	14	15	14	13	11	08	06	07	10	11	10	06	03	01	00														
l^I	l^{II}	B	+ 30	+ 40	+ 50	+ 60	+ 70	+ 80	+ 90	+100	+110	+120	+130	+140	+150	+160	+170	+180	+190	+200	+210	+220	+230	+240	km/sec

TABLE 4 *(continued)*

l^I	l^{II}	B	+30	+40	+50	+60	+70	+80	+90	+100	+110	+120	+130	+140	+150	+160	+170	+180	+190	+200	+210	+220	+230	+240	km/sec
$b^I = -2.0°$		$b^{II} = -0.6$																							
322.0	354.3	20	30	22	15	07	01	00																	
323.0	355.3	20	38	25	13	06	02	01	00																
324.0	356.3	20	33	18	10	04	01	01	00																
325.0	357.3	20	43	24	12	05	02	01	00																
326.0	358.3	20		32	15	08	03	01	00																
327.0	359.3	20	55	36	19	08	06	05	04	03	02	01	00												
327.5	359.8	40		24	16	10	08	07	06	05	04	03	02	02	01	01	01	00							
328.0	000.3	40		31	19	10	07	06	05	05	04	03	02	02	01	00									
329.0	001.3	20		31	17	10	06	05	05	06	05	04	03	02	02	01	01	00	05	04	04	03	03	04	04
330.0	002.3	20		24	13	08	06	04	02	02	02	02	02	02	02	01	01	00	05	04	04	03	03	04	04
331.0	003.3	20			12	09	08	07	05	05	06	05	04	03	02	02	02	02	02	02	02	02	02	02	04
332.0	004.3	20			15	10	06	04	02	02	01	00	00	00	00	00	01	01	02	02	02	02	02	02	04
333.0	005.3	20			16	10	07	04	03	02	02	02	01	01	01	01	02	02	02	02	02	02	02	02	04
333.5	005.8	40				11	08	05	04	03	03	02	02	02	02	02	02	02	02	02	02	02	02	02	04
334.0	006.3	40																							
334.5	006.8	40				07	04	03	02	02	02	02	02	02	02	02	02	02	02	02	02	02	02	02	04
335.0	007.3	40				08	05	04	04	03	03	03	03	03	03	03	03	03	03	03	03	03	03	03	04
335.5	007.8	40				18	12	08	06	04	04	04	04	04	04	04	04	04	04	04	04	04	04	04	04
336.0	008.3	40					13	10	07	05	04	04	05	05	05	05	05	05	05	05	05	05	05	05	05
336.5	008.8	40					16	13	10	09	06	05	04	05	05	06	06	06	06	06	06	06	06	06	06
337.0	009.3	40				13	10	10	08	07	06	05	04	04	04	04	04	04	04	04	04	04	04	04	04
337.5	009.8	40					11	11	10	09	07	06	05	05	05	05	05	05	05	05	05	05	05	05	05
338.0	010.3	40					17	17	16	13	09	07	06	06	06	06	06	06	06	06	06	06	06	06	06
339.0	011.3	40																							
340.0	012.3	40					13	14	11	09	07	06	05	05	05	05	05	05	05	05	05	05	05	05	05
341.0	013.3	20																							
342.0	014.3	40					11	09	08	07	07	06	06	06	06	06	07	07	07	06	06	05	05	05	05
343.0	015.3	20						12	16	12	10	09	07	07	07	07	07	06	06	05	05	05	05	05	05
344.0	016.3	40							14	12	10	10	08	08	08	08	08	08	08	07	07	07	07	07	07
345.0	016.8	40							18	14	12	11	09	09	09	09	09	09	09	08	08	08	08	08	08
345.5	017.3	40								16	13	12	11	10	10	10	10	10	10	09	09	09	09	09	09
346.0	017.8	40								20	15	14	12	12	12	12	12	12	12	11	11	11	11	11	11
346.5	018.3	40									18	16	14	13	13	13	13	13	13	13	13	13	13	13	13
347.0	018.8	40									22	19	17	16	15	15	15	15	15	15	15	15	15	15	15
347.5	019.3	40										24	21	20	19	18	18	18	18	18	18	18	18	18	18
348.0	019.8	40											26	24	23	22	22	22	22	22	22	22	22	22	22
348.5	020.3	40												29	28	27	27	27	27	27	27	27	27	27	27
349.0	020.8	40													33	32	32	32	32	32	32	32	32	32	32
349.5	021.3	40														37	37	37	37	37	37	37	37	37	37
350.0	021.8	40															42	42	42	42	42	42	42	42	42
	022.3	40																48	48	48	48	48	48	48	48
l^I	l^{II}	B	+30	+40	+50	+60	+70	+80	+90	+100	+110	+120	+130	+140	+150	+160	+170	+180	+190	+200	+210	+220	+230	+240	km/sec

TABLE 4 *(continued)*

l^I	b^I	l^{II}	b^{II}	-270	-280	-290	-300	km/sec
323.5	-1.0	355.8	+0.4	00				
324.0	-1.0	356.3	+0.4	01	01	01	01	
323.5	-1.5	355.8	-0.1	01	00			
324.0	-1.5	356.3	-0.1	03	02	02	02	
324.5	-1.5	356.8	-0.1	01	01	01	00	
324.5	-2.0	356.8	-0.6	01	01	01	01	

l^I	b^I	l^{II}	b^{II}	+270	+280	+290	+300	km/sec
328.5	-1.0	000.8	+0.4	01	01	00		
329.0	-1.0	001.3	+0.4	01	00			
329.5	-1.5	001.8	-0.1	03	02	01	01	
330.0	-1.5	002.3	-0.1	03	02	01	01	
330.5	-1.5	002.8	-0.1	02	01	01	00	
331.0	-1.5	003.3	-0.1	01	00			
330.0	-2.0	002.3	-0.6	03	03	02	01	
331.0	-2.0	003.3	-0.6	03	01	00		

smooth isophote could be drawn, the original measurements were reinspected. In a few cases the zero level had to be shifted 1 unit, in several other cases the intensities of part of the profile had to be changed. No change of more than 2 units was permitted.

3.2. *Tables and contour diagrams*

The intensities given in tables 4 and 5 include these changes. For each position the bandwidth used has been indicated under B in the third column. The circumstance that different bandwidths had been used for different parts of the programme did not cause difficulties. The features which needed a narrower band were measured with a narrow band (20 kc/s; e.g. the 3-kpc arm). Only at positive velocities from $l^{II} = 12°$ to 22° too broad a band was used for the feature visible at about + 130 km/sec.

The isophote charts are in figures 7, 8, 9, 10 and 11. As a bright region is visible at $l^{II} = -3°$ and $V = +100$ km/sec in the diagram for $b^I = -0°.5$ ($b^{II} = +0°.9$), it was decided to take more profiles at higher latitudes; these profiles were measured in March 1963; the intensities are given in table 5. An isophote chart of this region at $b^I = 0°.1$ ($b^{II} = +1°.5$) is given in figure 7. In this case the grid used was in new galactic co-ordinates. So the old galactic co-ordinates have not been computed and are not given in this table.

3.3. *The combined D.T.M. – Dwingeloo diagram at* $b^I = -1°.5$ ($b^{II} = -0°.1$)

In figure 1 a rough *l–V* diagram has been given in which the measurements made at the Department of Terrestrial Magnetism of the Carnegie Institution of Washington (D.T.M.) were included.

The same chart is given again in figure 12, now with more isophotes drawn in. The chart was constructed as explained in the following. The D.T.M. chart which was kindly put at our disposal by Dr B. F. Burke, gives only the negative-velocity side of the diagram, with the exception of the disk (BURKE and TUVE, 1962).

The profiles of the 3-kpc arm were compared with ours in the common region $l^I = 320°$ to 325°. The agreement was not as good as one would expect. The mean integrated Dwingeloo profile was 26 ± 6 per cent higher than the mean D.T.M. profile (integrated between the limits 2 and 3, see section 4.2). But the most troublesome were the shifts in velocity and zero level. If we assume that on the average the central structure is symmetrical with respect to $l^{II} = 0°$ and $V = 0$ km/sec, and if we use only the part between $l^{II} = 5°$ and 22°, to avoid the disk (cf. section 4.7), we can make another, be it indirect, comparison between the Dwingeloo and D.T.M. scales. Integration of the Dwingeloo intensities at positive velocities between $l^{II} = 5°$ and 22° and of the D.T.M. measures at negative velocities between $l^{II} = -5°$ and $-22°$ (using the integration limits indicated in section 4.2) showed that the integrated D.T.M.

TABLE 5

l^{II}	b^{II}	+30	+40	+50	+60	+70	+80	+90	+100	+110	+120	+130	+140	+150	+160	+170	+180	km/sec
356.01	1.99	15	12	10	08	06	05	04	03	02	01	01	01	01	00			
357.01	1.99	14	12	11	10	08	07	06	05	04	04	04	04	03	03	02	01	01	00	
358.00	1.99	15	11	09	08	07	05	04	03	03	03	03	02	03	03	03	03	03	03	03	03	03	03	03	02	02	01	01	01	00	
355.76	1.50	20	15	10	10	11	10	09	06	04	03	03	02	02	02	02	02	01	00												
356.26	1.50	20	15	13	12	11	11	11	10	09	07	05	04	03	02	01	01	01	01	01	00										
356.76	1.48	16	14	12	11	10	09	09	09	09	10	10	10	09	08	07	06	04	03	02	01	01	00								
357.50	1.50	14	11	09	09	08	07	07	06	06	06	06	06	06	06	06	05	05	04	03	02	02	01	00							
358.01	1.49	16	12	09	08	07	06	06	06	06	06	07	07	07	06	06	06	05	05	05	05	04	04	04	03	03	03	03	02	02	02	01	01	01	00
358.50	1.50	00	17	10	08	04	04	04	04	05	05	05	06	06	06	07	07	07	07	07	06	05	05	04	03	02	02	02	02	03	02	02	01	01	00
359.01	1.49	00	17	12	09	07	05	04	04	04	04	03	03	03	03	03	03	03	03	02	02	02	02	01	01	01	00								
355.25	1.23	24	19	15	12	11	09	08	06	05	04	04	03	03	02	02	01	01	01	00											
354.02	0.99	25	21	17	15	13	11	09	06	04	03	02	01	01	01	01	00														
354.51	1.01	00	17	13	12	12	11	09	07	06	05	04	03	02	02	01	01	01	01	01	01	01	02	01	01	01	01	01	00	00	01	01	00		
354.52	0.49	00	00	20	12	10	09	08	08	07	04	02	00	01	03	03	03	02	00												

results were very close to those for Dwingeloo. They were only 10 per cent higher. This may be taken as an indication that there is indeed a good approach to large-scale symmetry. It may also indicate that the systematic differences between the two series of observations are not very large.

We decided to construct the chart of figure 12 without changing the D.T.M. intensities. From the foregoing it is clear that one should be careful in using this chart. The part from $l^{II} = -25°$ to $-8°$ has been taken from the D.T.M. chart. The intensities might be 10 to 30 per cent too low compared to the rest, which was derived from the Dwingeloo measurements. The connection of the two parts at $l^{II} = -8°$ did not give difficulties, because the differences were small on this scale.

4. Analysis

4.1. *Description of the principal features*

From the contour maps (figures 7 to 11) and the combined map (figure 12) one can immediately see that the distribution has an "arm-like" structure. The most outstanding arm is the 3-kpc arm, which crosses the line $l^{II} = 0°$ at -53 km/sec. We shall discuss this arm in detail in chapters 5 to 8. The other arms will be indicated by names, which have been chosen rather arbitrarily. We can distinguish (figure 13):

1) *The expanding arm at* $+135$ *km/sec.* This arm can be best followed on the maps for $b^{I} = 0°.1$ to $-1°.0$

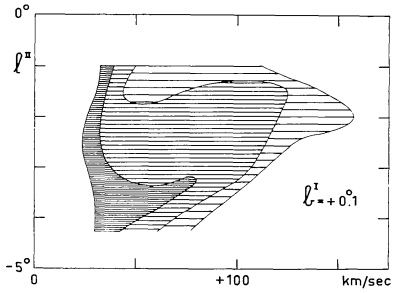

Figure 7

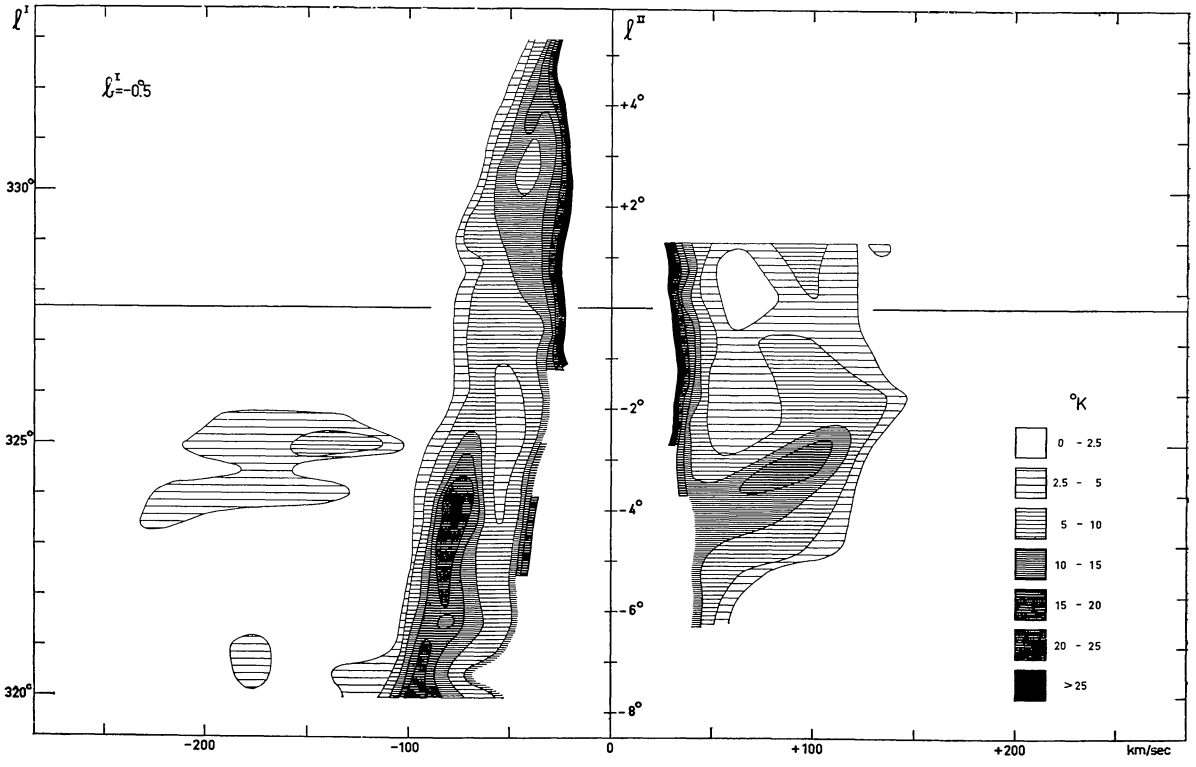

Figure 8

Figures 7–11. Contours of equal brightness temperature derived from the "survey" measurements. The main maximum has not been observed. The white lines in the black areas are the isophotes for 30 and 40 units (≈ °K). In some of the white parts contours of zero intensity have been drawn.

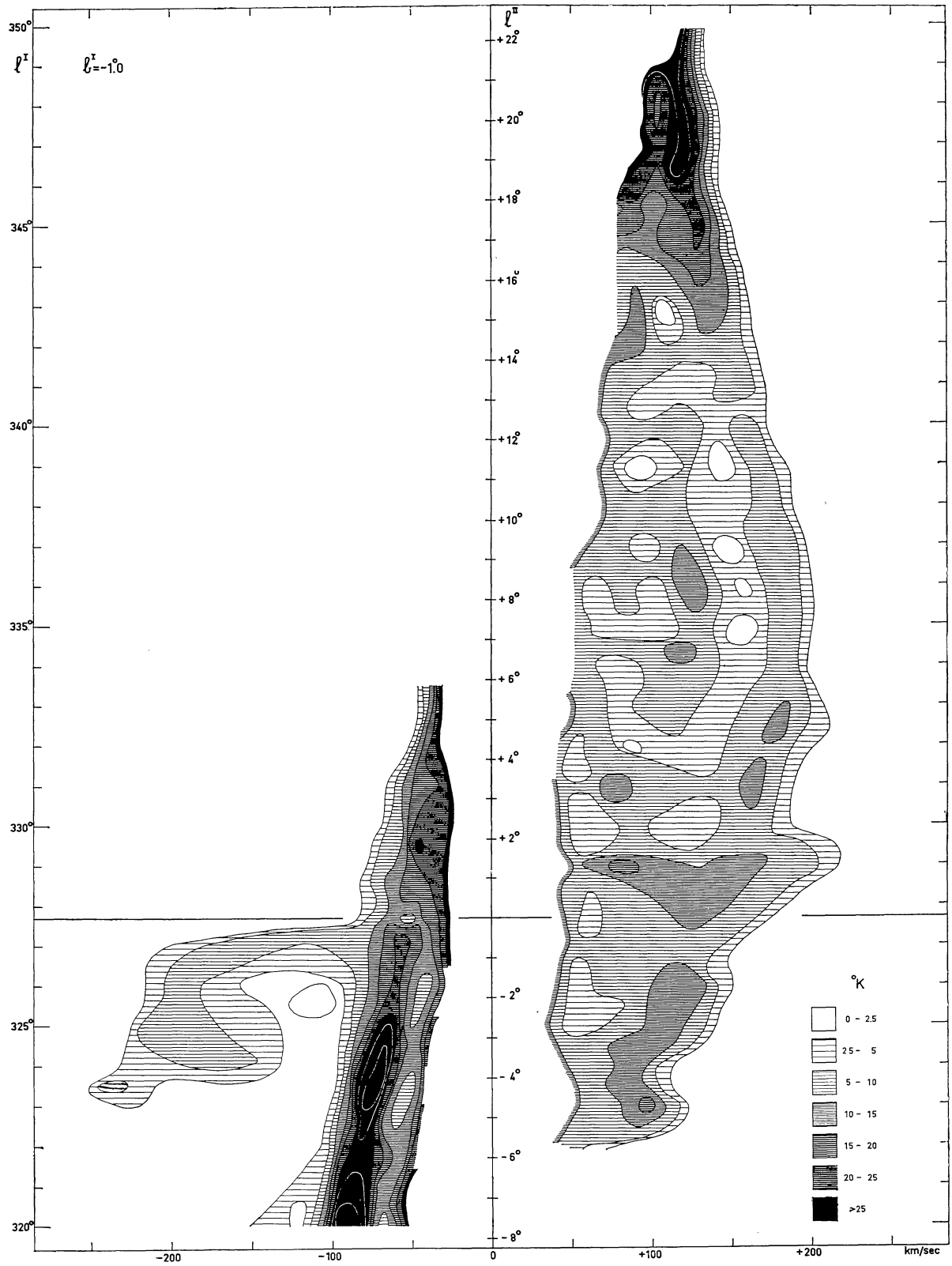

Figure 9

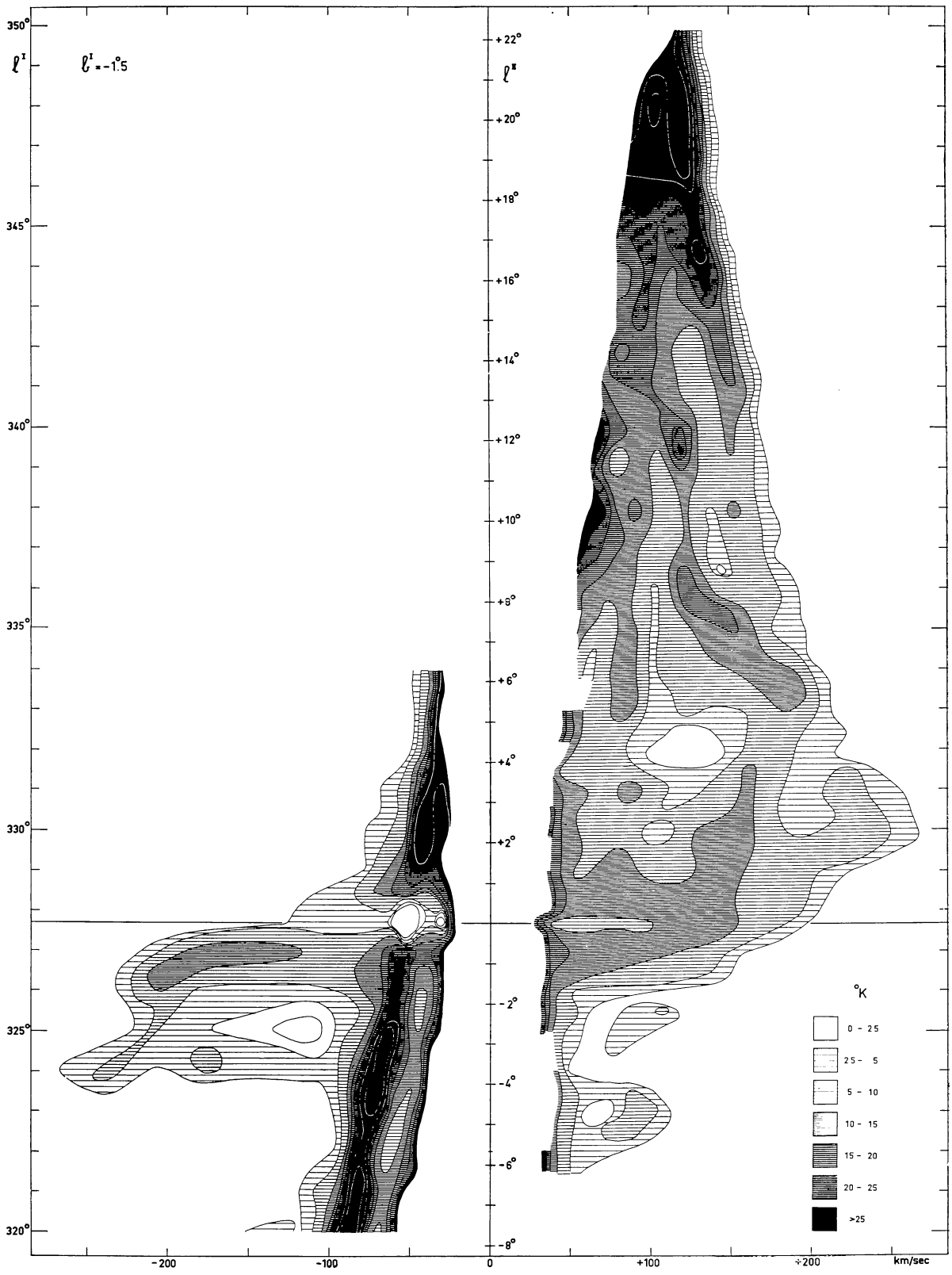

Figure 10

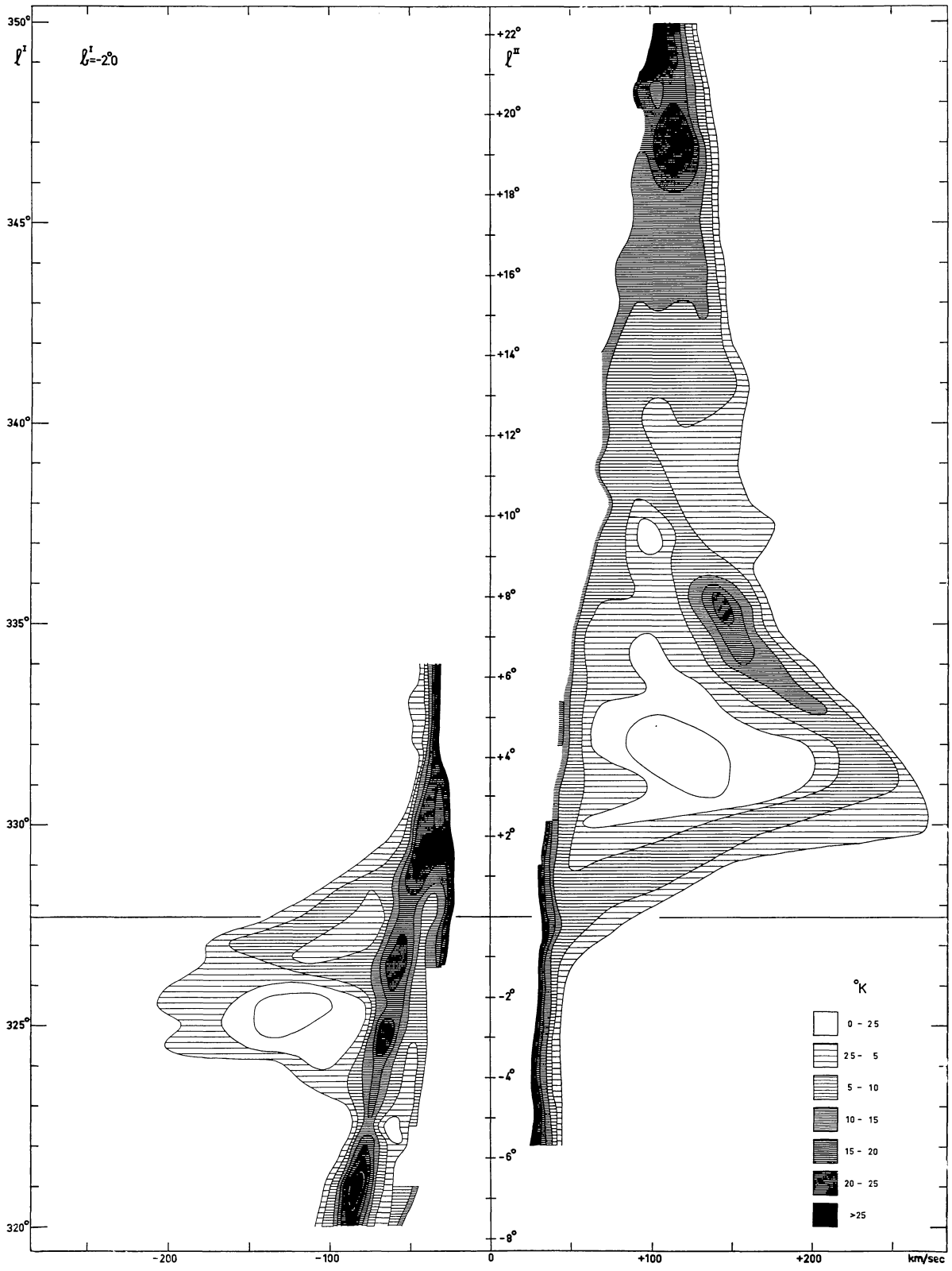

Figure 11

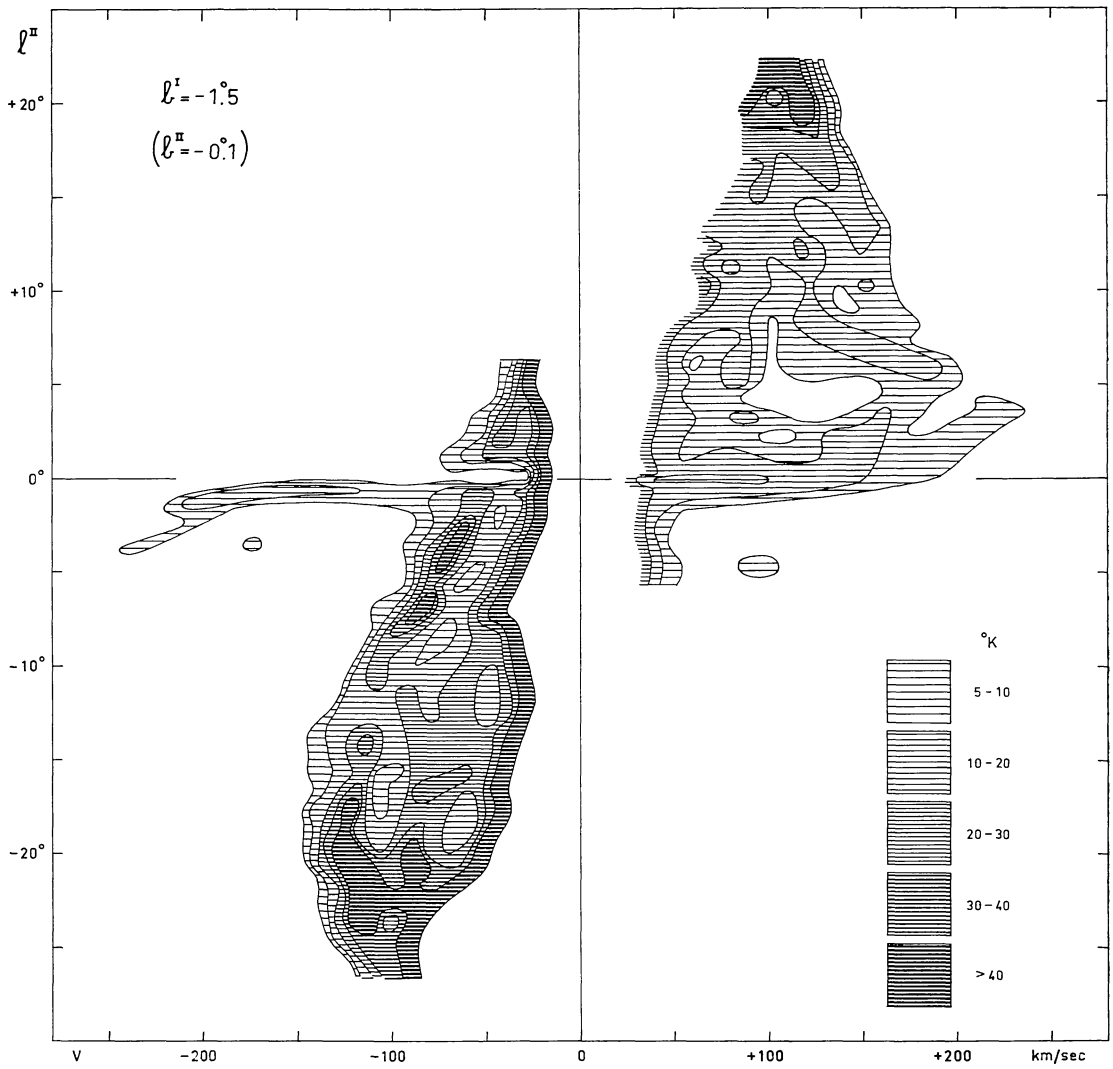

Figure 12. Combined chart for the longitude interval $-27°$ to $+22°$. The part between $-8°$ and $+22°$ is based on the observations in Dwingeloo, that for the lower longitudes on observations at D.T.M. (BURKE and TUVE, 1962).

(figures 7, 8 and 9). It becomes visible at $l^{II} = -5°$ at $+100$ km/sec (see also section 4.4). It crosses $l^{II} = 0°$ at $+135$ km/sec. As no trace of any absorption has been found at this longitude and in this velocity range, the arm is at a larger distance than the nucleus. Thus it is expanding, just like the 3-kpc arm. However, the expansion velocity is much higher. At positive longitudes the arm can be clearly followed up to $l^{II} = +22°$, where it disappears in the general galactic radiation. At this point it has a velocity nearly equal to the velocity of the 3-kpc arm at the corresponding negative longitude.

The other features at a lower positive velocity which are present in figure 9 can be better traced in the map for latitude $b^{I} = -1°.5$ ($b^{II} = -0°.1$) (figure 10).

2) *A very narrow arm* runs from $l^{II} = +9°$ (perhaps $l^{II} = +12°$) at $V \approx +80$ km/sec down to $l^{II} = +1°$, remaining at the same velocity. Here it might become the emission at $l^{II} = 0°$ at $+100$ km/sec, which is clearly visible in the map for $b^{I} = -0°.5$ ($b^{II} = +0°.9$) (figure 8). In this case the arm decreases strongly in velocity at $l^{II} = -3°$.

3) *The connecting arm.* In figure 10 an arm appears at $l^{II} = +18°$, at $V = +90$ km/sec. It keeps the same

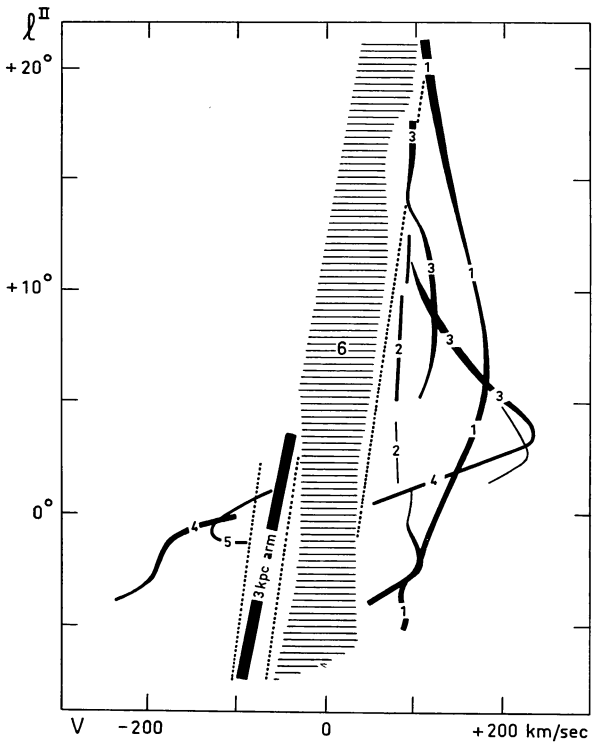

Figure 13. *l–V* chart with numbered features as described in section 4.1. The width of the lines gives the approximate intensity. The dotted lines are the integration limits described in section 4.2.

velocity down to $l^{II} = +13°$, where the velocity increases rather abruptly to about +120 km/sec. At $l^{II} = +8°$ the velocity increases again very rapidly. However, at this longitude the feature can be seen much stronger in figure 11 ($b^I = -2°.0$). In this map the arm becomes visible at $l^{II} = +11°$, at $V = +90$ km/sec; it reaches its maximum velocity of +230 km/sec at $l^{II} = +3°$.

4) *The nuclear disk.* Beyond this point a sharp decrease of velocity occurs in the feature just described, and at $l^{II} = 0°$ it is likely that the velocity is zero. At this point pure rotation seems to be present, and it was assumed earlier (ROUGOOR and OORT, 1960) that the H I emission found here comes from a small fast rotating disk around the nucleus. This disk will be discussed in detail in chapters 9 and 10. The part of this disk at negative velocities is a very outstanding feature, which is visible on all contour maps.

5) *The contracting or expanding arm at* -110 *km/sec.* On the map for $b^I = -2°.0$ (figure 11) a small arm crossing the longitude of the centre at a velocity of −110 km/sec is observed. One cannot decide whether this arm is in front of the nucleus or beyond.

6) *The main maximum.* In all contour maps the edges of the main maximum can be seen. It is assumed that most of this emission does not come from the central region, but from regions farther from the centre where the gas follows practically circular orbits. However, it is likely that part of the gas in the central region will likewise have a small velocity in the line of sight and will therefore not be recognized by its velocity as belonging to the central region. In section 4.5 an estimate of this part will be given.

4.2. *Integration limits*

The integration over the profile of 21-cm line emission gives N_H, the total number of H I atoms in the line of sight per unit area, provided the optical depth is small and the antenna beam is filled completely. If we want to get an estimate of the total mass of hydrogen in the central part the main maximum must obviously be omitted, at least provisionally, in these integrations. The limits of the part to be excluded were fixed as follows. It was considered that the pronounced trough between the main maximum and the 3-kpc arm, which is so clearly visible in figures 8, 9, 10 and 11, gives a natural separation between the most pronounced features in the central region at negative longitude and the "normally" moving gas, and that this would be a reasonable first-approximation for a dividing line between the central region and the more normal outer parts of our Galaxy. The centre of the trough can be represented by a straight line in the *l–V* diagram, which cuts the line $l^{II} = 0°$ at −40 km/sec and increases by +3.5 km/sec per degree longitude. In the following this will be denoted as limit 2. It was then assumed, somewhat arbitrarily, that the limit at the right-hand side of the main maximum would be a line parallel to the first and cutting the line $l^{II} = 0°$ at +40 km/sec (to be called limit 1). By this procedure the "main maximum" is reasonably separated from the low-intensity features. A third limit (limit 3) has been drawn which cuts the line $l^{II} = 0°$ at −80 km/sec and has the same slope as the other limits. This separates the disk from the 3-kpc arm. Figure 13 shows these three limits as dotted lines.

4.3. *Numbers of H I atoms per cm² (N_H)*

Using the demarcation limits defined in the preceding section we have determined the numbers of neutral hydrogen atoms in each of the three features from the usual formula (VAN DE HULST, MULLER and OORT, 1954), assuming that the optical depth is small,

$$N_H = 1.835 \times 10^{13} \int T dV.$$

T is the brightness temperature in °K, V is in cm/sec. The resulting values of N_H are given in table 6. As the data were not complete for all longitudes some numbers had to be interpolated between the results found for adjacent longitudes. Such interpolated numbers have been underlined.

Table 7 shows the average ($\bar{N}_H$) for $b^I = -1°.0$, $-1°.5$ and $-2°.0$. A comparison between the negative and positive velocities is shown in the upper part of

TABLE 6

N_H (10^{21} atoms/cm²)

		negative velocities												positive velocities			
	b^I	-0°.5			-1°.0			-1°.5			-2°.0			-0°.5	-1°.0	-1°.5	-2°.0
	b^{II}	+0°.9			+0°.4			-0°.1			-0°.6			+0°.9	+0°.4	-0°.1	-0°.6
l^I	l^{II}	d	3	total	d	3	total	d	3	total	d	3	total	total	total	total	total
320.0	352.3	0.33	1.17	1.50	0.33	2.36	2.69	0.33	1.92	2.25	0.10	0.95	1.05				
320.5	352.8	0.40	0.97	1.38	0.18	2.05	2.24	0.09	1.74	1.83	0.10	1.10	1.21				
321.0	353.3	0.34	1.01	1.35	0.28	1.82	2.10	0.18	1.80	1.98	0.11	1.26	1.37				
321.5	353.8	0.01	0.93	0.94	0.14	1.64	1.78	0.09	1.40	1.49	0.03	0.90	0.93				
322.0	354.3	0.05	1.03	1.07	0.11	1.53	1.64	0.06	1.16	1.23	0.00	0.67	0.67			1.33	0.69
322.5	354.8	0.02	0.97	0.99	0.10	1.38	1.49	0.01	1.14	1.15	0.00	0.28	0.28				
323.0	355.3	0.03	1.01	1.04	0.15	1.66	1.81	0.03	1.64	1.67	0.00	0.56	0.56				0.76
323.5	355.8	0.39	1.07	1.47	0.60	2.00	2.60	0.35	2.01	2.36	0.21	0.69	0.90				
324.0	356.3	0.77	1.10	1.87	1.05	1.85	2.91	1.37	1.82	3.19	0.30	0.67	0.97			0.76	0.31
324.5	356.8	0.39	0.72	1.12	0.92	1.66	2.58	1.10	1.87	2.97	0.70	0.85	1.55			0.86	
325.0	357.3	0.91	0.53	1.44	1.09	1.37	2.46	0.61	1.55	2.15	0.36	0.83	1.19	1.64		0.65	0.19
325.5	357.8	0.45	0.38	0.83	0.80	1.12	1.92	0.97	1.06	2.03	0.48	0.69	1.16	1.20	1.64	0.83	0.83
326.0	358.3	0.01	0.31	0.32	0.69	1.03	1.71	1.33	1.28	2.61	0.72	0.94	1.66	1.57	2.08	0.86	0.26
326.5	358.8	0.03	0.39	0.41	1.18	1.12	2.30	2.43	1.27	3.70	0.96	1.13	2.09	1.00	1.54	1.71	0.27
327.0	359.3	0.01	0.49	0.50	1.28	1.17	2.45	2.48	1.23	3.70	0.94	0.92	1.86	1.01	1.78	2.15	0.27
327.3	359.6							1.60	0.54	2.15							
327.5	359.8	0.01	0.38	0.39	0.27	0.92	1.18	0.98	0.05	1.03				0.71	1.86	2.83	0.88
327.7	000.0	0.03	0.47	0.50	0.06	0.82	0.88	0.38	-0.46	-0.11	0.55	0.73	1.28			2.67	
328.0	000.3	0.03	0.54	0.57	0.06	0.86	0.92	0.32	-0.03	0.29	0.50	0.74	1.24	0.58	2.22	3.37	0.67
328.5	000.8	0.00	0.49	0.49	0.06	1.04	1.10	0.30	1.02	1.32	0.24	0.99	1.23	0.54	2.62	3.26	0.95
329.0	001.3	0.03	0.58	0.61	0.02	0.97	0.99	0.03	1.17	1.20	0.11	0.94	1.05	0.89	3.60	3.11	1.23
329.5	001.8	0.03	0.78	0.81	0.04	1.17	1.21	0.06	1.36	1.41	0.05	0.82	0.88		1.95	3.29	1.53
330.0	002.3	0.00	0.61	0.61	0.01	1.04	1.05	0.06	1.28	1.34	0.00	0.71	0.71		1.28	3.00	1.83
330.5	002.8	0.00	0.50	0.50				0.00	1.13	1.13					1.66	2.66	1.53
331.0	003.3	0.00	0.59	0.59	0.00	1.01	1.01	0.03	1.19	1.22	0.00	0.59	0.59		2.22	2.50	1.23
331.5	003.8	0.00	0.63	0.63	0.00	1.00	1.00	0.00	1.09	1.09	0.00	0.58	0.58		1.65	1.98	0.99
332.0	004.3	0.00	0.83	0.83	0.00	1.22	1.22	0.00	1.24	1.24	0.00	1.02	1.02		1.27	1.29	0.75
332.5	004.8	0.00	0.81	0.81	0.00	1.17	1.17	0.00	1.30	1.30	0.00	0.86	0.86		1.76	1.48	1.07
333.0	005.3				0.00	1.02	1.02				0.00	0.98	0.98		1.78	1.97	1.38

positive velocities				
	b^I	-1°.0	-1°.5	-2°.0
	b^{II}	+0°.4	-0°.1	-0°.6
l^I	l^{II}	total	total	total
333.5	005.8	1.68	2.24	1.51
334.0	006.3	1.37	2.50	1.64
334.5	006.8	1.88	2.22	1.50
335.0	007.3	0.98	2.08	1.54
335.5	007.8	1.47	2.25	1.71
336.0	008.3	1.45	2.00	1.34
336.5	008.8	1.68	1.77	1.02
337.0	009.3	1.30	1.60	0.81
337.5	009.8	1.50	1.81	0.89
338.0	010.3	1.05	1.68	0.72
338.5	010.8	1.14	1.54	0.70
339.0	011.3	0.71	1.70	0.69

positive velocities				
	b^I	-1°.0	-1°.5	-2°.0
	b^{II}	+0°.4	-0°.1	-0°.6
l^I	l^{II}	total	total	total
339.5	011.8	0.98	1.88	0.65
340.0	012.3	1.24	1.93	0.61
340.5	012.8	0.61	1.66	0.74
341.0	013.3	0.81	1.57	0.87
341.5	013.8	0.83	1.82	0.79
342.0	014.3	0.99	1.47	0.71
342.5	014.8	0.89	1.54	0.83
343.0	015.3	0.94	1.78	0.95
343.5	015.8	1.19	1.78	1.00
344.0	016.3	1.27	1.87	1.05
344.5	016.8	1.48	2.10	0.91
345.0	017.3	1.43	1.59	0.77

positive velocities				
	b^I	-1°.0	-1°.5	-2°.0
	b^{II}	+0°.4	-0°.1	-0°.6
l^I	l^{II}	total	total	total
345.5	017.8	1.17	1.60	0.86
346.0	018.3	1.32	1.68	0.95
346.5	018.8	1.35	1.81	1.05
347.0	019.3	1.46	1.90	1.15
347.5	019.8	1.34	1.98	0.88
348.0	020.3	1.11	1.57	0.61
348.5	020.8	0.92	1.39	0.53
349.0	021.3	0.81	1.16	0.53
349.5	021.8	0.50	0.54	0.36
350.0	022.3	0.62	0.48	0.20

d : nuclear disk, integration from $-\infty$ km/sec to limit 3
3 : 3 kpc arm, integration from limit 3 to 2
total : integration from $-\infty$ km/sec to limit 2
} see section 4.2

TABLE 7

$\bar{N}_H$ (10^{21} atoms/cm²)

l^{II}	neg.	pos.	l^{II}	pos.
-7.7	2.00	--	7.8	1.81
-7.2	1.76	--	8.3	1.60
-6.7	1.82	--	8.8	1.49
-6.2	1.40	--	9.3	1.84
-5.7	1.18	--	9.8	1.40
-5.2	0.97	--	10.3	1.15
-4.7	1.35	--	10.8	1.13
-4.2	1.95	--	11.3	1.03
-3.7	2.36	--	11.8	1.17
-3.2	2.37	--	12.3	1.26
-2.7	1.93	--	12.8	1.00
-2.2	1.70	0.90	13.3	1.08
-1.7	1.99	1.07	13.8	1.15
-1.2	2.70	1.17	14.3	1.06
-0.7	2.67	1.40	14.8	1.09
-0.2	--	1.86	15.3	1.22
0.0	0.69	--	13.8	1.32
0.3	0.82	2.09	16.3	1.40
0.8	1.22	2.28	16.8	1.50
1.3	1.08	2.65	17.3	1.26
1.8	1.17	2.26	17.8	1.21
2.3	1.03	2.04	18.3	1.32
2.8	--	1.95	18.8	1.40
3.3	0.94	1.98	19.3	1.50
3.8	0.89	1.54	19.8	1.40
4.3	1.16	1.10	20.3	1.10
4.8	1.11	1.44	20.8	0.95
5.3	--	1.71	21.3	0.83
6.3	--	1.84	21.8	0.47
6.8	--	1.87	22.3	0.43
7.3	--	1.53		

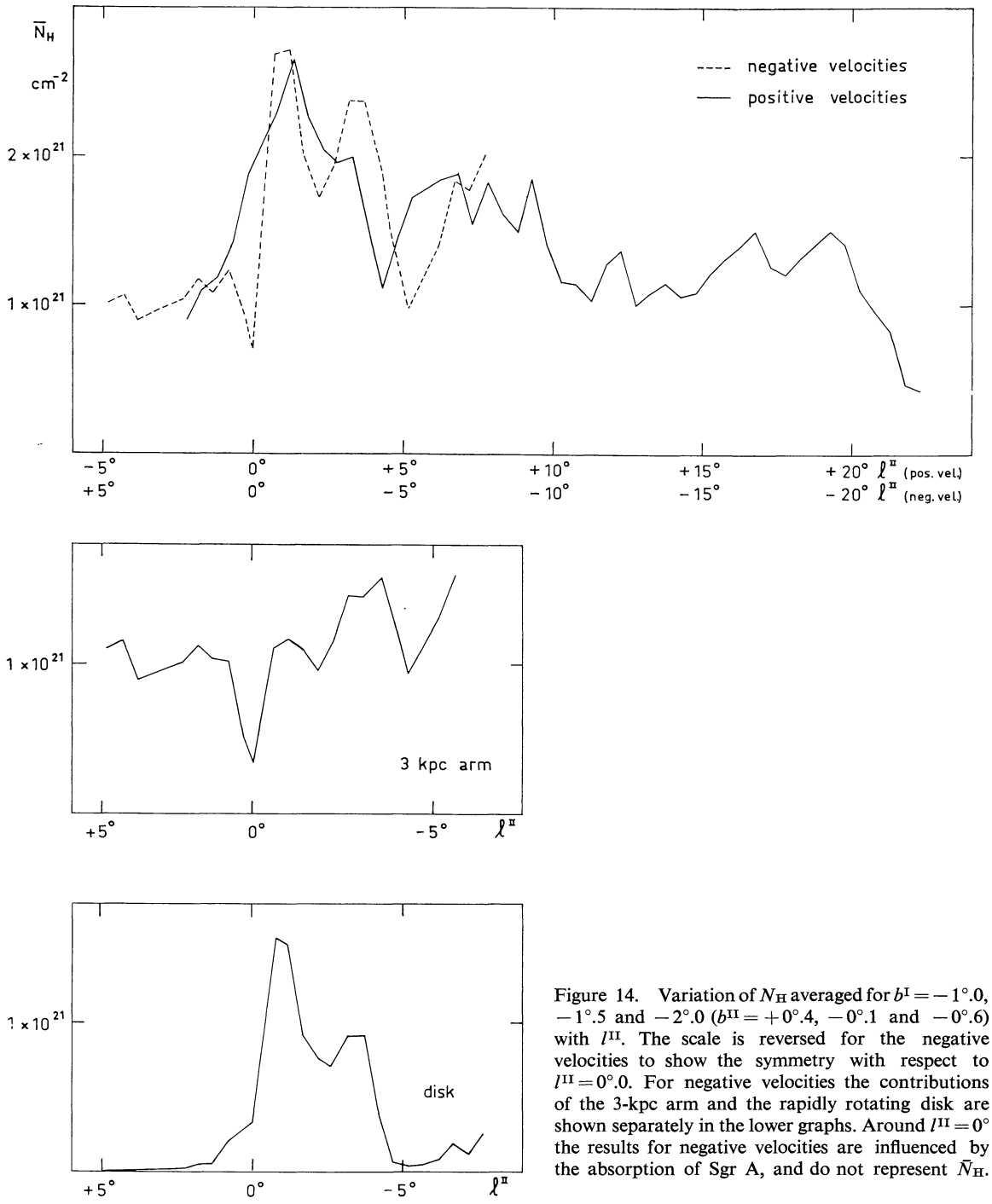

Figure 14. Variation of N_H averaged for $b^I = -1°.0$, $-1°.5$ and $-2°.0$ ($b^{II} = +0°.4$, $-0°.1$ and $-0°.6$) with l^{II}. The scale is reversed for the negative velocities to show the symmetry with respect to $l^{II} = 0°.0$. For negative velocities the contributions of the 3-kpc arm and the rapidly rotating disk are shown separately in the lower graphs. Around $l^{II} = 0°$ the results for negative velocities are influenced by the absorption of Sgr A, and do not represent $\bar{N}_H$.

figure 14; in order to facilitate the comparison the signs of the longitudes have been reversed for the negative velocities.

It will be noted that there is a remarkable symmetry between the values of N_H for positive and negative velocities. For both there is a steep increase towards $l^{II} = 0°$. At negative velocities the curve is sharply depressed by absorption due to the source Sgr A. Both

positive and negative velocities have a maximum at about 1° from the centre, while there appears to be a minimum around longitude 5°. In a rough way we can say that the N_H curve consists of a more or less constant part, from $l^{II} = +5°$ to $+20°$, and a high part between $l^{II} = 0°$ and approximately 3°. In the case of the negative velocities these two parts are clearly distinguished by different features, viz. the 3-kpc arm and the disk (limit 3). This separation is shown in the lower part of figure 14 for the average of the three latitudes.

4.4. *The positive velocity feature at* $l^{II} = -5°$, $b^{II} = +0°.7$

The expanding arm at positive velocities already described in section 4.1 has a very remarkable, sudden start at about $l^{II} = -5°$. No gas with high positive velocity has been found at longitudes below $l^{II} = -6°$.

The feature is very different from the 3-kpc arm, where the negative velocity at the "forbidden" side of the nucleus (i.e. the side where, in the case of simple rotation, no negative velocities should occur) is relatively small, and can be understood by an expansion velocity of about 50 km/sec superposed on a rotation of roughly 200 km/sec. How striking the difference between the two "forbidden" features is, can best be seen by comparing the contours in the lower right-hand quadrant of figure 8 with those in the upper left quadrant. In the positive-velocity feature the forbidden velocities are very much higher. So much so, that they are hard to explain by the superposition of an expansional motion on a normal rotation (see section 4.5). The sudden appearance of the positive-velocity "arm" around $l^{II} = -5°$ and the sharp rise in velocity between $-5°$ and $-3°$ are also quite different from what we observe in the opposite quadrant for the 3-kpc arm. These facts indicate that the feature must be rather close to the centre. It cannot be closer than 1.0 kpc; on the other hand it is unlikely that it is much farther than 1.5 kpc, because in that case the sudden drop at $l^{II} = -5°$ would mean a sudden ending of the arm, which is not commonly observed in central parts of spirals.

The feature concerned is also distinguished by the fact that it lies at a considerable distance from the galactic plane. As it is still of considerable intensity at $b^{II} = +0°.9$, new observations were made in 1963 at higher latitudes, in order to obtain profiles of the entire

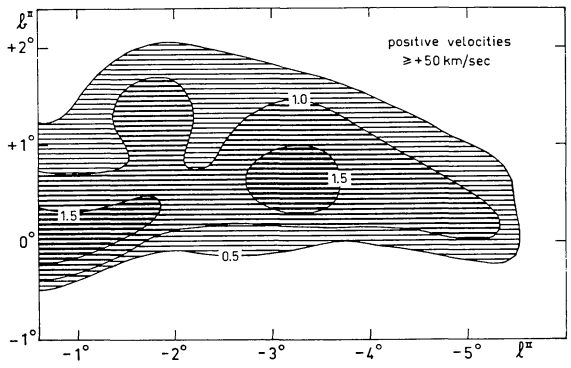

Figure 15. Contours of equal N_H for the positive-velocity feature at negative longitudes. Units are 10^{21} atoms/cm^2. The figure shows the large deviation of the feature from the galactic plane.

mass. In order to get a clear picture we have integrated all emission with velocities above +50 km/sec. The result is shown in figure 15, which shows contours of equal numbers of hydrogen atoms per cm^2. Between $l^{II} = -2°$ and $-5°$ the average latitude b^{II} is about $+0°.7$, corresponding with a distance z from the mean galactic plane of +120 pc.

If one tries to explain these velocities by a rotational velocity plus an expansion velocity, one is forced to assume either a very high velocity of expansion, or a low rotational velocity. As we do not find expansion velocities higher than 135 km/sec at $l^{II} = 0°$, it is rather unlikely that between $l^{II} = -2°$ and $-4°$ we should have expansion velocities of the order of 400 km/sec, such as would be required if the feature had a normal rotational velocity. The existence of this feature therefore indicates that at least some of the gas in the central region has an abnormally low velocity of rotation. This phenomenon is considered quantitatively in the next section.

4.5. *Four velocity models*

In order to locate the features of figure 13 at a certain distance from the centre we will now discuss four different velocity models. The characteristics are in table 8. All the models are axi-symmetrical, so there is only one rotation- and one expansion-curve for each model. We realize the inadequacy of this assumption. The distribution of the gas is notably asymmetrical, and it is very probable that the velocity field will likewise show systematic deviations from axial symmetry. If, as seems quite possible, the expansion is caused by an

TABLE 8

Rotation and expansion velocities assumed in the different models (in km/sec)

R (kpc)	Rotation velocities				Expansion velocities			
	1 pure rot.	2 high rot. low exp.	3 low rot. low exp.	4 higher rot. high exp.	1 pure rot.	2 high rot. low exp.	3 low rot. low exp.	4 higher rot. high exp.
0.75	258	258	15	0	0	185	175	265
1.00	248	248	40	40	0	140	150	240
1.25	240	240	65	120	0	90	125	215
1.50	232	232	90	140	0	40	100	190
1.75	224	224	115	177	0	7	75	165
2.00	216	216	140	190	0	0	50	140
2.50	204	204	180	195	0	0	18	90
3.00	200	200	198	200	0	0	0	40
3.50	205	205	204	205	0	0	0	10
4.00	210	210	210	210	0	0	0	0

explosion in the nuclear region some 10^7 years ago, there is certainly no reason to expect that the resulting gas motions would be axi-symmetrical. But the available data are entirely insufficient to determine such deviations from symmetry.

For each model we can at once compute for any point in the central region the velocity in the line of sight which would be seen by an observer near the Sun who would be at rest with respect to the galactic centre. We shall denote this velocity by U. To obtain the velocity V with respect to the local standard of rest, we have to correct with a velocity component due to the movement of the local gas around the galactic centre ($R_0 = 10$ kpc, $\Theta_0 = 250$ km/sec). In figure 16 different lines of equal U are drawn for each model. The part within $R = 700$ pc has been left out. It will be discussed in the last part of this paper (part IV, nuclear disk). The shaded part gives the position of the emission found between limits 1 and 2 in diagrams like figure 12, i.e., the part in which we cannot distinguish the gas in the central region because its velocity lies within the range covered by the main maximum.

Model 1 (Pure rotation)

We should distinguish three different rotations:

a) The circular velocity, defined as the velocity of a body moving in a circular orbit, and subjected exclusively to the gravitational force of the system.

b) The average transverse (rotational) component of the motion of the hydrogen. We shall call this the velocity of rotation of the gas. In the outer parts of galaxies, where expansional motions and forces other than gravitation may be comparatively small, the velocity of rotation of the gas may be practically equal to the circular velocities defined under a). In regions where magnetic forces are large, or where there are considerable deviations from axial symmetry in the velocity field, or where, alternatively, the gas has larger systematic motions in radial direction, the gas rotation may differ very greatly from the circular velocities considered in a).

c) The average rotation of the stars. This will generally differ from the circular velocity. Especially in the central regions of galaxies the differences may be quite large.

The rotation curve for model 1 has already been described (ROUGOOR and OORT, 1960). It has been determined by a comparison of the Galactic System with M 31. Outside the central regions velocities of the rotation can be determined quite well in both systems. For M 31 these were taken from the investigation by VAN DE HULST, RAIMOND and VAN WOERDEN (1957). As these velocities refer to the gaseous substratum they may be considered to represent circular velocities. In the central part there are no reliable 21-cm measurements. Here we have made use of data on the distribution of light. If one assumes that the ratio of mass to light is constant, and if the value of this constant is determined from the part where 21-cm measurements are available, one can then find the distribution of mass density. From this we have computed the circular velocities in the central part of M 31. We have used these,

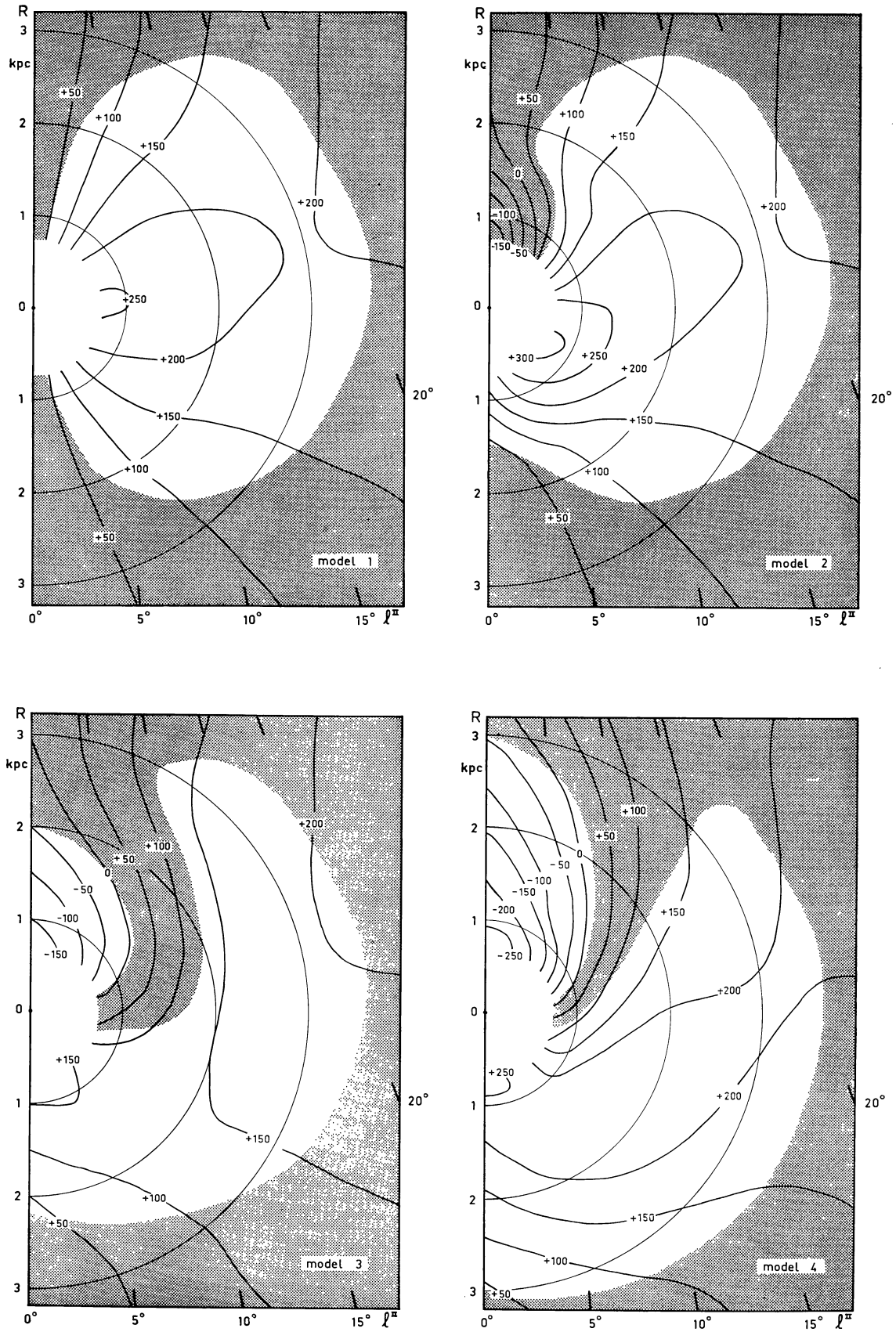

Figure 16. Lines of equal velocity with respect to the galactic centre (U). The galactic centre is at $R=0$, the Sun at $R=10$ kpc *above* this point. The shaded areas are regions where the velocity is within limits 1 and 2 (the "invisible" part). The region within $R=750$ pc has been left blank (see part IV).

in turn, to estimate the circular velocities in the central part of the Galactic System, on the assumption that the mass distribution in the central regions would be similar in the two systems. The rotation curves outside the central regions *are* quite similar, except that the velocities of rotation in the Galactic System are smaller by a factor of about 0.79. The same factor has been applied to reduce the curve for the central part of M 31 to that for the Galactic System. That the curve for the circular velocities so obtained may be meaningful is indicated by the fact that it agrees well with the rotational velocities derived from observations of the nuclear disk in the Galactic System (cf. section 10.3).

Model 1 is intended only for comparison with the other models, since it cannot correspond to the actual situation. At $l^{II} = 0°$ the model allows only velocities around zero km/sec. To include the observed expansion velocities one can either postulate expansion within $R = 700$ pc only – which is very improbable, see below – or we can add some expansion throughout the whole inner region, as in the next model.

Model 2

This has the same rotation curve as before, while some general expansion has been added (185 km/sec at $R = 750$ pc, 0 km/sec at $R = 2$ kpc; see also table 8). Only half of the figure – positive longitudes – has been drawn, the other half is nearly symmetric if the sign of the velocity is changed. The shaded part in figure 16 has not changed very much in this model, except for longitudes close to the nucleus. Formally "forbidden" velocities are now possible in the region $R < 1$ kpc, while in the upper part of the figure the velocities are somewhat larger than before. This model fits the observed expansion velocities at $l^{II} = 0°$. However, the positive-velocity feature at $l^{II} = -5°$, described earlier, does not fit this model. At this longitude we find velocities around -100 km/sec. To include this feature in the model we might, either increase the expansion velocity at say $R = 2$ kpc to several hundreds of km/sec, or we might decrease the rotational velocity of the gas. The former is very improbable, because the largest observed expansion velocity at $l^{II} = 0°.0$ is 135 km/sec. Another objection is that the radial velocities at $l^{II} = +5°$ would become extremely high, which has not been observed either. We are therefore led to consider the following model.

Model 3

The velocity of rotation of the gas between $R = 750$ and 3 000 pc has been assumed to be very much lower than the circular velocity. Only at $R = 3$ kpc the two become equal. The rotational velocity is assumed to be almost zero at $R = 700$ pc, and to increase linearly up to $R = 2$ kpc. The expansion velocity is somewhat higher than in model 2, and becomes zero at $R = 3$ kpc.

The "invisible" part of the H I has changed considerably. In figure 16 a large tongue intrudes the whole central region. The positive-velocity feature can be fitted in this model. However, at positive longitudes the positive velocities are much too small, about 130 km/sec instead of 200 km/sec. In order to reach this value we have considered model 4.

Model 4

It has to be kept in mind that all these models are quite arbitrary. At each distance from the nucleus we can have a set of both rotation and expansion velocities which satisfies the observed values. Even more serious is the fact that different features at the same distance from the nucleus may have different rotation and expansion velocities, i.e., that there is no axial-symmetry. In model 4 we have tried to find some compromise between models 2 and 3. The rotation curve is low at $R = 1$ kpc, but increases rapidly to higher R. The expansion velocities are rather high: at $R = 750$ pc, 265 km/sec; at $R = 3$ kpc, 40 km/sec. The tongue of the "invisible" part is not so pronounced as in model 3. The positive-velocity features at $l^{II} = -5°$ and $+5°$ can easily be located in this diagram. The schematic picture of the run of the arms in the central region shown in figure 1 has been drawn using a model like this. For a given line of sight there are always two positions giving the same radial velocity, just as in the case of pure rotation. In SCHMIDT's (1957) investigation of the inner region ($R < 10$ kpc) this ambiguity was eliminated by considering the difference in the distribution in latitude. In the present case this is more difficult, because all the gas is fairly close to the centre. If we follow, for instance, the lines $U = +200$ km/sec in model 4, we can conclude that the difference in width for features on these two lines must be extremely small. As the largest part of the expanding arm (feature 1, section 4.1) has $U = +200$ km/sec it should follow one

of these lines. We have chosen the lower one. The other line will be followed partly by the connecting arm.

4.6. *The H I density as a function of the distance to the centre*

For each of the models the length of the line of sight in the non-shaded part was measured. Together with the values of N_H already determined we can now compute the H I density, if we assume it to be a function of R only. This is certainly not generally true, but we may hope that at the side of positive velocities the gas is sufficiently spread out over the region concerned to obtain in this way at least an approximate idea of the densities. At negative velocities we have only the 3-kpc arm and the disk, and a determination of $n_H(R)$ in this way would be meaningless.

The computations are based on the average values of N_H for the three zones $b^I = -1°.0$, $-1°.5$ and $-2°.0$, multiplied by the factor 1.41 (see section 4.7). We first started to determine the density for the ring between $R = 3.0$ and 3.5 kpc. Longitude $l^{II} = 21°$ was left out because the length of the line of sight in the non-shaded region was too uncertain. The lines $l^{II} = 18°$, 19° and 20° are situated fully in the interval $R = 3.0$ to $R = 3.5$ kpc for the region concerned. The density for this region was derived from N_H at these longitudes and the lengths of the lines of sight in the non-shaded part. The density is found to be 0.21 atoms/cm^3. Assuming that at other longitudes the density for this interval of R is the same, we derived the density between 2.5 and 3.0 kpc from the N_H values at $l^{II} = 15°$, 16° and 17°. This procedure was continued down to $R = 750$ pc. The results are shown in figure 17 for models 1 and 4. Between 1.75 and 3.5 kpc the densities are the same for the two models. For $R = 750$ pc to 1.75 kpc model 1 has rather low densities. They are nearly twice as large for model 4, this being caused by the smaller interval in the line of sight which is cut off by the integration limits. In both models there is a minimum at $R = 2.3$ kpc. The increase at higher R might indicate that the expanding arm at + 135 km/sec becomes tangential to the line of sight at this distance from the centre (at $l^{II} > 20°$). The maximum at $R = 1.5$ kpc in model 4 is due to the appearance of the connecting arm at $l^{II} = 10°$. If we follow the 3-kpc arm and the connecting arm in model 4, we get the impression that the latter might be the continuation of the 3-kpc arm. This agrees with the latitude distribution of these features.

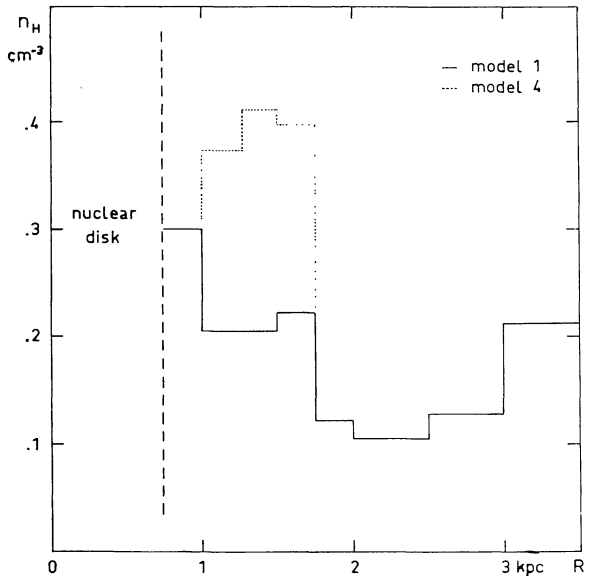

Figure 17

The minimum longitude we have used was $l^{II} = +5°$. At lower longitudes we measure the radiation from the disk, as can be seen from the l–V diagrams at negative velocities (assuming the disk to be symmetrical).

4.7. *Thickness of the gas layer; total H I mass*

In the last section we discussed the density of the H I gas. To get the total amount of gas we have to consider first the latitude distribution. From $l^{II} = +5°$ to +22° we have values for N_H for only three latitudes. In parts III and IV we shall determine the latitude distribution for the 3-kpc arm and the nuclear disk from measure-

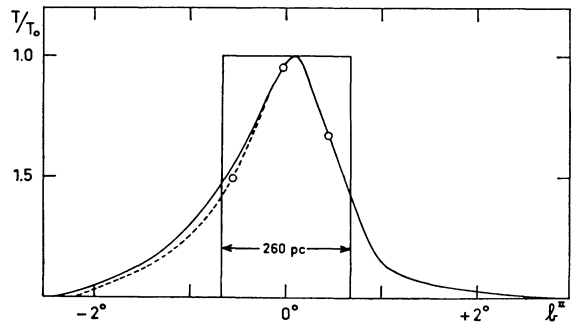

Figure 18. Average scan in galactic latitude from the preliminary measurements. The top is normalised to intensity 1. The circles refer to mean values for longitudes $l^{II} = +5°$ to +22° taken from table 6. The rectangle has the same area as the area under the curve and represents a homogeneous layer with a thickness of 260 pc.

ments made over a larger latitude interval. In order to get at least *some* indication of the distribution at higher latitudes for longitudes between 5° and 22° we have used the B_α measurements (see section 2.2), which were part of the preliminary programme in 1956. The curve of figure 18 is the average of 16 such measurements between longitudes $l^{II} = 8°$ and 19°. These measurements cover the velocities above limit 1 reasonably well, because a large bandwidth was used (30 km/sec). No absolute scale was determined; the peak value of the curve was normalized to one. The three small circles give values of N_H calculated from table 6 by averaging over all longitudes from $l^{II} = 5°$ to 22°. They have been multiplied by a factor which made the average for $b^I = -1°.5$ (corresponding in this longitude range with $b^{II} = -0°.04$) coincide with the curve. The smallness of the deviations between the curve and the other two small circles indicates that the relative distribution derived from the B_α measurements is not too bad; this notwithstanding the circumstance that the drift of the receiver was still considerable at that time. From the curve in figure 18 we can get some idea about the wings of the latitude distribution. A small correction, indicated by the dashed line, has been applied to match the circle at $b^I = -2°.0$ ($b^{II} = -0°.6$). A rectangle has been drawn in, which has the same area as the curve. It extends from $b^{II} = -0°.67$ to $b^{II} = +0°.69$. The effective thickness of the layer is, therefore, 1°.36. The layer is exactly symmetrical with respect to the new galactic plane. N_H for this layer is 1.80×10^{21} atoms/cm^2. If the distance is 11 kpc (most of the emission comes from a distance slightly larger than the distance to the centre; see model 4) the layer has a thickness of 260 pc.

The thickness between the points where the ordinate of the curve is half the peak value, is 1°.15, corresponding to 240 pc. This value is close to the value of 270 pc which SCHMIDT (1957) found for the whole inner region within $R = 10$ kpc. The width of the nuclear disk is much smaller (see section 10.2). A value for the 3-kpc arm cannot be given, because of its complex structure (see section 6.5).

In order to get the variation of N_H with longitude for the homogeneous layer of 260 pc as defined by the rectangle of figure 18, we have to multiply the average N_H of table 7 for the three latitudes by a factor of 1.41. The same factor has been applied for the densities derived in section 4.6. From these densities we can now find the total mass of neutral hydrogen $M(R)$ between about 750 pc and 3 kpc, assuming a layer of 240 pc thickness and radial symmetry of the density.

Table 9 gives the results expressed in solar masses for the distance intervals concerned.

TABLE 9

R (kpc)	$M(R)$ (10^7 solar masses) Model 1	Model 4
0.75–1.00	0.2	0.2
1.00–1.25	0.2	0.4
1.25–1.50	0.2	0.5
1.50–1.75	0.3	0.5
1.75–2.00	0.2	0.2
2.00–2.50	0.4	0.4
2.50–3.00	0.6	0.6
3.00–3.50	1.2	1.2
0.75–3.50	3.3	4.0

The total mass is not too different from two times the mass of one galactocentric quadrant of the 3-kpc arm as derived in section 6.6. The mean density over the whole region concerned is 0.16 atoms/cm^3 for model 1 and 0.19 for model 4.

The symmetry of the H I mass in the central region is clearly shown by an integration over longitude. We interpolated the values of $\bar{N}_H$ in table 7 for whole and half degrees of l^{II}. The longitude interval $l^{II} = -1°.0$ to $-7°.5$ was taken for the negative velocities, for the positive velocities the interval was reversed: $+1°.0$ to $+7°.5$. From this integration it follows that the negative velocity side contributes 49.8 per cent of the emission and the positive side 50.2 per cent. The symmetry of the emission around $l^{II} = 0°$ is therefore perfect.

PART III

THE 3-KPC ARM

5. Observations and tables

The broad band which can be seen in figures 8 to 12 from $l^{II} = -7°.7$ at $V = -90$ km/sec up to $l^{II} = +4°$ at $V = -30$ km/sec has been called the 3-kpc arm. It

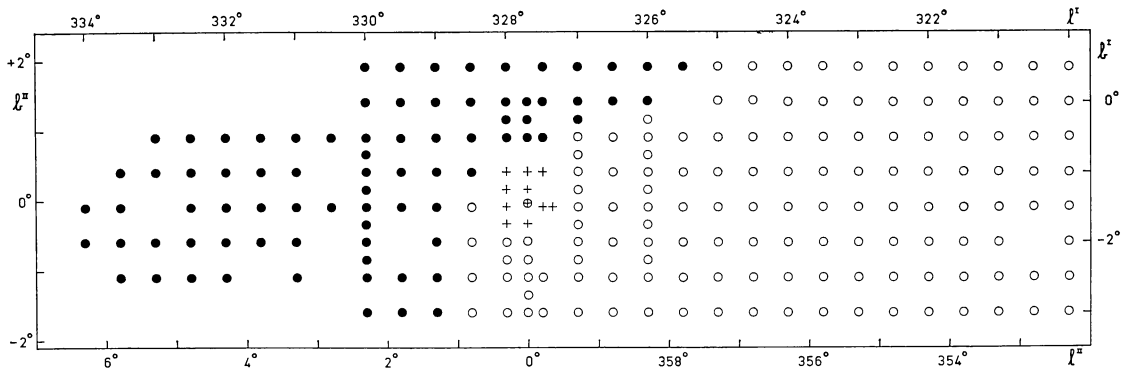

Figure 19. Positions where profiles of the 3-kpc arm were taken. Open circles represent profiles which are not (seriously) blended by emission of the main maximum. At the position of the filled circles there *is* serious blending. Crosses indicate profiles strongly influenced by the source Sgr A, shown by an encircled cross.

is still recognizable at $l^{II} = +6°$ as a small hump in the left-hand slope of the main maximum. Observations by Kerr (private communication) in Parkes and by BURKE and TUVE (1962) in Washington below $l^{II} = -7°.7$ demonstrate that this arm can be followed down to $l^{II} = -22°$. At that longitude its distance from the centre has to be at least 3.7 kpc (assuming $R_0 = 10$ kpc). We can distinguish the following parts:

a) $l^{II} = -22°$ to $-7°.7$. This part will be described later. It has been observed extensively from Parkes with the 210-ft telescope. Profiles were taken with a spacing in longitude of 1°. At each longitude the latitude interval was between $b^{II} = +2°$ and $-2°$ with 0°.1 spacing.

b) $l^{II} = -7°.7$ to $-2°.7$. In this longitude interval the profile of the arm is practically undisturbed by other emissions, either from the main maximum or from the nuclear disk.

c) $l^{II} = -2°.7$ to $-0°.7$. The profile is reasonably pure, except for a slight blending by the nuclear disk.

d) $l^{II} = -0°.7$ to $+0°.8$. The source Sgr A causes absorption in nearly all the profiles except in those 1° or more from the galactic plane. This absorption will be discussed in chapter 7.

e) $l^{II} = +0°.8$ to $+6°.3$. All over this range the profiles of the 3-kpc arm are seriously blended with the main maximum. This maximum is composed of numerous near-by and far-away clouds and arms. It is impossible to separate these from the 3-kpc arm.

Beside the observations already described in the "general survey", many additional measurements were made in the frequency interval of the arm, especially at larger distances from the galactic plane. The positions where measurements referring to the 3-kpc arm were made are shown in figure 19. Open circles indicate

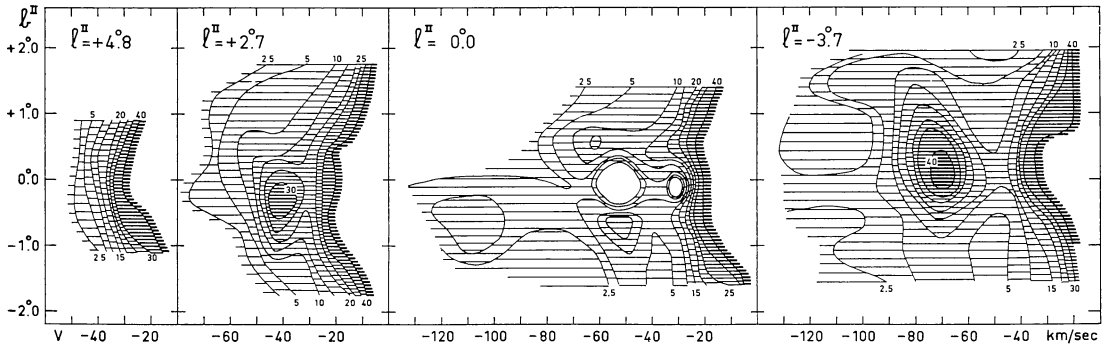

Figure 20. Four characteristic examples of b–V charts for the 3-kpc arm. The numbers give brightness temperatures. At $l^{II} = -3°.7$ the arm is completely separated from the main maximum. The chart for $l^{II} = 0°.0$ shows the absorption due to Sgr A. At $l^{II} = 2°.7$ there is already a strong blending. At $l^{II} = +4°.8$ the arm has practically disappeared. In the maps for $l^{II} = -3°.7$ and 0°.0 the "rolling" motion described in chapter 8 can clearly be seen.

TABLE 10

b^I	b^{II}	-20		-25		-30		-35		-40		-45		-50		-55		-60		-65		-70		-75		-80		-85		-90		-95		-100		-105		-110		-115		-120		-125		-130			km/sec
l^I = 320°.0	l^{II} = 352°.3																																																
+0.5	+1.8	39	34	31	29	28	26	22	18	15	12	10	08	07	06	05	05	04	04	04	03	03	03	03	03	03	02	02	02	02	02	02	02	02	02	02	02	02	02	02	02	02	02	02	02	02	02	02	01
+0.0	+1.3	54	45	40	37	35	36	35	33	31	26	20	15	12	09	07	06	06	07	07	08	08	08	09	09	09	08	07	07	06	06	05	04	05	05	05	05	05	05	05	05	05	05	05	05	04	04	04	04
-0.5	+0.8	00	00	55	48	43	41	40	41	40	35	30	24	19	15	11	09	07	07	08	08	09	10	11	12	13	14	16	17	19	21	24	24	22	17	14	10	08	06	05	04	04	04	04	03	03	03	02	02
-1.0	+0.3	00	00	00	00	00	60	54	49	44	44	45	43	39	31	24	19	15	12	10	09	09	11	15	21	32	40	45	46	53	57	53	44	34	24	16	11	09	06	05	03	02	01	01	02	03	03	04	04
-1.5	-0.2	00	00	00	00	00	57	49	42	39	40	44	47	48	45	39	30	23	18	14	10	08	07	11	18	29	40	49	51	48	43	35	27	19	14	10	07	05	03	03	02	02	02	03	03	04	04	04	04
-2.0	-0.7	00	00	00	58	50	42	32	26	23	20	18	17	17	16	15	11	08	05	04	04	04	05	08	11	16	21	25	26	24	20	16	10	07	05	04	03	02	01	01	01	01	01	02	02	02	02	02	01
-2.5	-1.2	00	00	59	50	39	30	22	17	12	10	09	07	06	06	05	05	05	05	06	06	06	07	09	11	13	15	16	17	17	15	13	10	08	06	06	05	04	04	03	03	02	02	02	02	02	02	02	02
-3.0	-1.7	52	47	42	36	29	22	17	13	09	07	06	05	05	04	04	04	04	04	04	04	04	04	05	06	06	07	07	06	06	05	05	04	04	03	03	02	02	01	01	01	01	01	01	01	01	01	01	01
l^I = 320°.5	l^{II} = 352°.8																																																
+0.5	+1.8	45	36	33	29	26	23	19	15	12	10	07	06	05	05	05	05	04	04	04	04	04	04	05	04	04	03	04	04	04	04	04	03	03	03	02	02	02	02	02	02	02	02	02	02	02	02	02	02
+0.0	+1.3	55	45	37	32	30	28	26	24	20	17	15	12	09	07	06	06	07	07	08	09	09	09	09	09	09	09	08	07	07	06	06	05	05	05	05	04	04	03	03	03	03	03	04	04	04	04	04	04
-0.5	+0.8	00	00	53	44	37	34	33	33	32	29	24	19	15	13	12	12	12	11	11	11	11	11	10	10	10	11	12	15	19	21	21	19	15	11	08	05	04	03	03	03	03	03	04	04	04	04	04	03
-1.0	+0.3	00	00	00	00	00	54	49	46	44	43	42	40	37	33	29	24	20	17	15	14	14	16	20	25	30	34	39	42	46	45	40	32	24	15	11	07	05	03	03	02	02	02	02	02	03	03	03	02
-1.5	-0.2	00	00	00	00	00	54	49	45	44	46	49	51	50	45	38	30	23	18	13	12	12	16	23	29	36	42	43	41	33	26	21	17	13	09	07	05	04	03	03	02	02	02	01	01	00			
-2.5	-1.2	59	50	42	37	30	24	19	15	12	10	09	08	07	06	05	05	05	05	05	06	07	09	11	15	18	20	20	19	18	16	12	09	07	05	04	03	03	03	03	03	03	03	03	02	01			
-3.0	-1.7	42	36	30	26	21	16	12	09	08	07	06	05	05	04	04	03	03	03	04	05	06	06	07	08	09	09	08	07	06	05	04	04	03	03	03	02	02	02	02	01	01	01	01	01	01			
l^I = 321°.0	l^{II} = 353°.3																																																
+0.5	+1.8	45	38	33	27	23	19	16	13	09	07	05	04	04	03	03	03	03	03	03	04	04	04	04	05	04	04	05	05	05	04	04	03	03	02	02	02	01	01	01	01	01	01	01	01	01	00		
+0.0	+1.3	56	46	38	32	26	21	17	15	12	10	09	08	07	07	06	07	07	07	08	09	10	10	10	10	10	09	09	08	07	06	06	05	04	03	03	02	02	02	01	02	02	03	02	02	02	03	03	02
-0.5	+0.8	00	00	53	43	35	31	30	29	27	24	21	18	14	10	10	09	09	09	10	10	10	10	10	11	12	14	16	18	21	21	19	15	12	08	04	03	01	01	00	01	01	01	01	01	01	01	01	01
-1.0	+0.3	00	00	00	00	00	00	57	53	49	49	49	45	37	30	24	19	16	14	13	12	13	15	20	23	29	33	38	39	39	35	29	24	18	12	08	06	04	03	03	03	03	03	03	02	02	02	02	02
-1.5	-0.2	00	00	00	00	60	53	49	47	48	49	49	48	44	35	29	22	17	13	12	12	16	21	28	35	45	47	44	35	26	20	15	13	10	08	07	06	05	05	04	03	02	02	01	01	01	01	00	
-2.0	-0.7	58	52	46	40	33	28	22	19	17	16	14	12	09	08	08	07	06	05	05	05	07	10	17	23	31	37	38	32	24	16	10	07	05	03	02	02	02	02	02	02	02	02	02	02	01	01	01	01
-2.5	-1.2	48	40	35	29	23	20	16	13	11	09	08	07	06	05	05	05	04	05	05	06	07	09	12	14	15	17	17	15	13	10	08	06	05	04	03	03	03	03	03	03	03	03	03	03	03			
-3.0	-1.7	37	31	26	21	17	14	10	08	07	06	05	05	04	04	04	04	04	05	06	07	08	08	09	09	09	08	07	06	05	04	04	04	04	03	02	02	02	02	02	02	01	01	01	01	01			
l^I = 321°.5	l^{II} = 353°.8																																																
+0.5	+1.8	33	29	27	26	25	24	20	15	10	06	04	03	03	02	03	02	02	02	02	02	02	02	03	03	03	04	04	04	04	04	03	03	02	02	01	01	01	01	01	01	01	01	01	01	00			
+0.0	+1.3	49	42	36	31	26	22	19	16	13	10	08	07	07	06	06	06	07	08	09	10	10	10	10	09	08	08	07	07	06	06	05	05	04	03														
-0.5	+0.8	00	53	43	33	26	24	26	25	22	18	14	11	08	06	05	06	08	09	11	12	14	15	16	15	13	13	15	15	16	13	11	08	05	02	01	00												
-1.0	+0.3	00	00	00	00	00	57	51	45	39	34	30	25	21	18	15	14	14	14	16	18	21	23	25	26	28	28	29	29	27	25	22	17	11	07	05	04	03	03	03	02	01	01	01	01	01	01	01	01
-1.5	-0.2	00	00	00	00	59	49	44	40	38	35	31	27	23	19	16	14	12	10	10	10	12	15	23	35	44	43	38	25	16	08	06	05	04	04	04	03	03	02	02	01	01	01	00					
-2.0	-0.7	00	00	51	43	34	27	22	18	15	13	11	09	07	06	06	05	05	05	05	07	11	15	20	24	29	27	20	14	09	05	03	02	01	01	01	01	01	01	01	01	00							
-2.5	-1.2	50	43	37	30	25	20	16	13	11	09	08	07	06	05	05	05	05	06	09	12	15	17	18	19	18	16	14	12	10	07	05	04	04	03	03	03	03	02	02	02	02	02	02	02				
-3.0	-1.7	34	29	25	20	16	13	11	10	08	06	05	05	04	04	04	04	06	07	09	10	11	11	10	09	08	07	05	04	04	03	03	02	02	02	02	02	02	02	02	02	01	01	01					
l^I = 322°.0	l^{II} = 354°.3																																																
+0.5	+1.8	31	29	27	26	25	23	19	14	10	07	05	04	03	02	02	02	02	02	02	02	02	03	03	03	03	04	04	04	04	04	04	03	03	02	02	02	01	01	01	01	00							
+0.0	+1.3	00	00	00	00	00	00	00	00	14	11	09	07	06	05	05	05	05	05	06	06	07	08	08	09	09	08	08	07	06	06	05	05	04	04	03	03	02	03	02	01	01	01	01	01	01	01		
-0.5	+0.8	48	40	32	28	27	27	26	23	20	17	14	10	09	08	08	08	08	09	10	11	13	14	17	19	20	20	19	17	16	13	09	06	04	02	01	00												
-1.0	+0.3	00	00	00	54	48	45	43	40	36	32	28	24	20	16	13	12	11	12	15	17	20	23	25	27	29	29	29	26	23	19	15	11	08	05	03	02	01	00										
-1.5	-0.2	00	00	00	00	56	51	49	45	43	39	34	26	20	17	14	11	09	07	08	09	13	17	24	29	33	32	26	18	10	06	04	03	02	02	02	01	01	01	01	01	01	01	00					
-2.0	-0.7	00	59	49	39	31	26	22	18	15	13	11	08	05	04	03	02	03	04	06	08	11	15	19	20	19	15	11	07	03	02	01	01	00															
-2.5	-1.2	57	49	42	33	25	19	15	12	09	09	07	06	05	05	04	05	05	06	09	12	14	15	14	12	10	08	07	06	05	04	03	02	02	02	02	01	01	01	01	01	01	01	01	01	01			
-3.0	-1.7	38	33	27	22	18	16	13	11	10	08	07	06	05	04	04	04	06	08	11	11	09	08	08	08	07	07	06	05	04	03	02	02	02	01	01	01	01	01	01	01	01	01	01					
l^I = 322°.5	l^{II} = 354°.8																																																
+0.5	+1.8	34	30	26	22	17	14	11	08	06	05	05	04	04	04	03	03	02	02	03	03	04	06	07	07	07	07	06	06	05	05	04	04	03	02	02	01	01	01	01	01	01	01	01	00				
+0.0	+1.3	48	45	40	33	28	24	21	18	15	13	11	08	06	05	05	05	05	05	05	06	08	11	14	15	14	11	10	09	08	06	06	05	04	04	03	03	02	02	02	02	01	01	01	00				
-0.5	+0.8	55	50	44	39	34	31	30	29	27	24	19	14	10	08	06	05	06	08	09	10	12	13	16	18	21	21	20	17	14	10	08	05	02	01	00													
-1.0	+0.3	00	00	58	52	47	44	40	37	34	31	25	20	16	13	11	10	10	10	11	12	15	20	27	30	33	30	25	20	17	15	13	10	08	05	03	01	00											
-1.5	-0.2	00	00	00	55	50	46	44	43	42	38	30	23	16	12	09	07	06	08	11	14	19	25	32	33	29	23	16	11	07	05	04	02	01	01	00													
-2.0	-0.7	60	52	42	35	30	26	23	20	18	15	11	08	06	04	03	02	01	01	02	03	05	08	10	10	09	06	03	02	01	01	00																	
-2.5	-1.2	51	42	34	28	22	17	14	11	09	07	06	05	04	04	04	03	03	03	03	04	04	05	06	06	06	05	05	05	04	03	03	02	02	02	02	01	01	01	01	01								
-3.0	-1.7	43	38	30	24	20	17	15	13	11	09	07	06	04	04	04	04	04	05	05	05	05	06	06	06	05	05	05	05	04	04	03	03	02	02	02	02	01	01	01	01	01	01						
b^I	b^{II}	-20		-25		-30		-35		-40		-45		-50		-55		-60		-65		-70		-75		-80		-85		-90		-95		-100		-105		-110		-115		-120		-125		-130			km/sec

TABLE 10 *(continued)*

b^I	b^{II}	-20	-25	-30	-35	-40	-45	-50	-55	-60	-65	-70	-75	-80	-85	-90	-95	-100	-105	-110	-115	-120	-125	km/sec
$l^I = 323.°0$	$l^{II} = 355.°3$																							
+0.5	+1.9	41	38	32	26	19	14	10	08	07	07	06	06	06	06	06	06	06	07	07	07	07	08	08	09	09	09	08	07	06	05	04	03	03	02	02	02	01	01	01	00							
+0.0	+1.4	46	46	41	36	31	29	28	27	23	16	12	10	08	07	07	07	07	08	09	10	11	12	12	13	12	10	09	07	06	05	04	03	02	02	01	01	01	01	01	01	00						
-0.5	+0.9	49	45	41	38	36	36	34	32	29	23	17	12	09	07	06	06	06	07	09	11	13	15	19	21	24	24	22	17	12	08	05	04	02	01	01	01	00										
-1.0	+0.4	00	00	56	51	46	42	38	34	30	24	18	14	11	10	10	10	11	13	19	26	33	41	43	41	34	28	20	14	10	08	05	03	02	01	00											
-1.5	-0.1	00	00	00	55	50	45	41	37	34	27	21	16	13	11	10	11	13	16	24	31	39	42	42	38	31	25	18	12	08	06	04	02	02	01	00											
-2.0	-0.6	54	47	39	34	31	29	25	21	17	13	09	06	04	04	04	04	05	06	08	11	14	16	16	12	09	06	04	04	03	03	02	01	00													
-2.5	-1.1	50	43	36	29	23	18	14	11	09	07	05	04	03	03	03	02	02	02	03	03	03	04	04	05	06	06	06	06	05	05	04	03	02	02	01	01	01	01	01	01	01					
-3.0	-1.6	43	37	31	24	19	17	14	12	10	08	07	06	05	04	03	03	03	03	03	03	04	04	05	05	06	06	07	06	06	05	04	03	03	02	02	01	01	01	02	02	02	02					
$l^I = 323.°5$	$l^{II} = 355.°8$																							
+0.5	+1.9	47	43	35	26	18	13	10	08	06	05	04	04	04	04	04	04	04	05	05	06	06	06	07	07	08	08	08	08	07	06	06	05	04	03	03	02	01	01	01	01	00						
+0.0	+1.4	46	39	33	29	27	26	24	21	16	12	09	07	06	06	06	06	06	07	08	09	10	11	12	14	15	15	14	12	10	08	07	06	05	05	04	04	04	03	03	03	03	03	02	02			
-0.5	+0.9	48	42	38	37	38	38	36	33	27	18	12	08	06	05	05	05	06	09	13	16	19	23	26	26	24	21	17	11	07	04	03	01	01	01	00												
-1.0	+0.4	00	00	56	49	44	41	38	34	29	22	15	11	09	09	10	12	14	17	23	37	44	48	49	45	38	32	26	19	14	10	05	01	00														
-1.5	-0.1	00	00	59	49	44	40	36	32	28	21	13	09	09	10	11	13	16	19	34	43	51	52	47	41	32	26	19	13	09	06	05	04	03	02	02	02	02	02	02	02	02	02	01	01	00		
-2.0	-0.6	50	42	35	30	27	24	21	17	14	10	07	05	04	03	04	05	07	09	12	14	15	15	15	13	10	09	07	06	05	04	03	03	03	03	03	03	03	02	02	02	02	02	01	01	01		
-2.5	-1.1	44	37	30	24	19	16	13	10	08	07	05	04	03	03	03	04	04	05	05	06	06	06	06	06	06	06	05	05	04	03	03	03	02	02	02	02	02	02	02	02							
-3.0	-1.6	36	31	26	21	17	14	12	10	08	90	70	60	50	40	40	30	03	03	04	05	05	05	05	05	05	05	05	04	04	04	03	03	03	02	02	02	02	02	02								
$l^I = 324.°0$	$l^{II} = 356.°3$																							
+0.5	+1.9	48	41	30	20	12	07	05	04	03	03	02	02	02	02	02	02	03	03	03	03	03	03	04	04	04	05	05	05	04	03	03	03	02	02	01	01	01	01	01	01	01						
+0.0	+1.4	40	34	27	22	20	18	16	13	10	08	07	06	05	05	05	05	05	07	08	09	11	12	13	14	15	14	13	11	09	08	07	06	06	06	06	06	06	05	05	04							
-0.5	+0.9	41	35	33	33	34	32	29	23	18	13	09	07	06	06	05	06	08	11	15	19	22	24	25	24	23	19	15	10	07	05	03	02	02	02	01	01	01	01	01	01	02	02	02	02	03		
-1.0	+0.4	54	47	45	45	44	43	39	34	27	19	13	11	11	11	13	16	21	26	34	39	41	40	38	34	28	23	18	14	09	05	03	02	01	01	01	01	00	00	00	01	01	01	01	01	02		
-1.5	-0.1	00	59	52	48	45	42	38	32	25	17	13	10	11	14	16	19	22	28	37	44	46	41	35	27	22	17	13	09	08	06	05	04	04	03	03	03	03	03	03	03	03	03	03	04	04		
-2.0	-0.6	51	43	35	30	24	20	17	14	10	07	05	04	04	05	06	07	09	11	13	14	15	15	13	11	09	07	05	04	03	03	03	02	02	02	02	02	02	02	02	02	02	02	02	02			
-2.5	-1.1	37	28	23	19	16	14	12	10	08	06	05	04	04	03	04	04	05	06	07	08	08	08	08	08	07	06	05	04	04	03	03	03	03	03	03	03	03	03	02	02							
-3.0	-1.6	29	24	20	17	14	12	11	09	07	06	05	04	04	04	04	05	06	07	07	08	08	08	07	06	05	04	04	03	03	02	02	02	02	02	02	02	02	02	02	02							
$l^I = 324.°5$	$l^{II} = 356.°8$																							
+0.5	+1.9	42	32	22	15	09	07	05	04	03	03	03	03	02	02	02	02	03	03	04	04	04	05	05	05	05	05	04	04	03	03	02	02	02	02	02	02	02	02	01								
+0.0	+1.4	33	26	20	16	13	11	10	08	07	06	05	04	05	04	04	05	06	07	08	09	10	10	10	10	10	10	08	07	06	06	05	05	05	05	05	05	05	05	05	05							
-0.5	+0.9	37	32	28	26	25	24	22	19	15	11	08	06	04	03	04	04	06	08	11	15	18	18	17	15	12	09	07	05	04	03	02	02	02	02	02	01	01	01	01	01	01	01	01	01	01	01	01
-1.0	+0.4	52	44	41	42	42	39	34	29	24	20	15	12	12	14	17	20	24	29	37	40	38	33	28	23	18	15	12	09	07	06	03	02	01	01	01	00	00	00	00	00	01	01	01	01	01		
-1.5	-0.1	00	58	52	45	46	42	37	30	23	17	14	13	14	17	21	26	34	44	52	51	45	33	24	17	12	10	09	08	07	06	05	04	03	02	01	01	01	02	02	02	02	02	03	03	03		
-2.0	-0.6	51	44	35	29	24	20	16	12	09	06	06	05	05	06	08	12	16	21	25	23	20	17	13	09	06	04	03	02	02	02	02	02	02	02	02	02	01	01	01	01	01	01	02	02			
-2.5	-1.1	38	29	23	19	17	14	12	10	08	06	05	04	03	03	05	07	09	12	13	14	12	10	09	07	06	05	04	04	04	03	03	02	02	02	02	02	02	02									
-3.0	-1.6	31	26	22	18	16	13	11	09	07	06	05	05	05	06	07	09	11	12	11	10	08	07	05	05	04	04	03	03	03	02	02	02	02	02	02	02	02	02									
$l^I = 325.°0$	$l^{II} = 357.°3$																							
+0.5	+1.9	26	19	15	11	08	06	05	03	03	02	02	02	02	02	02	03	03	04	04	04	04	04	04	04	03	03	02	02	02	02	01	01	01	01													
+0.0	+1.4	31	25	17	13	09	07	06	05	04	04	03	03	03	03	03	04	05	05	05	06	06	05	05	05	05	05	04	04	03	03	04	03	03	04	04	04	04	04	04							
-0.5	+0.9	36	27	21	18	17	17	15	13	10	07	04	03	03	02	03	05	07	08	11	12	13	12	10	08	07	05	04	04	03	03	03	03	04	04	05	05	05	05	05	05	05						
-1.0	+0.4	52	45	40	36	32	30	27	23	19	14	12	10	10	11	15	20	26	29	30	29	26	23	20	17	14	11	08	06	04	03	02	02	01	01	01	01	01	01	01	02	02	02					
-1.5	-0.1	55	47	40	35	31	28	25	20	16	12	10	10	13	17	23	30	38	44	43	35	26	18	12	09	08	07	07	06	05	04	03	02	01	01	00	00	00	00	00	00	01	01					
-2.0	-0.6	42	34	29	26	22	19	16	13	10	07	06	06	06	08	13	17	21	24	24	22	17	11	06	03	02	02	02	02	02	02	02	02	01	01	01	01	01	01	00								
-2.5	-1.1	43	35	32	27	22	18	15	12	09	07	06	05	06	08	10	12	13	13	10	08	06	04	04	03	02	02	02	02	02	02	02	01	01	01	01	01											
-3.0	-1.6	40	35	30	25	20	15	11	09	07	06	05	05	05	06	07	08	09	08	07	06	04	03	03	02	02	02	02	02	02	02	02	02	02	02	02	02	02	02	02								
$l^I = 325.°5$	$l^{II} = 357.°8$																							
+0.5	+1.9	23	18	15	14	13	12	11	09	06	04	03	03	03	03	03	03	04	04	04	03	03	03	02	02	02	02	01	01	01	01	01	01	01	01	01	01	01	01	00								
-0.5	+0.9	36	26	20	16	13	11	10	09	07	05	04	03	03	04	05	07	07	08	08	08	07	06	04	03	02	02	01	01	01	01	01	01	01	01	01	01	02	02	02	02	03						
-1.0	+0.4	49	40	33	29	25	22	19	16	13	11	09	09	11	13	17	20	23	24	23	20	18	15	13	12	10	08	07	05	04	03	01	01	00	00	00	00	00	00	00	00	00	01	01				
-1.5	-0.1	00	00	00	00	00	21	17	14	11	07	06	09	14	18	23	26	27	26	23	18	13	09	07	06	05	05	04																				
-2.0	-0.6	42	39	34	30	26	23	18	13	08	04	04	05	09	12	16	17	17	15	14	12	11	08	04	02	02	02	02	03	03	03	02	01	00														
-2.5	-1.1	56	53	47	37	27	19	14	10	07	06	06	06	07	09	10	11	11	10	08	07	06	05	04	03	03	03	03	03	03	03	03	03	03	02													
-3.0	-1.6	45	39	32	25	17	12	08	06	05	05	05	06	07	07	07	06	05	04	03	03	02	02	02	02	02	01	02	02	01	01	01	02	02	02	02	02											

b^I	b^{II}	-20	-25	-30	-35	-40	-45	-50	-55	-60	-65	-70	-75	-80	-85	-90	-95	-100	-105	-110	-115	-120	-125	km/sec

TABLE 10 *(continued)*

b^{I}	b^{II}	- 20		- 25		- 30		- 35		- 40		- 45		- 50		- 55		- 60		- 65		- 70		- 75		- 80		- 85		- 90		- 95		-100		-105		-110		-115		km/sec
$\ell^{I} = 326^{\circ}.0$	$\ell^{II} = 358^{\circ}.3$																																									
+0.5	+1.9	22	17	14	12	10	09	08	06	05	04	03	02	03	03	03	03	03	03	03	02	02	02	02	01	01	01	01	01	01	01	01	01	01	01	01	01	01				
+0.0	+1.4	25	20	14	12	09	07	05	04	04	03	03	03	03	03	04	04	03	03	04	04	03	03	03	02	01	01	01	01	01	01	01	01	01	01	01	01	01				
-0.25	+1.1	41	31	22	17	14	12	09	07	05	04	04	03	03	03	03	03	03	04	05	05	05	04	04	03	03	02	02	02	02	01	01	01	01	01	01	01	01	01	01	01	01
-0.5	+0.9	35	27	20	16	13	11	09	07	06	05	05	05	05	05	05	06	06	07	07	06	05	04	03	02	02	01	01	01	01	01	00										
-0.75	+0.6	42	33	25	20	16	14	12	10	08	07	06	05	06	07	08	09	11	11	11	11	10	09	07	06	05	04	03	02	02	02	02	02	02	02	02	01	01	01	01	01	01
-1.0	+0.4	42	35	29	24	19	16	13	11	10	08	08	10	13	15	18	20	21	20	19	18	16	14	12	10	08	06	05	04	03	03	02	01	01	01	00	00	00	01	01	01	01
-1.25	+0.1	58	48	40	32	26	22	18	13	09	08	11	13	16	20	23	25	25	24	23	21	19	16	14	13	11	10	09	08	07	06	05	05	04	04	03	03	02	02	03	03	03
-1.5	-0.1	55	46	40	32	27	20	16	13	10	08	09	12	18	22	25	26	28	28	23	19	16	13	12	11	10	09	08	07	06	06	05	05	04	04	04	03	03	03	03	03	03
-1.75	-0.4	59	52	44	38	31	23	11	06	05	06	07	10	14	18	22	23	23	22	20	18	15	12	09	07	06	06	06	06	06	06	05	05	04	04	04	03	03	03	03	03	02
-2.0	-0.6	00	00	00	00	00	00	00	00	08	06	06	07	12	16	19	21	21	20	17	14	12	10	09	08	07	06	05	04													
-2.25	-0.9	00	56	47	34	24	16	08	05	03	03	04	05	06	07	09	10	10	09	09	08	07	06	05	04	03	03	03	03	03	02	02	02	01	01	01	01	01	01	01	01	01
-2.5	-1.1	57	51	39	28	19	12	08	06	05	05	05	05	06	08	08	08	08	08	08	07	06	05	05	04	04	04	04	04	03	03	03	02	02	02	01						
-3.0	-1.6	40	36	29	21	15	10	08	06	05	05	05	05	06	06	06	05	04	04	03	03	03	02	02	02	02	02	02	02	02	02	02	02	02								
$\ell^{I} = 326^{\circ}.5$	$\ell^{II} = 358^{\circ}.8$																																									
+0.5	+1.9	22	17	13	10	07	05	03	02	01	01	01	02	02	02	02	02	02	01	01	01	01	02	01	01	00																
+0.0	+1.4	26	21	16	13	10	07	06	05	04	04	04	04	03	03	03	03	03	03	02	02	02	02	02	02	02	02	02	02	02	02	02	02	02	02	02	02	02				
-0.5	+0.9	38	30	24	20	17	14	11	09	08	07	06	06	05	05	05	07	08	08	08	06	05	04	03	02	02	02	02	01	01	01	01	00									
-1.0	+0.4	50	40	32	26	21	18	15	13	12	11	12	13	16	18	20	21	20	19	18	17	15	14	12	10	09	08	07	06	05	05	04	04	04	04	03	03	03	03	03	03	04
-1.5	-0.1	00	53	43	35	28	23	17	14	13	12	13	15	19	22	25	25	25	22	19	17	14	12	12	11	11	11	10	09	08	07	07	06	06	06	06	06	06	07	07	07	07
-2.0	-0.6	00	51	40	33	24	18	13	11	10	10	10	12	17	21	23	24	24	22	20	16	13	10	08	08	08	08	08	07	07	06	06	06	06	06	06	06	06	06	06	06	06
-2.5	-1.1	48	39	28	21	15	11	09	07	06	06	07	09	10	11	11	12	12	11	11	10	09	07	06	05	05	05	05	05	05	05	05	04	04	04	03	03					
-3.0	-1.6	28	23	18	13	09	07	05	04	04	04	05	05	05	05	04	04	04	03	03	03	02	02	02	02	01	01	01	01	01	02	02	02	03	03							
$\ell^{I} = 327^{\circ}.0$	$\ell^{II} = 359^{\circ}.3$																																									
+0.5	+1.9	21	17	14	12	09	07	05	04	03	03	03	02	02	03	03	03	02	02	02	02	02	01	01	01	01	01	00														
+0.0	+1.4	33	27	23	19	15	11	07	06	05	05	04	04	04	04	03	03	03	03	02	02	02	02	02	02	02	02	02	02	02	02	02	02									
-0.25	+1.1	39	32	25	21	16	14	10	07	06	05	04	04	04	04	04	04	04	03	03	02	02	02	02	02	03	02	02	02	02	02	02	01	01	01	01	01	01	01	01	01	00
-0.5	+0.9	44	36	29	23	18	14	11	09	08	08	08	08	08	08	08	09	09	09	08	07	06	05	04	03	02	01	01	01	00												
-0.75	+0.6	55	42	32	27	22	18	16	14	12	11	11	11	12	13	14	16	18	18	17	15	13	11	10	08	07	05	04	03	02	02	01	01	01	01	01	02	02	02	02	01	01
-1.0	+0.4	52	41	32	27	23	19	17	15	14	14	16	17	19	20	22	21	21	19	17	15	14	13	11	10	08	07	06	06	06	06	06	06	06	05	05	05	05	04	04	04	05
-1.25	+0.1	57	45	32	28	24	20	17	15	15	16	17	18	20	21	21	21	20	18	16	14	13	11	10	09	07	07	06	06	05	05	05	06	06	07	07	07	08	08	09	09	09
-1.5	-0.1	00	52	41	33	27	24	21	19	17	17	19	20	21	23	24	23	22	19	17	14	12	11	10	10	09	08	07	06	06	06	06	06	06	06	06	07	08	09	09	10	11
-1.75	-0.4	58	52	45	36	28	24	19	16	14	14	16	18	20	22	23	23	21	19	17	14	11	09	09	08	08	07	07	07	07	07	07	07	07	08	08	08	09	09	09	09	10
-2.0	-0.6	49	41	34	26	20	17	14	12	10	10	13	16	18	20	21	20	19	17	14	10	07	05	04	04	04	04	04	03	03	03	03	03	03	03	04	04	05	05	05	06	06
-2.25	-0.9	41	34	27	21	15	10	07	07	07	07	09	12	15	15	15	14	14	13	10	08	06	04	04	04	04	04	04	04	04	04	03	03	03	03	04	04	05	05	05	04	04
-2.5	-1.1	34	28	22	16	11	08	07	06	07	08	09	11	12	12	12	11	09	09	08	07	06	04	03	03	03	03	03	03	03	03	03	03									
-3.0	-1.6	28	23	17	12	09	07	06	05	05	05	05	06	06	05	04	03	03	02	02	02	01	01	01	01	01	01	01	01	02	02	02	02									
$\ell^{I} = 327^{\circ}.3$	$\ell^{II} = 359^{\circ}.6$																																									
-1.5	-0.1	39	33	24	16	13	13	12	12	13	12	11	08	02	-02	00	07	11	11	10	09	09	08	08	08	08	08	07	07	07	07	07	07	07	07	07	07	08	08	08	08	08
$\ell^{I} = 327^{\circ}.5$	$\ell^{II} = 359^{\circ}.8$																																									
+0.5	+1.9	19	15	12	09	07	05	04	03	03	03	03	02	02	02	02	02	02	02	01	01	01	01	01	01	01	01	01	01	01	01	01	01	01	01	00						
+0.0	+1.4	33	28	22	17	13	09	06	05	04	04	04	04	04	04	03	03	03	03	02	02	02	02	02	01	01	01	01	01	01	01	01	01	01	01	01						
-0.5	+0.9	44	36	27	20	15	12	09	08	07	06	07	07	06	06	06	06	06	06	06	05	05	04	03	02	02	01	01	01	00												
-1.0	+0.4	56	42	32	26	21	19	17	16	15	15	15	14	13	12	13	14	16	16	15	14	13	11	09	08	06	05	04	04	03	03	02	02	02	02	02	02	02	02	02	02	02
-1.5	-0.1	40	29	19	11	04	05	09	09	09	08	07	-02	-16	-23	-15	-02	05	08	08	07	06	05	05	05	05	05	05	05	05	05	05	05	06	06	06	06	06	05	05	05	05
-2.5	-1.1	33	27	22	17	11	08	05	04	05	07	09	12	13	12	11	08	06	04	03	03	03	03	03	03	04	04	04	04	04	04	04	04									
-3.0	-1.6	24	21	17	12	08	06	05	05	04	05	06	07	07	06	05	04	03	02	02	01	01	01	01	01	01	01	02	02	02	02	02	02									
$\ell^{I} = 327^{\circ}.7$	$\ell^{II} = 000^{\circ}.0$																																									
+0.0	+1.4	33	26	17	14	09	06	04	04	03	03	03	03	03	03	03	02	02	01	00																						
-0.25	+1.2	36	31	25	19	15	11	09	07	07	06	06	05	05	05	05	04	04	04	04	03	03	02	02	02	02	01	01	01	01	01	00										
-0.5	+0.9	43	35	27	21	16	13	11	10	09	08	07	07	07	07	07	07	07	06	06	05	05	04	03	02	02	01	01	00													
-0.75	+0.7	55	45	34	29	24	21	17	15	13	13	13	13	13	14	14	15	15	15	13	11	10	08	06	05	04	03	02	01	01	00											
-1.0	+0.4	56	45	33	26	22	20	18	16	16	15	15	12	09	07	08	10	13	14	13	11	09	07	06	04	04	03	02	01	01	00											
b^{I}	b^{II}	- 20		- 25		- 30		- 35		- 40		- 45		- 50		- 55		- 60		- 65		- 70		- 75		- 80		- 85		- 90		- 95		-100		-105		-110		-115		km/sec

TABLE 10 *(continued)*

b^I	b^I	-20	-25	-30	-35	-40	-45	-50	-55	-60	-65	-70	-75	-80	-85	-90	-95	-100	-105	-110	-115	km/sec
-1.25	+0.2	47	34	21	13	07	06	09	10	08	07	05	-04	-15	-24	-20	-07	03	07	08	07	06	05	04	03	02	02	01	01	01	00			
-1.5	-0.1	44	30	18	03	-08	-03	04	04	03	02	-02	-14	-33	-43	-35	-20	-04	02	04	04	03	02	02	02	03	04	04	04	04	03	03	03	03	03	03	03	03	03	04	04	03	03
-1.75	-0.4	44	35	25	17	07	05	08	08	07	07	05	01	-05	-07	-05	02	06	06	05	04																						
-2.0	-0.6	45	38	26	20	13	10	08	08	08	09	13	15	18	19	17	15	11	07	05	04	04	04	04	04	04	04	04	05	05	05	05	06	06	06	06	06	06	05	05	05	04	
-2.25	-0.9	34	27	19	13	08	07	06	05	05	07	10	13	16	15	13	10	07	05	04	03	02	02	02	02	02	02	02	03	03	03	04	04	04	05	05	05	05	04	04	03		
-2.5	-1.1	27	22	17	12	07	05	04	04	05	07	08	10	10	09	07	05	03	02	02	01	01	01	02	02	02	02	02	02	02	02	03	03	04	05	05	05	05	04	03	02		
-2.75	-1.4	24	20	15	10	06	05	04	04	04	05	06	07	06	06	05	03	02	01	00	00	00	00	00	01	01	01	01	01	01	02	02	02	02	02	02	01	01	00				
-3.0	-1.6	19	16	13	09	06	05	04	04	05	05	06	06	06	05	04	02	01	01	00	00	00	00	00	01	01	01	01	01	01	01	01	01	00									
$\ell^I = 328.^\circ0$		$\ell^{II} = 000.^\circ3$																																
+0.5	+1.9	14	11	08	07	05	04	03	02	03	02	02	03	03	03	03	02	02	02	02	01	01	01	01	01	01	01	00															
+0.0	+1.4	27	22	18	15	11	08	06	05	05	06	05	05	05	05	05	04	04	03	03	02	02	02	02	01	01	01	01	01	01	01	01	01	01	01	01							
-0.25	+1.2	37	31	25	20	15	12	09	07	06	05	06	06	06	06	05	04	04	03	03	03	03	03	03	02	02	02	02	01	01	01	01	01	01	01	01	01	01	01				
-0.5	+0.9	40	34	27	22	18	15	13	11	10	10	10	10	09	09	09	08	08	07	06	05	04	04	03	02	02	01	01	01	00													
-1.0	+0.4	00	49	35	29	25	23	21	19	17	16	15	15	14	14	14	13	13	11	10	09	07	06	04	03	03	02	02	01	01	01	00											
-1.25	+0.2	00	42	29	18	10	08	07	07	06	04	02	00	-02	-04	-05	-03	00	04	06	06	05	04	03	02	01	01	01	01	01	00												
-1.5	-0.1	44	32	20	10	03	05	07	05	03	02	00	-05	-12	-16	-13	-05	03	06	07	06	05	05	04	04	03	03	03	03	03	03	03	03	03	03	03							
-1.75	-0.4	56	43	27	18	11	09	08	07	07	07	08	04	-03	-08	-08	-03	03	05	05	05	05	05	05	05	06	06	06	05	05	05	05	05	05	05	05	04						
-2.0	-0.6	46	34	23	18	12	10	08	07	09	11	14	17	18	18	16	13	10	07	05	04	04	04	05	05	05	05	06	06	06	06	07	07	07	07	06	06	05					
-2.25	-0.9	36	27	18	13	09	06	05	06	09	11	14	16	17	16	14	11	08	06	05	04	04	04	05	05	06	06	07	07	06	06	06	06	06	06	06	06						
-2.5	-1.1	28	21	15	09	05	05	06	07	08	10	12	12	11	09	07	06	04	04	03	03	03	04	04	04	03	03	03	03														
-3.0	-1.6	22	19	16	12	08	06	05	05	06	06	07	07	07	07	06	05	04	03	02	02	02	02	02	02	03	03	03	04	04	04												
$\ell^I = 328.^\circ5$		$\ell^{II} = 000.^\circ8$																																
+0.5	+1.9	11	10	09	08	06	05	05	04	04	03	04	04	04	04	04	04	04	03	02	02	01	02	02	02	02	02	02	02	02	02	01	01	01									
+0.0	+1.4	21	17	15	13	10	08	06	06	05	05	05	05	05	06	06	06	06	05	06	07	06	05	04	03	02	02	01	01	01	01	02	01	01	00								
-0.5	+0.9	43	36	31	27	21	17	13	10	09	10	10	10	10	09	09	08	07	06	04	03	03	02	01	01	00																	
-1.0	+0.4	00	50	36	30	25	23	21	20	19	19	19	18	18	17	16	15	14	13	12	10	09	08	06	05	04	03	02	01	01	01	01	01	00									
-1.5	-0.1	00	46	30	25	22	20	18	14	10	11	14	16	19	19	17	16	15	15	15	14	12	10	09	08	06	05	05	04	04	04	03	03	03	03	03	02	02					
-2.0	-0.6	37	29	22	18	14	14	15	16	19	22	23	23	21	19	16	13	11	09	07	06	06	05	05	05	06	06	06	06	05	04	04	03	03	03	02	01	00					
-2.5	-1.1	24	17	13	10	08	08	08	10	12	15	16	17	15	13	11	09	07	06	05	05	05	04	04	04	04	04	04	04	04	04												
-3.0	-1.6	19	14	10	08	07	06	06	06	06	06	07	07	06	05	04	03	02	02	01	01	01	01	01	01	01	01	01	01	01	01												
$\ell^I = 329.^\circ0$		$\ell^{II} = 001.^\circ3$																																
+0.5	+1.9	10	08	06	05	04	04	04	03	03	04	04	04	04	04	04	04	03	03	03	02	02	02	01	01	01	00																
+0.0	+1.4	17	14	12	10	08	07	06	05	05	05	05	05	05	05	05	05	05	05	04	04	03	03	02	01	01	01	00															
-0.5	+0.9	37	33	29	24	19	16	13	11	10	10	10	10	09	09	09	08	08	07	06	06	04	03	03	02	01	01	01	00														
-1.0	+0.4	58	50	40	33	26	23	22	22	23	23	22	21	19	16	14	12	10	09	08	07	06	05	04	03	02	01	00															
-1.5	-1.1	60	52	43	35	29	26	24	23	24	26	27	27	27	24	21	18	14	12	11	10	09	08	07	05	03	02	01	01	01	01	00											
-2.0	-0.6	39	32	25	20	18	18	21	23	25	27	28	24	19	15	12	09	07	06	05	05	04	03	03	03	03	02	02	02	01	01	01	01	01	01	01	01	01	00				
-2.5	-1.1	28	22	17	15	14	13	12	12	12	13	12	12	10	08	06	05	05	04	04	03	03	02	02	02	02	01	01	01														
-3.0	-1.6	18	14	11	09	08	07	06	06	06	06	06	05	05	04	03	02	02	02	02	02	02	02	02	02	02	02	02	02	02	02	02	02	02									
$\ell^I = 329.^\circ5$		$\ell^{II} = 001.^\circ8$																																
+0.5	+1.9	09	07	05	04	04	04	04	04	03	02	02	02	03	03	03	02	02	02	02	01	01	01	01	00																		
+0.0	+1.4	16	13	11	09	08	07	06	06	05	05	05	05	05	05	05	04	04	03	03	02	02	01	01	01	01	01	01	00														
-0.5	+0.9	32	28	24	21	18	17	14	13	13	13	13	13	13	12	11	10	09	08	07	06	05	04	02	01	01	01	01	00														
-1.0	+0.4	45	39	33	27	23	21	22	23	24	25	26	25	23	16	12	10	09	08	07	06	05	04	03	02	01	01	00															
-1.5	-0.1	53	48	41	35	30	27	28	31	35	36	34	29	22	16	11	09	07	07	06	06	05	05	04	03	02	01	00															
-2.5	-1.1	27	22	18	15	12	11	10	10	10	09	09	07	06	05	04	03	03	03	03	03	03	02	02	02	02	02	02	02	02	02												
-3.0	-1.6	14	11	10	08	07	06	04	04	04	04	03	03	03	03	02	02	01	01	01	01	01	01	01	01	01	01	01	01	01	01												
$\ell^I = 330.^\circ0$		$\ell^{II} = 002.^\circ3$																																
+0.5	+1.9	10	08	07	06	05	05	04	04	04	03	03	02	02	02	02	02	02	02	02	01	01	01	01	01	01	00																
+0.0	+1.4	15	13	12	11	10	09	09	09	08	08	08	08	07	07	06	05	05	04	03	03	02	02	02	01	01	01	01	01	01	01	00											
-0.5	+0.9	29	26	22	19	16	14	12	11	10	10	10	11	12	12	11	09	07	05	03	02	01	01	00																			
-0.75	+0.7	43	37	29	24	21	18	16	15	14	13	13	13	13	12	12	10	08	06	04	01	00																					
-1.0	+0.4	41	34	28	24	22	21	22	22	23	23	22	20	18	15	12	10	08	06	05	03	02	01	01	01	00																	
-1.25	+0.2	45	37	29	25	24	25	27	29	30	30	28	23	16	12	08	06	05	05	05	04	04	03	02	01	00																	
b^I	b^{II}	-20	-25	-30	-35	-40	-45	-50	-55	-60	-65	-70	-75	-80	-85	-90	-95	-100	-105	-110	-115	km/sec

TABLE 10 *(continued)*

b^I	b^{II}	−20	−25	−30	−35	−40	−45	−50	−55	−60	−65	−70	−75	−80	km/sec
−1.5	−0.1	48	38	31	26	24	26	29	34	37	36	33	26	19	11	08	06	05	05	05	04	04	03	03	02	02	01	01	00
−1.75	−0.3	48	42	31	25	20	19	23	29	32	31	24	18	12	06	03	02	01	00										
−2.0	−0.6	43	38	29	22	17	17	20	22	24	25	21	15	08	05	03	02	01	01	00									
−2.25	−0.8	00	31	25	20	16	13	13	14	16	16	14	10	07	04	02	01	00											
−2.5	−1.1	27	24	20	15	11	08	08	08	08	07	06	05	04	04	03	02	02	01	01	01	01	01	01	01	01	01	01	00
−3.0	−1.6	15	13	11	09	07	06	05	04	03	02	02	02	02	02	02	02	02	01	01	01	01	01	01	00				
$l^I = 330.°5$	$l^{II} = 002.°8$																												
−0.5	+0.9	31	25	19	16	14	12	10	09	08	08	09	09	11	12	11	08	05	03	01	00								
−1.5	−0.1	52	43	35	27	23	23	28	35	38	34	29	19	13	08	06	05	04	04	03	03	02	01	00					
$l^I = 331.°0$	$l^{II} = 003.°3$																												
−0.5	+0.9	36	28	20	16	13	11	09	09	10	11	12	11	10	09	07	04	03	01	00									
−1.0	+0.4	52	43	32	25	21	19	17	18	19	20	18	16	14	13	11	09	06	05	04	03	00							
−1.5	−0.1	60	49	38	30	27	29	31	31	29	25	19	13	10	08	06	06	05	04	03	02	02	01	01	01	00			
−2.0	−0.6	49	40	32	26	21	19	20	19	16	11	06	03	01	00														
−2.5	−1.1	34	30	25	21	15	11	08	06	04	03	02	02	01	01	00													
$l^I = 331.°5$	$l^{II} = 003.°8$																												
−0.5	+0.9	40	31	22	18	15	14	15	16	16	15	12	09	06	04	03	02	02	01	00									
−1.0	+0.4	59	48	37	31	26	24	24	25	24	21	18	15	11	08	05	03	01	00										
−1.5	−0.1	00	00	49	40	35	33	31	27	23	19	15	12	09	06	04	02	01	01	01	00								
−2.0	−0.6	51	43	37	34	30	26	21	16	11	06	01	00																
$l^I = 332.°0$	$l^{II} = 004.°3$																												
−0.5	+0.9	41	35	29	25	21	19	16	14	12	10	08	05	03	01	01	00												
−1.0	+0.4	00	50	43	39	34	29	24	21	18	15	11	07	03	01	00													
−1.5	−0.1	59	48	42	40	40	37	30	21	14	09	06	03	02	01	01	00												
−2.0	−0.6	48	42	39	36	34	31	24	15	08	06	04	03	02	01	00													
−2.5	−1.1	29	25	22	19	14	10	06	03	01	00																		
$l^I = 332.°5$	$l^{II} = 004.°8$																												
−0.5	+0.9	52	48	38	31	22	18	15	11	08	05	04	02	01	00														
−1.0	+0.4	00	00	52	44	35	27	21	18	15	11	05	02	00															
−1.5	−0.1	00	54	51	48	44	36	28	19	13	08	05	03	01	00														
−2.0	−0.6	44	39	34	34	33	28	19	12	05	03	03	03	01	00														
−2.5	−1.1	30	28	25	22	18	14	09	04	02	01	01	01	02	02	01	01	00											
$l^I = 333.°0$	$l^{II} = 005.°3$																												
−0.5	+0.9	48	39	29	21	14	10	07	04	03	01	00																	
−1.0	+0.4	00	00	46	39	32	26	19	14	09	06	04	03	01	01	00													
−2.0	−0.6	47	44	42	39	34	28	18	12	06	04	03	03	03	02	01	00												
−2.5	−1.1	33	29	25	21	16	13	10	07	04	03	02	01	01	00														
$l^I = 333.°5$	$l^{II} = 005.°8$																												
−1.0	+0.4	00	00	48	40	31	25	17	12	08	05	03	02	01	01	00													
−1.5	−0.1	00	59	54	45	35	27	17	11	07	06	04	03	02	01	00													
−2.0	−0.6	53	52	49	43	34	28	18	11	06	04	02	01	00	00	01	01	01	01	00									
−2.5	−1.1	35	33	29	25	20	17	13	10	07	05	04	03	01	01	00													
$l^I = 334.°0$	$l^{II} = 006.°3$																												
−1.5	−0.1	00	00	54	45	36	24	16	11	07	05	04	02	02	01	00													
−2.0	−0.6	00	59	48	41	32	25	17	13	08	05	02	01	00	00	01	01	01	01	00									
b^I	b^{II}	−20	−25	−30	−35	−40	−45	−50	−55	−60	−65	−70	−75	−80	km/sec

positions where the 3-kpc arm is not too much blended or is not blended at all. Profiles taken at these positions were used for a velocity and mass analysis as described in chapter 6. Dots refer to positions where blending is so strong that the profiles could not be used in the velocity analysis. Crosses are at positions where there is apparently strong absorption by Sgr A.

Nearly all profiles were measured with a bandwidth of 20 kc/s and a few with 10 kc/s. In the latter case this has already been indicated in the general survey. Numerical values of all the profiles are in table 10 for each 2.5 km/sec; this spacing gives all the details. The arrangement of the table is different from that in table 4. At each longitude the various latitudes have been brought together. This was done because in the analysis of the next chapter b–V diagrams are mainly used. Figure 20 shows four examples of these diagrams, at $l^{II} = -3°.7$, $0°.0$, $+2°.3$ and $+4°.8$, respectively. The effects of the blending with other features can be clearly seen. At $l^{II} = 0°.0$ one observes the absorption by Sgr A. The first two diagrams show the effect of "rolling", which will be described in chapter 8.

6. Analysis

6.1. *Determination of velocities and profiles of the arm*

As the 3-kpc arm stands fairly apart from the main maximum, only the wings of the features in the princi-

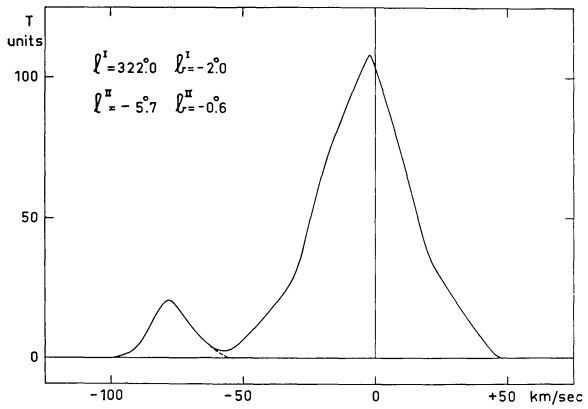

Figure 21. An example of an easy separation from the main maximum.

pal maximum interfere with it; these wings are extremely uncertain. Because of this we just guessed by visual inspection the separation of the 3-kpc arm from the main maximum, and, on the other side, its separation from the nuclear disk. This latter only influences the 3-kpc arm from $l^{II} = -2°.7$ to $-0°.7$. Figure 21 shows an example of how the separation was made for a position where a complete profile has been measured. The separation was more difficult at larger distances from the galactic plane, the intensities becoming rather low. The separation enables us to find N_H, the numbers of H I atoms in the line of sight per cm^2 in the arm. The results are given in section 6.4. From the guessed profile of the 3-kpc arm the median velocity V_m was determined, which has been used for further analysis. The results are in table 11. The profiles were now read off at equal velocities relative to V_m, and, for each latitude, the curves so obtained were averaged for the eleven longitudes measured in the interval $l^I = 320°$ to $325°$ ($l^{II} = -7°.7$ to $-2°.7$). These average profiles are shown in figure 22. The lower part of figure 22 gives the same for the interval $l^I = 325°.5$ to $328°.5$ ($l^{II} = -2°.2$ to $+0°.8$) (seven profiles, as $l^{II} = 0°.0$ was left out) for those latitudes where it was possible to determine V_m up to $l^I = 328°.5$, i.e., for $b^I = -2°.0$, $-2°.5$ and $-3°.0$ ($b^{II} = -0°.6$, $-1°.1$ and $-1°.6$).

From these figures one may get an impression of the manner in which the separation was made. The lower part of figure 22 shows clearly the serious blending by the nuclear disk, and the stronger blending by the main maximum.

6.2. *Reference velocities and systematic deviations*

At the latitudes $b^I = -0°.5$, $-1°.0$, $-1°.5$ and $-2°.0$ ($b^{II} = +0°.9$, $+0°.4$, $-0°.1$ and $-0°.6$) V_m could be determined with high precision. For each longitude in the interval $l^I = 320°$ to $327°$ ($l^{II} = -7°.7$ to $-0°.7$) a weighted mean V_m was determined from these four latitudes, using the areas under the profiles (which are practically proportional to N_H) as weights. The variation of this mean V_m as a function of longitude turned out to be very smooth and nearly linear.

The curve for V_m can be fitted to the following simple model, in which the arm is supposed to be circular and to have, over the interval considered, the same velocity of rotation and of expansion everywhere. We assumed that the arm becomes tangential at $l^{II} = -22°$, and that, therefore, its distance from the centre is 4 kpc. The expansion velocity was taken as 53 km/sec, as derived in section 7.3. The rotational velocity can be determined

TABLE 11
V_m (km/sec)

l^I \ b^I	+0.5	0.0	-0.5	-1.0	-1.5	-2.0	-2.5	-3.0
320.0	69.6	75.7	93.4	91.0	88.9	87.7	88.6	85.2
320.5	69.6	78.1	91.9	88.7	85.4		85.2	80.2
321.0	81.9	76.8	88.7	86.7	83.5	84.0	83.1	76.8
321.5	82.7	74.7	79.5	83.3	81.7	79.9	77.6	72.6
322.0	86.5	80.4	78.9	81.1	80.3	76.7	73.0	71.7
322.5	81.0	81.2	79.6	81.5	77.2	76.4	78.5	76.4
323.0	78.5	76.8	78.7	78.0	74.6	73.3	82.7	80.6
323.5	80.2	81.2	75.8	74.5	72.4	72.8	79.8	78.5
324.0	81.0	80.0	75.1	71.8	69.8	69.5	74.1	70.9
324.5	75.1	76.4	73.5	69.2	65.2	67.0	69.0	65.4
325.0	67.5	70.5	70.6	67.5	62.9	63.5	61.6	60.3
325.5			67.1	65.8	60.8	60.8	59.5	52.3
326.0		68.8	61.2 65.8	59.9 62.5	62.9 60.1	62.2 61.2	60.6	53.1
326.5			63.3	63.3	58.7	59.1	59.9	50.6
327.0			59.1 62.2	60.1 57.8	56.3 54.0	55.9 55.9	53.1	47.7
327.5							50.6	49.0
327.7						52.1 51.3	49.0 46.0	46.8
328.0						51.5 50.2	49.0	48.1
328.5					57.4	47.5	48.1	45.6

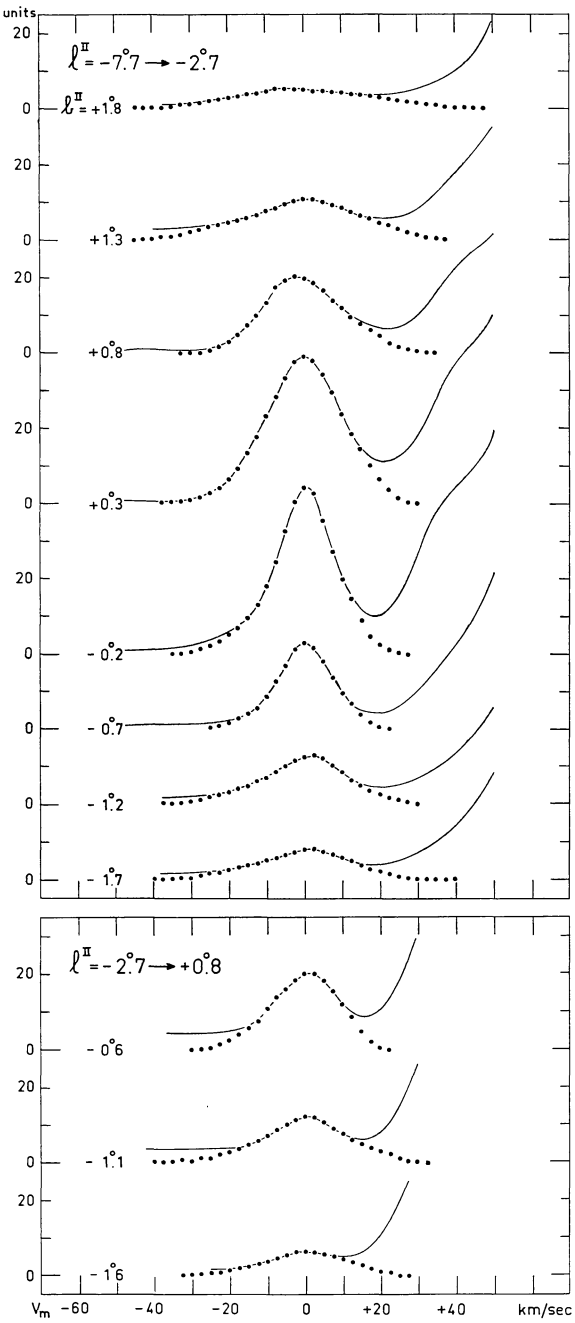

Figure 22. Averages of eleven profiles for $l^{II} = -7°.7$ to $-2°.7$ and of seven profiles for $l^{II} = -2°.7$ to $+0°.8$. The full-drawn curves are the observed profiles. The dots give the contribution due to the 3-kpc arm. This contribution has been estimated from the individual profiles.

at the tangential point; the old Australian value is $V = 122$ km/sec or $U = 203$ km/sec, assuming $\Theta_0 = 250$ km/sec. We have used $U = 204$ km/sec. However, for the transformation from U to the local standard of rest $\Theta_0 = 216$ km/sec has been used. As all computations had been finished before the new value of 250 km/sec was proposed, and the changes which would have resulted from a change to this new value would have been unimportant, it was decided to leave the results as they were. They are shown in table 12. For comparison we have added the unweighted average of the peak velocities for the same four latitudes. It may be noted that these averages fit the model equally well. In both cases the mean deviation from the model without regard to sign is ± 0.25 km/sec.

In the further analysis the velocities of the model have been used as reference velocities, relative to which we have studied the systematic motions within the arm. The deviations are by no means random. They are shown graphically in the upper part of figure 23, which indicates contours of equal deviation. A discussion will be given in chapter 8.

6.3. *The widths of the profiles*

The rather smooth kinematic structure of the arm can also be observed in the halfwidths of the profiles (the interval between the velocities where the intensity has dropped to half the peak value, figure 23). Comparison of the diagrams for systematic motions and halfwidths in figure 23 shows that there is but little correlation between the features on both charts. A discussion is given in chapter 8.

6.4. *Numbers of H atoms per cm² (N_H)*

By integrating the estimated emission of the 3-kpc arm we find N_H, the number of H I atoms in the line of sight. The results are in table 13 and in the lower part of figure 23. At higher longitudes we have taken double the free half of the profile at the negative side of the peak of the 3-kpc arm.

In the computations the arm was assumed to be optically thin. If we take account of the optical depth, assuming a temperature of 100 °K, the correct values of N_H become 2 per cent higher for higher latitudes and about 20 per cent higher for the central core of the arm.

6.5. *The emission as a function of galactic longitude and latitude*

Adding the four values for N_H for those latitudes at which complete observations for all longitudes were

TABLE 12

Velocities of the 3-kpc arm (in km/sec)

(All velocites are relative to the local standard of rest)

l^{I}	l^{II}	Model velocity	Weighted mean V_m	Model minus observed	Unweighted mean peak velocity	Model minus observed
320°	− 7°.7	− 89.3	− 90.4	+ 1.1	− 90.7	+ 1.4
320.5	− 7.2	− 87.1	− 87.7	+ 0.6	− 88.8	+ 1.7
321	− 6.7	− 85.1	− 85.4	+ 0.3	− 86.5	+ 1.4
321.5	− 6.2	− 82.8	− 81.5	− 1.3	− 82.5	− 0.3
322	− 5.7	− 80.6	− 79.7	− 0.9	− 80.2	− 0.4
322.5	− 5.2	− 78.1	− 79.4	+ 1.3	− 79.1	+ 1.0
323	− 4.7	− 76.0	− 76.4	+ 0.4	− 76.8	+ 0.8
323.5	− 4.2	− 73.6	− 73.8	+ 0.2	− 73.6	0.0
324	− 3.7	− 71.2	− 71.5	+ 0.3	− 71.1	− 0.1
324.5	− 3.2	− 68.8	− 68.0	− 0.8	− 67.9	− 0.9
325	− 2.7	− 66.5	− 65.4	− 1.1	− 65.6	− 0.9
325.5	− 2.2	− 64.0	− 63.4	− 0.6	− 62.5	− 1.5
326	− 1.7	− 61.6	− 61.7	+ 0.1	− 61.0	− 0.6
326.5	− 1.2	− 59.1	− 60.8	+ 1.7	− 58.9	− 0.2
327	− 0.7	− 56.6	− 57.8	+ 1.3	− 56.8	+ 0.2

made, viz. $b^{I} = -0°.5$, $-1°.0$, $-1°.5$ and $-2°.0$ ($b^{II} = +0°.9$, $+0°.4$, $-0°.1$ and $-0°.6$), we get a measure for the emission of the arm as a function of longitude (figure 24). The scale at the right-hand side will be discussed below. From this figure it can be seen that in the longitudes considered the emission is rather constant.

The general distribution in galactic latitude was studied by averaging over the various longitudes. We have split the longitude interval into two parts: $l^{I} = 320°$ to 325° ($l^{II} = -7°.7$ to $-2°.7$, heavy line in figure 25), and $l^{I} = 325°.5$ to 330° ($l^{II} = -2°.2$ to $+2°.3$, thin curve). The longitudes $l^{I} = 327°.5$, 327°.7 and 328°.0 ($l^{II} = -0°.2$, 0°.0 and $+0°.3$) have been omitted, so as to avoid too strong an influence of Sgr A. At high positive latitudes the distribution could not be obtained for the higher longitude interval, the intensities being too low. At high negative latitudes, between $b^{I} = -2°.0$ and $-3°.0$ ($b^{II} = -0°.6$ and $-1°.6$), the distributions for the two longitude intervals are practically identical. In the interval $l^{I} = 320°$ to 325° the distribution is quite symmetrical; the mean latitude is $b^{I} = -1°.20$ ($b^{II} = +0°.18$). It seems to be composed of a rather flat distribution with a superimposed sharp peak. The peak component is almost Gaussian, with $(N_H)_{max} = 1.30 \times 10^{21}$ atoms/cm^2, $b^{II}_{max} = +0°.18$, and a width between half-intensity points of 0°.71. This value is only slightly larger than the antenna pattern (0°.56), the corrected width thus being around 0°.3, or 40 pc (at a distance of about 7 kpc). The distribution in latitude for the second longitude interval, from $l^{II} = 325°.5$ to 330°, does not show this small peak. However, the accuracy is far less, especially at the latitude of this peak, where the absorption is strong.

The halfwidth of the underlying extended component is about 3°. The far wings were extrapolated, as indicated by the dashed lines of figure 25. Of course it is possible that there is still emission at far higher elevation from the plane.

6.6. *Total H I mass*

Integration of this distribution gives the number of H I atoms in the arm in a layer of 1 cm thickness perpendicular to the galactic plane and passing through the observer. In computing these numbers the distance was assumed to be 7 kpc. For the longitude interval $l^{I} = 320°$ to 325° the average number of atoms in such a slice is 1.6×10^{42}, corresponding to a mass of 1.4×10^{-15} solar masses. A correction for optical depth of 5 per cent has been applied. In the same longitude interval the mean value of N_H for the four latitudes between $b^{I} = -0°.5$ and $-2°.0$ was found to

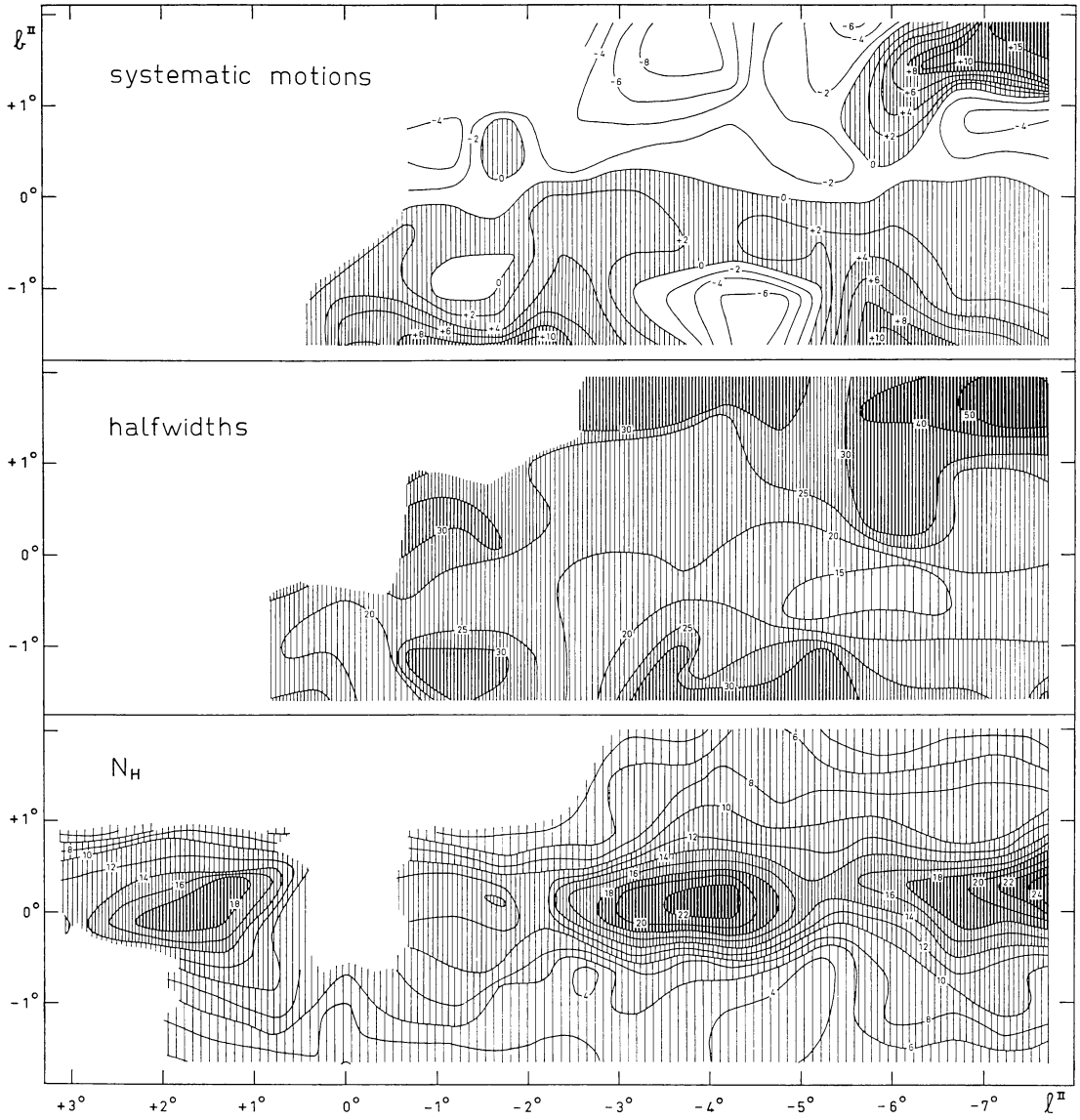

Figure 23. Contours of equal systematic motions (deviations from the reference velocities) in km/sec, half widths in km/sec and N_H in units of 10^{20} atoms/cm^2. The latter chart could be extended to higher longitudes because only half of the profile has been used. In the upper chart the positive systematic motions are hatched.

be 1.4×10^{21} atoms/cm^2 (section 6.5). The number of atoms in a slice is thus a factor 1.1×10^{21} higher. The scale on the right-hand side of figure 24 has been obtained by applying this factor. For the longitude interval $l^{I} = 325°.5$ to 330° the average number of atoms in a slice was found to be 1.0×10^{42}. Comparing this with the corresponding average of N_H we obtain a factor of 0.9×10^{21}, somewhat lower than the factor for the other longitude interval. However, between $l^{I} = 325°.5$ and 330° the values of N_H are quite uncertain, due to the possibility that the influence of Sgr A extends farther than the positions which have been omitted, and because at greater distances from the plane the determination of the contribution of the 3-kpc arm was very uncertain for these longitudes. For these reasons we assume that the values for the lower longitude interval are more reliable and they are used in the following computation.

TABLE 13

N_H (10^{21} atoms/cm^2)

l^I \ b^I	+0.5	0.0	-0.5	-1.0	-1.5	-2.0	-2.5	-3.0
320.0	0.34	0.73	1.37	2.53	1.93	0.95	0.92	0.45
320.5	0.47	0.81	0.95	2.12	1.75		1.04	0.55
321.0	0.40	0.78	0.91	1.89	1.80	1.24	0.81	0.52
321.5	0.29	0.74	1.04	1.79	1.29	0.89	0.90	0.54
322.0	0.28	0.70	1.14	1.63	1.07	0.69	0.69	0.50
322.5	0.45	0.76	1.05	1.39	1.12	0.28	0.32	0.41
323.0	0.74	0.72	1.04	1.68	1.71	0.57	0.33	0.37
323.5	0.61	0.90	1.10	2.05	2.11	0.72	0.40	0.37
324.0	0.37	0.74	1.14	1.95	2.01	0.69	0.50	0.46
324.5	0.39	0.73	0.74	1.75	2.00	0.86	0.61	0.55
325.0	0.31	0.40	0.52	1.41	1.58	0.36	0.52	0.33
325.5			0.42	1.12	1.03	0.64	0.52	0.32
326.0		0.25	0.39 0.60	1.08 1.41	1.26 1.06	0.96 0.48	0.49	0.33
326.5			0.34	1.30	1.14	0.99	0.75	0.27
327.0			0.53 0.96	1.25 1.21	1.19 1.00	0.84 0.73	0.72	0.29
327.5							0.48	0.27
327.7						0.62 0.51	0.33 0.26	0.22
328.0				0.81		0.66 0.65	0.53	0.39
328.5			0.60	1.59	1.04	1.06	0.87	0.33
329.0				1.83	1.77	1.17	0.68	0.30
329.5			0.96	1.49	1.87		0.52	0.22
330.0			0.53 0.52	1.38 1.53	1.80 1.11	0.79 0.53	0.38	
330.5			0.34		1.40			
331.0			0.49	1.16	1.54	0.63		

We assume that the average distance of the arm from the centre is 3 kpc. Its length is at least a quarter of the circumference of a circle, or 4 700 pc = 1.4×10^{22} cm. In order to obtain the mass of the arm we multiply this by the mean mass of a slice of 1 cm thickness, which was found to be 1.4×10^{-15} solar masses. So the H I mass of the observed part of the arm is at least 2.0×10^7 times the mass of the Sun. The total mass of the expanding arm might well be 50 per cent higher.

A comparison of this value with the total mass as found in section 4.7 (which has been principally determined from the positive-longitude side) shows that the arm contains about half the total mass. This supports to some extent the assumption made in drawing figure 1 that the 3-kpc arm is the only expanding feature in the longitude interval between $-5°$ and $-22°$.

The D.T.M. and C.S.I.R.O. (KERR, HINDMAN and GUM, 1959) measurements made in this interval (cf. figure 12) show that the simple structure which we have found in the interval $l^{II} = -3°$ to $-8°$, does not continue beyond $l^{II} = -12°$. At this longitude the distribution of the emission becomes more like that at positive velocities. There is an interruption in the arm between $-11°$ and $-13°$ longitude, and beyond that

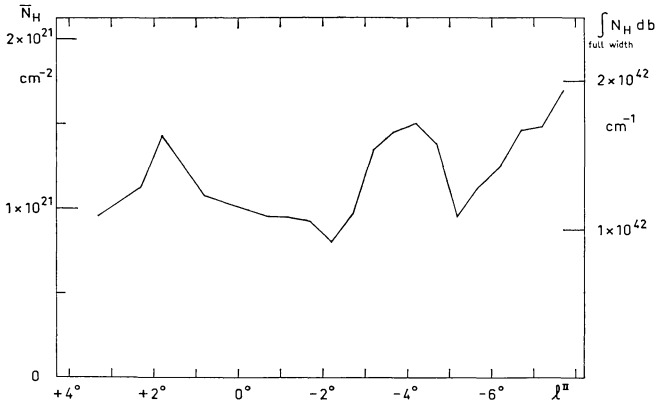

Figure 24. Variation with longitude of $\bar{N}_H$, averaged over latitudes $b^I = -0°.5$, $-1°.0$, $-1°.5$ and $-2°.0$ ($b^{II} = +0°.9$, $+0°.4$, $-0°.1$ and $-0°.6$). The ordinate at the right side gives the number of H I atoms in a slice of 1 cm thickness. Longitudes $l^I = 327°.5$, $327°.7$ and $328°$ ($l^{II} = -0°.2$, $0°.0$ and $+0°.3$) have been omitted because of the absorption effects.

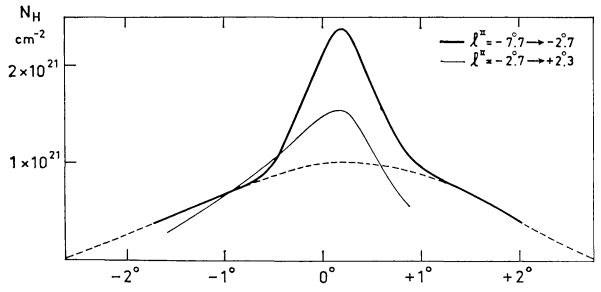

Figure 25. Distribution in latitude for two longitude ranges. The heavy curve has been corrected for optical depth. The dashed lines at both sides are the extrapolations used to determine the area under the curve. The dashed line near the centre separates the sharp core from the "normal" emission.

interval the structure is more complicated than in the longitudes above $-12°$. However, the 3-kpc arm remains the principal feature in this whole region. The general symmetry of the H I emission in the central region has already been discussed in section 4.7.

7. The absorption at Sagittarius A

7.1. *The source Sagittarius A*

The source Sgr A was among the first discovered radiosources. It has been discussed by a large number of authors. However, a satisfactory explanation of the nature of the source, or rather of the complex of sources, cannot yet be given. Insufficient angular resolution, especially at the lower frequencies, is the main obstacle for constructing a satisfactory model. The highest resolution, of 1′ in right-ascension, has been attained by the Soviet observers with the large Pulkovo telescope at 3-cm wavelength (PARIISKII, 1961). The resolution in declination was 40′. The measurements of LEQUEUX (1962) with an interferometer at $\lambda = 21$ cm yielded an east-west resolution of 2′. Both the Soviet and the French observations were made practically along an east-west line; the information on the real distribution is, therefore, incomplete. Complete information is given in the isophote chart by DRAKE (1959a, b, c), who observed at the minimum wavelength, $\lambda = 3$ cm, of the Green Bank 25-metre telescope, with a beamwidth of 6′. Cooper and Price (cf. KERR, 1962) obtained the same results at $\lambda = 10$ cm, with a similar beam. The measurements of Pariiskii and of Lequeux show that even a resolution of 6′ is insufficient to study the detailed structure. MILLS *et al.* (1958, p. 83) obtained at $\lambda = 3.5$ m a resolution of 0°.7, a resolution which, so far, has not been improved at such a long wavelength.

For our purpose a discussion of the source is needed for two reasons:

a) The distribution of the continuous radiation at $\lambda = 21$ cm influences the absorption profile as obtained in section 7.3.

b) The source is part of the nuclear disk, which will be described in part IV of this article.

The complex of sources which together are called Sgr A, consists of four components which are probably thermal, embedded in a larger concentration of emission which appears to be partly non-thermal. The data concerning the thermal components, which have been taken from the article of Lequeux, have been collected in table 14.

WESTERHOUT'S (1958) cross-section at $\lambda = 21$ cm through the nucleus along the galactic equator has been derived from his drift curves at constant declination. To improve the accuracy we have measured the distribution directly by scans along the galactic equator, moving the telescope at the appropriate rate in right-ascension and declination. From the discussions by Lequeux and by Pariiskii, together with our own measurements we can derive a satisfactory model of the continuous emission at $\lambda = 21$ cm. The fluxes of the thermal components at $\lambda = 21$ cm being known from

TABLE 14

Source	l^{II}	Diameter		(pc)	Flux [10^{-26} watt · m^{-2} · (c/s)$^{-1}$]	T_b (at $\lambda = 21$ cm) (°K)
A	− 0°.07	3′.5	0°.06	10	300	5 900
B1	+ 0.07	15	0.25	40	300	300
B2	+ 0.60	—	—	—	100	—
B3	− 0.64	—	—	—	15	—

the observations at shorter wavelengths, we can smear out the three strongest components with the beam of our antenna (0°.56). The broadened distributions in longitude (for $b^{II} = -0°.06$) are shown in the lower part of figure 26. The two brightest sources, which have both a flux density of 300×10^{-26} watt $\cdot$ m$^{-2} \cdot$ (c/s)$^{-1}$, have been assumed to lie at $l^{II} = +0°.07$ and $-0°.07$. For comparison we have drawn a scan on an arbitrary scale derived from Drake's chart at $\lambda = 3$ cm. The upper half of figure 26 shows the averaged scan with the Dwingeloo telescope. The Dwingeloo curve is rather accurately symmetric around $l^{II} = 0°.00$. The zero-point of galactic longitudes is indeed principally based on

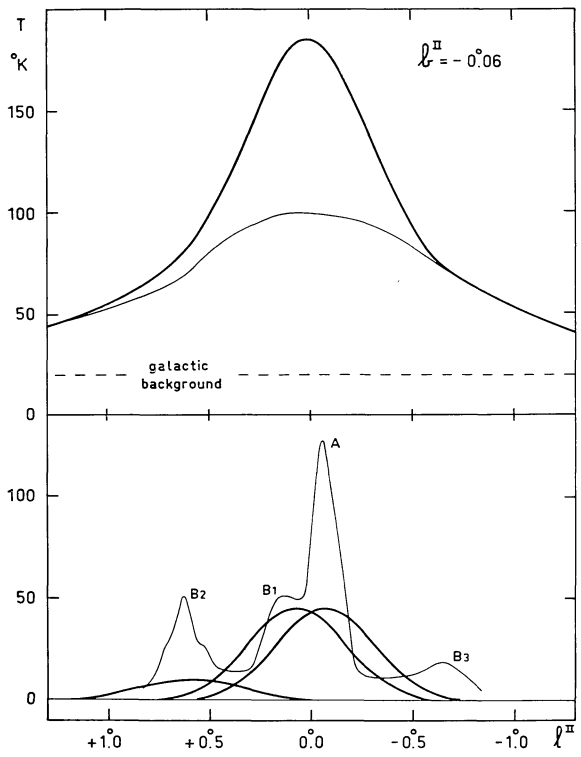

Figure 26. The distribution of continuous radiation in the Sagittarius source. The upper heavy curve gives the distribution along the galactic equator at $\lambda = 21$ cm as measured with the Dwingeloo telescope. In the lower part the thin line gives a scan on an arbitrary scale derived from Drake's isophote chart ($\lambda = 3$ cm). The different components are designated in the same way as was done by LEQUEUX (1962). The three heavy curves give components A, B1, B2, smoothed out by the beam of the Dwingeloo telescope. (Sources A and B1 have about the same total flux.) These components have been subtracted from the upper curve; the remaining radiation indicated by a thin line, comes from the extended source, which is partly thermal and partly non-thermal.

scans through the galactic centre at $\lambda = 21$ cm and with this resolution. It was somewhat surprising to see that the thermal components, which are so different from each other, did not spoil the symmetry.

We have subtracted the three sources from the observed 21-cm scan as shown in figure 26. The remaining distribution is again fairly symmetrical. The longitude of the point of symmetry is $l^{II} = -0°.02 \pm 0°.02$. After subtracting also the general galactic background radiation, estimated at 20 °K (WESTERHOUT, 1958), we are left with a source of 80 °K central temperature and 1°.7 halfwidth.

The four thermal sources can hardly have any effect on the distribution of the continuous radiation at $\lambda = 3.5$ m as observed by Mills, although they are all optically thick at this wavelength. Even source B1, which occupies an area of 0.06 square degrees at most, is small compared to Mills' beam of about 0.7 square degrees. Nevertheless an absorption dip is visible on the 3.5 m survey. The only possibility to understand the absorption dip is to assume an extended thermal source with a diameter of the order of one degree. It is impossible to derive from the dip at $\lambda = 3.5$ m the flux density of the thermal source, as the optical depth will be large over the whole area of the source.

If we assume, somewhat arbitrarily, that this thermal source absorbs half of the emission of the non-thermal source, we can derive from the 3.5 m survey the amount of non-thermal radiation at $\lambda = 21$ cm. At the latter wavelength the optical depth is small and we did not take it into account.

Mills' brightness temperature at $l^{II} = 0°$ is about 30 000 °K (this value is already corrected for half of the general galactic non-thermal background radiation of about 5 000 °K). Taking account of the absorption by the thermal source, we find 60 000 °K for the maximum of the non-thermal emission. Assuming a value of 1 430 for $T_{3.5\,m}/T_{21\,cm}$ (WESTERHOUT, 1958) we have a top of about 40 °K at $\lambda = 21$ cm for the non-thermal source. This is half the maximum intensity of the extended source of figure 26. The extended thermal source will therefore have about the same maximum brightness temperature of about 40 °K as the extended non-thermal source and a flux density of about $1\,000 \times 10^{-26}$ watt $\cdot$ m$^{-2} \cdot$ (c/s)$^{-1}$. This corresponds to 10 °K at $\lambda = 10$ cm and 1 °K at $\lambda = 3$ cm. The non-thermal source has at these wavelengths about half these values. From

Drake's isophote chart, Lequeux found about 700×10^{-26} watt $\cdot$ m$^{-2} \cdot$ (c/s)$^{-1}$ for the flux at ($\lambda = 3$ cm) of the whole complex within $T_b = 1$ °K, excluding the individual sources. This confirms that there *is* an extended thermal source, with a flux of the same order of magnitude as that found above. Many other combinations are possible. For instance, we can add some non-thermal radiation to the concentrated components. However, too large an admixture of such radiation would be in contradiction with LEQUEUX's interferometer measurements at $\lambda = 21$ cm (1962). We can also change the ratio between the extended thermal and non-thermal sources considerably; the intensities assumed above rest on the inaccurate values at $\lambda = 3.5$ m and 3 cm. For our interpretation of the absorption features, to be described in section 7.3, we shall use the intensity distribution in Sgr A as shown in figure 26. Its connection with the nuclear disk will be described in chapter 10.

7.2. *The expected profile*

A second difficulty in obtaining the correct absorption pattern lies in the determination of the "expected profile", i.e., the emission profile which would be observed if the source would not be present. The normal procedure for determining the expected profile at the position of a radio source is to measure a number of profiles around the source, and from these to interpolate the profile needed.

In the present case the following additional difficulties arise. In the first place the width of the H I layer is very small. This means that we have to obtain the expected profile from profiles at about the same latitude as the source, i.e., at $b^{\mathrm{I}} = -1°.5$ ($b^{\mathrm{II}} = -0°.1$). In the second place the source is extended in the direction of the galactic plane. As a consequence, we have to take the comparison profiles at fairly large distances from the source. Because of these large distances we have to apply a velocity correction. We have used the profiles at about 2°.5 from the source, i.e., at $l^{\mathrm{I}} = 325°.0$ ($l^{\mathrm{II}} = -2°.7$) and $l^{\mathrm{I}} = 330°.0$ ($l^{\mathrm{II}} = +2°.3$) for determining the expected profile. First, the shift in velocity between the two profiles was determined. This was done by matching the negative-velocity sides of the profiles, which are uncontaminated by radiation from the main maximum, and could therefore be matched with high precision (within about 0.5 km/sec). The shift was thus found to be 22.5 km/sec, or 4.5 km/sec per degree in longitude. By applying a shift of + 12.2 km/sec to the profile at $l^{\mathrm{I}} = 325°.0$ ($l^{\mathrm{II}} = -2°.7$) and − 10.3 km/sec to the profile at $l^{\mathrm{I}} = 330°.0$ ($l^{\mathrm{II}} = +2°.3$) the velocities of the two profiles were reduced to $l^{\mathrm{II}} = 0°.0$. The two profiles, shifted in this manner, are shown in the upper part of figure 27. They do not differ very much. We adopt the mean as expected profile; only above − 47 km/sec the profile at $l^{\mathrm{I}} = 325°$ ($l^{\mathrm{II}} = -2°.7$) was taken rather than the average of the two, because for these velocities the other is blended by the main maximum. At $l^{\mathrm{II}} = 0°.0$ no blending will occur for the velocities in which we are mainly interested (velocities below − 42 km/sec).

For comparison we have also drawn the mean profile at $b^{\mathrm{I}} = -1°.5$ ($b^{\mathrm{II}} = -0°.1$) for $l^{\mathrm{I}} = 320°$ to 325°

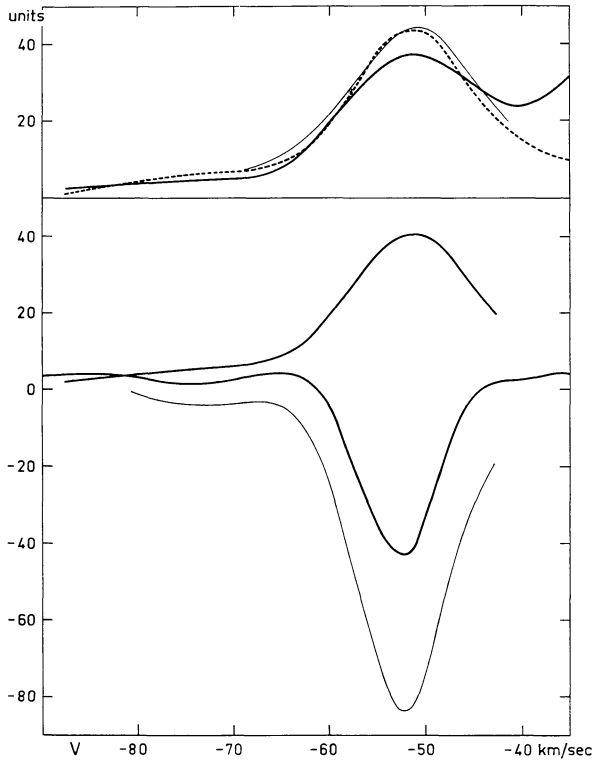

Figure 27. The absorption of Sgr A. The upper part shows emission profiles of the 3-kpc arm at $l^{\mathrm{II}} = -2°.7$, $b^{\mathrm{II}} = -0°.1$ (dashed curve) and $l^{\mathrm{II}} = +2°.3$, $b^{\mathrm{II}} = -0°.1$ (heavy curve); the thin line is the profile at $b^{\mathrm{II}} = -0°.1$ averaged over the longitude interval between $l^{\mathrm{II}} = -7°.7$ and $-2°.7$. The velocities are reduced to $l^{\mathrm{II}} = 0°.0$ as described in the text. The expected profile shown in the lower part is based on the curves in the upper part. The lower figure shows the observed (heavy curve) and the "true" (thin curve) absorption profiles.

($l^{II} = -7°.7$ to $-2°.3$). The close correspondence of this profile with the expected profile as derived above indicates that we may have some confidence in this expected profile. However, we must keep in mind that undoubtedly, local irregularities exist – as can be seen in figure 24, for instance – and that there must be a corresponding uncertainty in the expected profile.

7.3. *The true absorption*

The lower part of figure 27 gives the observed profile together with the expected profile. The difference between the two gives what is generally called the true absorption, which has been indicated by a thinner line. Both profiles and the absorption are symmetrical. The mean velocities, the halfwidths in km/sec and the central intensities in units ($\approx$ °K) are in table 15.

TABLE 15

	V (km/sec)	$(\Delta V)_{\frac{1}{2}}$ (km/sec)	Central temperature
Expected profile	51.4	17.0	41
Observed profile	52.8	9.3	– 43
Absorption	52.4	11.2	– 84

The smallness of the halfwidth of the absorption is remarkable as compared to that of the emission. The true absorption profiles of most strong radiosources e.g. Cas A and Tau A have small halfwidths. However, these radiosources have a small angular size and the small widths measured are due to the fact that there are only a few clouds between the source and the observer, each of which gives an absorption line broadened only by thermal motions and small internal cloud motions. If there are many clouds in front of the source, such as might be the case if the source has a considerable angular size, the width of the absorption profile should be equal to that of the expected emission profile. If we should not know the complicated structure of Sgr A, and if we should assume that the absorption profile was due to the combined effect of a large number of clouds, we should determine the optical depth of the 3-kpc arm in front of the source simply by the formula

$$\Delta T = T_c\,(1 - e^{-\tau}),$$

where $\Delta T = 84$ °K is the central true absorption, and $T_c = 165$ °K represents the central intensity of the source Sgr A (section 7.1). In that case τ would be equal to 0.71. The relation

$$T = T_{exc}\,(1 - e^{-\tau}),$$

where T is the maximum intensity of the expected emission profile (41 °K), and T_{exc} is the excitation temperature in the arm, then gives an excitation temperature of 81 °K.

However, both the complicated structure of Sgr A, as described in section 7.1, and the difference between the halfwidths of the absorption and the emission profiles indicate that the absorption cannot be treated in this simple manner. The observed halfwidth is considerably smaller than the halfwidth of the emission, while, on the other hand, it is considerably larger than the halfwidth we can expect for individual clouds.

The following analysis gives an example how the observed absorption might be interpreted. We want to stress that this interpretation is by no means the *only* possibility. A real analysis would only be possible by new observations with a very small bandfilter (of the order of 5 kc/s or less) and a much smaller angular beam (say about 0°.10). We suppose that there is only one cloud in front of the concentrated component A, and that the cloud covers this component completely. Let the optical depth be $\tau_{cloud}\,(V)$ and let the velocity be nearly equal to the central velocity of the whole absorption profile. The H I in front of the extended source (see section 7.1) will also cause an absorption. The halfwidth of this absorption will be approximately the same as that of the expected emission, because many clouds will contribute to this absorption. We shall denote its optical depth by $\overline{\tau\,(V)}$. A comparison of the expected emission profile with the true absorption, indicated that the velocity of the hypothetical cloud in front of component A may differ somewhat from the average velocity of the arm, as might have been expected. The brightness temperature of component A is about 45 °K. The maximum brightness temperature of the extended source is 80 °K (section 7.1). If the source B1, with a brightness temperature of 45° K, is extended enough to be covered by a large number of clouds, the observed absorption $\Delta T\,(V)$ in °K can now be written as

$$\Delta T\,(V) = (80 + 45)\,[1 - e^{-\overline{\tau(V)}}] + 45\,[1 - e^{-\tau_{cloud}(V)}].$$

We suppose that both $\overline{\tau\,(V)}$ and $\tau_{cloud}\,(V)$ have a

Gaussian distribution around the same average velocity; for the former we have assumed a halfwidth of 15 km/sec, comparable to that of the emission profile, while the halfwidth of the cloud was, rather arbitrarily, taken to be 4 km/sec. The optical thickness of the cloud was supposed to be large ($\tau = 3$ in the centre of the line).

The maximum value of $\Delta T(V)$ is 84 units, of which $45(1 - e^{-3}) = 43$ units would be due to the small cloud in front of component A. The remaining 41 units must be due to the extended source plus component B1. From the relation given above and the known maximum of the expected emission profile we then obtain $\bar{\tau}_{max} = 0.40$, and $T_{exc} = 125$ °K. In this case the excitation temperature is not different from what has been found elsewhere in the Galactic System (WESTERHOUT, 1957). One should expect that the absorption of the cloud in front of component A would be visible as a narrow dip below the broader absorption due to all clouds in front of the extended source plus B1. But, because of the large optical depth assumed for the individual cloud, the dip is smoothed out. The absorption computed from the above model is shown in figure 28, together with the observed true absorption.

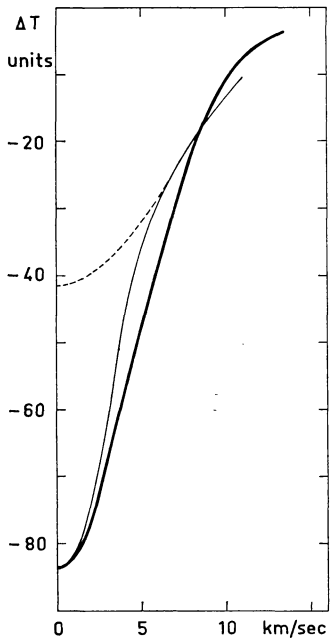

Figure 28. Observed true absorption (heavy line) and computed absorption (thin line). The dashed line shows the contribution of the broad component.

The agreement is quite reasonable. We did not try to get a better fit, because the uncertainties in the parameters governing the absorption are too large. As we have already pointed out, the model considered is quite arbitrary. We have given it only to indicate the uncertainty in the interpretation of the results, and, in particular, to show that there is no absolute need to assume a lower value for the excitation temperature in the 3-kpc arm, or a lower velocity dispersion for the part of the absorption profile that is due to the extended source. But one should not conclude from this example that the excitation temperature *is* really about 125 °K, but rather that the margin of uncertainty extends from about 60 to 125 °K. CLARK, RADHAKRISHNAN and WILSON (1962) have observed the absorption in Sgr A with an interferometer consisting of the two 90-ft dishes of the Owens Valley Radio Astronomy Observatory. They found a very narrow dip (width about 4 km/sec) at − 54 km/sec. Although their method is alright for point-sources, it is impossible to analyse the data for Sgr A without additional observations. Their results were derived from observations at a single east-west base-line of 300 wavelengths. It should be possible to derive a complete and decisive picture in l, b and V by this method by using different spacings and directions of the base-line.

8. General structure of the 3-kpc arm and comparison with the Andromeda nebula

In sections 6.2 and 6.3 we have found that the systematic motions and the values for the halfwidths of the profiles form a well-defined pattern on the sky. In figure 23 these patterns are shown together with the isophotes of N_H. Is there any correlation between these parameters? The N_H chart does not reveal anything unexpected. The arm shows patches such as we generally observe in spiral galaxies. On the chart of the systematic motions we should expect that negative and positive velocities would occur to about the same amounts on both sides of the axis of the arm, because the four inner latitudes (i.e. $b^{II} = +0°.9$, $+0°.4$, $-0°.1$ and $-0°.6$) were used to determine the reference velocities. It is striking that the 0 km/sec line practically coincides with the axis of the arm, as shown on the N_H chart over the whole longitude range considered. From the plot of the halfwidths we see that these have a tendency to be smaller near the central line, but the distribution is

rather irregular. The effect would have been somewhat more pronounced if the optical thickness of the arm had been taken into account. The halfwidth becomes exceptionally large in a region around $l^{II} = -7°$, $b^{II} = +1°.5$; in the same region there is a very pronounced positive systematic motion. The N_H contours, however, do not show any peculiarity in this direction. There might, however, be a relation between the minimum at $l^{II} = -5°.5$, between the patches of high N_H and the separation at the same longitude between positive and negative systematic motions at higher latitudes. At longitudes above $l^{II} = -2°$ we get a more complicated picture, but here the contours are less accurate. From the contours of systematic motion one gets the impression that in the strip about $b^{II} = -1°.0$ and $+1°.0$ the core of the arm is rolling around its axis with a velocity of about 2 km/sec. At larger distances from the axis the systematic motions do not follow this pattern. Here they apparently reflect more complicated gas streams at the surface of the arm.

It is of some interest to compare our observations of the inner arms in the Galactic System with observations of the Andromeda nebula. BAADE (1951, 1963; BAADE and MAYALL, 1951) has investigated the arms in the inner part of M 31, by studying the distribution of the dust and the emission nebulae. His innermost arms (N_1, N_2, S_1 and S_2 in his notation) are only visible by their dust components. These dust features at distances between 1 and 3 kpc from the nucleus (about 15′ along the major axis) are more irregular, and reflect probably the irregular structure we found at the positive-velocity side of our profiles.

Using a relatively high dispersion spectrograph, MÜNCH (1960) has observed emission of [O II] at $\lambda = 3\,727$ Å in the immediate vicinity of the centre of M 31. His observations extend to 600 pc. The observations along the minor axis indicate that there are considerable radial motions, up to about 40 km/sec within 300 pc from the nucleus. In the Galactic System COURTÈS and CRUVELLIER (1960a, b) have found H_α emission at about the same distance from the nucleus. There is no evidence for the existence of *radial* components in this case.

Perhaps a large region, between 0.5 and 3 or 4 kpc, in M 31 is devoid of gas, similar to the Galactic System at negative velocities, where no gas is found between the 3-kpc arm and the nuclear disk. A regular feature starts 8′ east of the nucleus, at a distance of 4 kpc. This feature is only clearly visible by its emission nebulae, of which 25 have been found in the range between the starting point and the turning point N_3 at 4.6 kpc on the north-following side of the major axis. From this turning point on a dust lane can be followed to a second group of seven emission nebulae. However, it is doubtful whether the arm N_3 is connected with this dust lane and the second group of emission nebulae, because the nebulae lie at a distance of 4 kpc from the centre, 8′ north of it. If they were part of this arm, this would again turn somewhat inwards, which is not very likely. It seems better to start with the second group (which might eventually be the continuation of the turning point N_2 at $R = 1.5$ kpc). South-west of these seven emission nebulae begins a very pronounced dust lane, in which no (or perhaps two) emission nebulae have been observed. The most probable reason for this absence of nebulae is the extremely heavy absorption. This dust lane comes out very neatly at the turning point S_3 on the major axis 30′ south-preceding the centre. Some eight emission nebulae have been found here.

Either of the two features described might correspond to the 3-kpc arm. There might be a possibility to test whether there exists in M 31 an expansion similar to that of the 3-kpc arm, by measuring the radial velocities of the few emission nebulae just mentioned. By observing the two groups of emission nebulae situated at about equal distances from the major axis it might be possible to eliminate the transverse component. In our galaxy WESTERHOUT (1958) found a ring of thermal emission at a distance of 5 kpc from the centre, just outside the 3-kpc arm, which latter probably has its tangential point at $l^{II} = -23°$ (figure 12), corresponding with $R = 4$ kpc. The sharp edges of the thermal emission at $l^{II} = \pm 30°$ have been confirmed by MATHEWSON, HEALEY and ROME (1962). The observed distribution of the thermal radio emission indicates that in our Galaxy the central region contains very few emission nebulae, just like in M 31. Another indication might be the absence of any emission around -50 km/sec, corresponding to the velocity of the 3-kpc arm, on the H II plates taken with the Fabry-Pérot interferometer of Courtès (private communication). However, this does not prove that there *is* no emission

in the arm, because on one hand the absorption in front of the arm is likely to be of the order of 10^m, and on the other hand the surface he has surveyed is so small (three fields of 9′ diameter) that there was little chance of finding large emission nebulae, even if they would be as frequent as in the outer arms.

PART IV
THE NUCLEAR DISK

9. Special measurements

We have seen from the l–V diagrams (figures 8 to 11) that there is evidence of a rapidly rotating disk of hydrogen extending to about 750 pc from the centre. In order to investigate the structure of this disk it was decided in the beginning of 1959 to make more detailed observations. As the velocities in the innermost part of this disk ($-2° < l^{II} < +2°$) showed a surprisingly steep slope in the l–V diagrams, we started our measurements in this inner region. For the negative velocities, where the disk stands quite apart, these observations were made from January until April 1959; for the positive velocities between June and November 1959. Profiles were taken with a spacing of 0°.25 in l and b, which is small compared with the beam of 0°.56. A good velocity definition was not necessary, because the profiles have a very broad distribution in velocity. So we chose C measurements (see section 2.2) for this programme. The eight channels of the receiver, which are 50 kc/s (10.6 km/sec) apart, cover a frequency range of 400 kc/s, or a velocity range of about 85 km/sec. The bandwidth used was 20 kc/s. The negative sides of the profiles were obtained in this manner by two measurements, each lasting 15 minutes. For the positive side we needed three measurements, because we also observed the velocity interval which the 3-kpc arm covers at the negative side. However, these C measurements are not very well suited for the investigation of this arm, because of the poor resolution in velocity. For a large part of the profiles more measurements were made in the same velocity interval, but at slightly different frequencies. Therefore these measurements improved the accuracy of the intensities, but did not add appreciably to the velocity resolution.

An example is given in figure 29. The 3-kpc arm is also drawn, for comparison. Figure 30 gives the

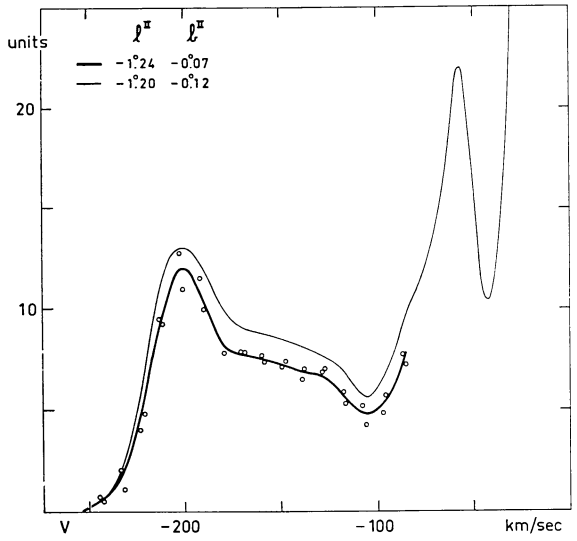

Figure 29. Sample of C measurements (circles and heavy curve). The heavy line is the adopted curve through the circles. The thin line gives, for comparison, a profile of the "general survey" at approximately the same position. The sharp peak at about −60 km/sec is due to the 3-kpc arm. The difference between the thin and heavy line demonstrates the difficulties in determining the zero level.

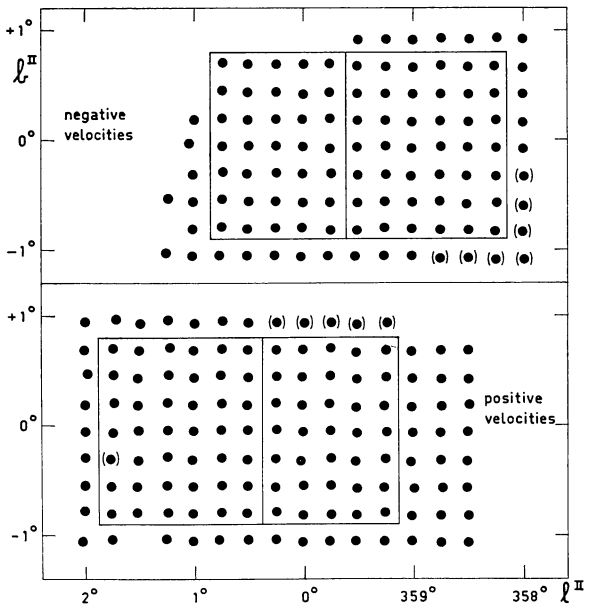

Figure 30. Positions where C measurements of the disk were made. Incomplete measurements are indicated by parentheses. The smaller and larger regions used for the integrations (see section 10.1) are indicated.

TABLE 16

(In order to avoid decimals in the table the unit used is half that used throughout this article, or about 0.5 °K)

l^{II}	b^{II}	- 90	-100	-110	-120	-130	-140	-150	-160	-170	-180	-190	-200	-210	-220	-230	-240	-250	km/sec
358.00	+0.92	04 02 01 02 02 03 04 05 05 06 06 06 06 06 05 05 05 04 04 03 03 03 02 02 01 01 01 00																	
358.20	+0.93	03 02 02 02 02 03 03 03 04 04 04 04 03 03 03 02 02 01 01 00																	
358.40	+0.92	03 03 03 03 03 03 03 03 03 03 03 03 02 02 01 01 01 00																	
358.74	+0.92	05 04 03 03 03 03 02 02 02 02 02 02 02 01 01 01 00																	
358.99	+0.91	06 05 04 03 03 02 02 02 01 01 01 00																	
359.24	+0.92	06 05 04 04 03 02 02 01 01 00																	
359.50	+0.91	05 04 04 03 02 02 01 01 00																	
359.75	+0.94	05 04 03 03 02 01 01 00																	
358.01	+0.66	06 04 03 02 02 02 03 04 05 05 06 06 07 07 07 08 08 08 08 08 08 07 07 06 06 05 05 03 02 01 00																	
358.26	+0.67	09 05 03 02 02 02 02 02 03 03 04 04 05 05 06 06 06 07 07 07 07 07 07 06 05 04 03 02 01 00																	
358.50	+0.66	08 05 03 03 03 03 03 03 04 04 04 04 04 04 05 05 05 05 06 06 06 06 05 04 03 02 01 01 00																	
358.75	+0.68	07 06 06 05 05 05 04 04 04 04 04 04 04 04 04 04 04 04 04 04 05 05 05 04 04 03 02 01 01 00																	
359.00	+0.66	07 06 06 06 06 06 05 05 05 04 04 04 04 04 04 04 04 03 03 03 03 02 02 02 02 01 01 00																	
359.25	+0.67	06 06 06 05 04 04 03 03 03 03 03 03 03 03 03 03 03 02 02 02 02 01 01 01 00																	
359.51	+0.67	06 06 06 05 05 04 04 03 03 03 03 03 03 03 03 03 02 02 02 02 01 01 01 01 00																	
359.76	+0.69	06 05 04 04 04 04 05 06 05 04 04 03 02 02 02 02 02 02 02 02 01 01 01 01 01 01 01 00																	
000.00	+0.69	05 03 03 02 02 02 03 03 03 02 02 01 01 01 00																	
000.25	+0.69	04 03 03 02 02 02 02 02 02 02 02 02 02 02 02 02 01 01 01 00 00 00 01 01 01 01 01 01 00																	
000.51	+0.69	03 02 02 02 02 01 01 01 01 01 01 01 01 01 01 01 01 01 01 00																	
000.74	+0.70	01 01 01 01 02 02 02 01 01 01 01 01 01 01 01 01 01 00																	
358.00	+0.42	05 04 03 03 03 03 03 04 04 05 06 07 08 09 10 10 10 10 11 11 12 12 12 12 12 11 09 06 04 02 01 00																	
358.26	+0.42	13 08 06 04 04 04 04 04 05 05 06 07 07 08 09 10 10 11 11 12 12 12 12 12 11 08 05 03 02 01 00																	
358.50	+0.41	14 10 08 06 06 06 06 06 06 06 06 06 06 06 06 07 08 09 11 12 13 13 14 14 13 11 07 04 03 02 01 01 00																	
358.75	+0.42	14 11 09 08 07 07 07 08 08 08 09 09 09 09 10 10 11 12 12 13 13 13 12 12 10 09 06 04 03 02 01 00																	
359.00	+0.42	14 12 10 09 08 09 09 10 10 11 11 12 12 13 13 13 13 12 12 11 10 09 08 07 05 04 03 02 02 01 00																	
359.25	+0.42	10 10 10 10 10 10 11 11 11 11 11 12 12 13 14 14 14 13 12 10 09 08 06 05 04 03 02 01 01 00																	
359.51	+0.42	13 12 12 11 10 10 10 10 10 10 10 10 10 10 10 09 09 08 08 07 06 05 04 03 02 01 01 00																	
359.76	+0.43	12 10 08 07 07 08 08 08 08 08 07 07 06 06 05 05 04 04 03 03 02 02 02 01 01 01 00																	
000.00	+0.42	08 07 06 05 05 05 05 04 04 03 02 02 02 01 01 01 01 02 02 02 01 01 01 01 01 02 02 02 01 01 01 01 00																	
000.25	+0.44	05 04 03 03 03 02 02 02 01 01 01 01 01 01 00																	
000.51	+0.43	04 03 03 03 02 02 02 02 02 02 02 02 02 02 01 01 01 00																	
000.74	+0.45	06 04 03 02 02 01 01 00																	
358.00	+0.16	04 04 04 04 05 06 06 07 07 08 08 08 08 09 09 09 09 10 11 12 13 14 16 17 17 17 14 09 06 04 02 01 00																	
358.25	+0.18	13 10 09 08 08 08 08 08 08 08 08 08 09 09 10 10 11 12 12 13 14 15 16 18 19 19 15 09 05 04 02 01 00																	
358.50	+0.16	17 13 09 07 06 07 08 09 09 09 09 09 09 09 09 10 11 12 13 15 16 17 19 22 24 25 22 17 12 06 04 03 02 01 00																	
358.75	+0.17	19 14 11 09 09 10 10 11 12 13 13 14 15 15 15 16 16 17 19 20 22 23 24 24 23 22 15 11 08 05 03 02 01 01 00																	
359.01	+0.16	17 14 13 13 12 12 13 15 16 18 19 20 20 21 22 22 23 24 24 24 24 23 22 21 19 16 11 08 06 05 03 02 01 00																	
359.25	+0.18	16 15 15 16 17 19 20 21 22 22 23 23 23 23 24 25 25 25 24 23 22 19 17 15 13 10 07 05 04 03 03 02 02 01 01 00																	
359.51	+0.17	16 15 15 16 17 20 23 24 24 23 23 23 22 22 21 20 19 17 15 13 12 10 09 07 06 04 03 02 01 01 00																	
359.76	+0.19	11 11 11 11 11 11 11 11 11 11 11 11 11 10 10 09 09 08 07 07 05 05 04 04 03 03 02 02 01 01 01 00																	
000.01	+0.18	04 04 04 04 04 04 03 03 03 03 02 02 02 02 02 02 03 03 03 03 03 03 03 03 03 02 02 01 01 01 01 01 00																	
000.25	+0.19	05 05 04 04 03 03 03 02 02 02 01 01 01 00																	
000.51	+0.18	08 07 06 05 04 03 03 02 01 01 01 00																	
000.75	+0.20	08 07 05 04 03 02 01 01 01 00																	
001.00	+0.18	05 04 02 01 00																	
358.00	-0.08	12 11 10 08 08 07 07 07 07 07 07 08 08 07 07 07 07 07 07 07 09 10 12 15 15 14 11 09 06 03 02 01 00																	
358.25	-0.07	08 08 08 08 08 08 08 08 08 08 08 08 08 09 09 09 09 09 09 10 11 13 15 17 17 16 13 11 07 04 02 01 00																	
358.51	-0.07	18 14 11 09 07 06 07 08 09 09 10 10 11 12 12 13 13 13 13 13 15 17 21 23 24 23 19 14 10 07 03 02 01 00																	
358.75	-0.06	18 15 13 12 11 12 13 14 15 16 16 16 17 17 18 18 18 18 18 19 22 24 27 28 26 23 18 13 08 05 03 02 01 00																	
359.01	-0.08	18 16 15 14 15 16 17 19 21 22 22 22 22 23 23 24 24 23 23 24 24 24 24 23 20 17 12 09 06 03 02 02 01 00																	
359.25	-0.06	18 17 17 17 18 20 22 24 26 27 28 28 29 29 29 29 28 28 26 25 22 20 18 15 13 10 07 06 04 03 02 02 01 01 01 00																	
359.51	-0.06	18 19 19 20 22 23 24 25 28 29 29 28 28 27 27 25 24 22 20 17 17 15 12 10 07 06 04 03 02 02 01 00																	
359.76	-0.07	14 15 15 15 15 15 15 15 15 15 15 15 14 14 13 12 11 10 09 07 06 05 04 03 03 03 02 02 02 01 01 01 00																	
000.01	-0.06	05 06 06 07 08 08 08 08 07 07 05 04 04 04 05 05 05 04 04 04 04 04 03 03 03 02 02 02 02 02 02 02 02 02 01 00																	
000.25	-0.05	09 08 08 07 07 07 07 07 05 04 03 02 02 03 03 04 04 03 03 03 03 02 02 02 02 02 01 01 01 00																	
l^{II}	b^{II}	- 90	-100	-110	-120	-130	-140	-150	-160	-170	-180	-190	-200	-210	-220	-230	-240	-250	km/sec

TABLE 16 *(continued)*

l^{II}	b^{II}	- 90	-100	-110	-120	-130	-140	-150	-160	-170	-180	-190	-200	-210	-220	-230	-240	-250	km/sec
000.51	-0.05	15 14 12 10 10 08 07 06 05 03 03 02 01 01 01 01 00																	
000.75	-0.05	15 08 06 04 03 02 02 02 02 02 02 02 02 01 01 01 01 00																	
001.05	-0.03	09 04 01 01 01 01 01 01 01 01 01 01 01 01 01 01 00																	
358.00	-0.33	-- -- -- -- 08 08 08 08 07 07 07 07 07 07 07 08 08 08 08 -- -- -- -- -- -- -- -- -- -- -- -- --																	
358.25	-0.33	09 08 08 08 08 08 08 08 08 08 08 08 09 09 09 09 08 08 07 07 08 10 12 13 14 14 12 09 05 03 01 00																	
358.52	-0.33	17 15 14 12 11 10 10 10 10 10 11 11 11 11 11 11 11 11 12 13 14 15 17 17 15 10 05 03 02 01 00																	
358.76	-0.32	18 17 15 14 13 13 13 14 15 16 16 16 15 15 15 14 14 14 14 14 14 15 15 15 14 12 08 04 02 01 00																	
359.02	-0.33	19 18 16 16 16 16 17 19 21 22 22 22 21 20 19 18 17 17 16 16 15 14 12 10 08 06 04 03 02 01 00																	
359.25	-0.31	16 16 17 18 18 20 22 23 24 25 26 26 25 24 23 22 20 19 17 16 14 11 09 06 05 03 02 01 00																	
359.51	-0.32	18 18 19 19 20 21 23 25 26 25 24 23 21 20 19 18 17 15 14 12 10 08 06 04 03 03 02 01 01 00																	
359.75	-0.31	14 15 16 17 17 18 18 18 17 16 16 15 14 13 12 11 09 08 07 06 06 05 04 03 03 03 02 02 01 01 00																	
000.01	-0.31	11 12 13 15 16 16 16 14 13 10 09 07 06 05 04 04 03 03 02 02 02 01 01 01 01 01 01 01 01 01 01 01 01 01 01 01 01 01 01																	
000.25	-0.30	13 14 15 15 15 15 14 11 09 07 06 05 03 02 02 01 01 00																	
000.52	-0.31	19 17 15 13 12 11 10 09 08 06 04 02 01 00																	
000.74	-0.29	17 13 10 07 05 04 03 02 01 01 01 01 00																	
001.01	-0.32	11 09 07 05 04 03 02 01 01 00																	
358.01	-0.59	-- -- -- -- 04 04 05 05 05 05 05 05 06 06 06 06 07 07 -- -- -- -- -- -- -- -- -- -- -- -- --																	
358.25	-0.57	08 07 07 07 07 07 07 08 08 08 08 09 09 09 09 08 08 07 06 06 08 10 11 12 11 09 07 05 03 01 00																	
358.52	-0.58	10 09 08 08 07 07 07 07 08 08 09 10 10 10 10 10 09 08 07 07 08 08 09 09 09 08 05 04 02 01 00																	
358.76	-0.56	17 14 12 11 10 10 10 10 10 10 10 10 09 09 09 09 08 08 08 07 07 07 06 06 06 05 04 02 01 01 00																	
359.01	-0.57	16 14 12 11 11 11 12 12 12 12 12 12 12 12 11 11 10 09 08 07 06 05 05 04 03 02 01 01 00																	
359.26	-0.56	11 11 11 12 12 13 13 14 14 14 14 14 14 13 12 12 11 10 09 07 06 05 04 03 02 01 01 00																	
359.51	-0.57	10 11 12 13 14 15 15 15 14 14 13 13 12 11 10 10 09 08 07 07 06 05 04 03 02 01 00																	
359.76	-0.57	12 12 12 14 16 16 15 15 13 12 11 09 08 07 07 06 06 05 05 04 04 03 03 02 02 01 01 01 00																	
000.01	-0.57	13 13 15 16 17 18 16 15 13 11 09 08 06 05 04 03 02 02 01 01 01 01 01 01 01 01 01 01 01 01 01 01 00																	
000.26	-0.56	15 15 16 16 15 14 12 11 09 07 05 04 03 02 02 01 01 01 01 00																	
000.51	-0.56	16 15 14 13 12 10 09 07 06 04 03 02 01 01 00																	
000.75	-0.54	16 13 11 09 08 06 05 04 03 02 01 01 00																	
001.01	-0.56	12 10 07 06 04 03 02 01 01 00																	
001.24	-0.53	07 06 06 05 04 03 01 00																	
358.01	-0.84	-- -- -- -- 07 06 05 04 04 03 03 04 05 05 06 07 08 09 10 -- -- -- -- -- -- -- -- -- -- -- -- --																	
358.26	-0.83	10 09 07 06 05 04 03 03 03 03 03 03 03 03 04 06 08 08 07 06 06 06 07 08 08 06 04 02 01 01 01 00																	
358.51	-0.82	08 07 07 07 06 06 05 05 05 05 05 04 04 04 04 05 05 06 06 06 06 06 06 06 05 03 02 01 00																	
358.76	-0.82	12 10 08 08 07 07 07 07 07 07 07 07 07 07 06 06 06 05 05 04 04 03 03 03 02 02 01 00																	
359.02	-0.82	11 10 09 08 09 10 12 12 10 08 08 07 07 07 07 06 06 05 05 04 03 03 02 02 02 01 01 00																	
359.27	-0.80	09 06 05 06 08 11 12 12 10 09 08 08 08 07 07 06 06 05 05 04 03 03 02 01 01 01 00																	
359.52	-0.82	08 05 05 06 09 11 13 12 10 08 07 07 07 06 06 06 05 05 04 03 03 02 01 01 00																	
359.76	-0.82	08 08 09 10 12 13 12 10 08 06 06 05 05 05 04 04 03 03 03 03 02 02 01 01 00																	
000.02	-0.80	09 10 11 12 15 15 12 09 06 05 04 04 03 03 02 02 01 01 01 01 01 00																	
000.26	-0.80	11 11 11 11 11 10 10 08 06 05 04 03 02 02 01 01 01 01 01 01 00																	
000.52	-0.81	11 11 10 09 08 07 06 05 04 03 02 01 00																	
000.75	-0.79	10 09 08 07 06 05 05 04 03 03 02 02 01 01 01 00																	
001.02	-0.81	09 07 06 05 04 03 02 02 01 01 01 00																	
358.01	-1.09	-- 03 02 01 01 01 00																	
358.26	-1.09	-- 02 02 02 01 01 00																	
358.51	-1.07	-- 03 02 01 01 00																	
358.76	-1.08	-- 04 03 02 02 01 01 00																	
359.02	-1.06	10 08 07 07 06 06 05 05 05 05 05 04 03 03 02 02 02 02 01 01 01 01 01 01 01 01 01 01 01 01 01 00																	
359.27	-1.05	08 07 07 07 06 06 06 06 06 05 05 05 05 04 04 04 04 03 03 03 02 02 02 01 01 01 01 01 00																	
359.53	-1.06	07 07 08 08 08 07 07 06 06 05 05 04 04 04 04 04 03 03 03 03 03 02 02 02 01 01 01 01 01 00																	
359.77	-1.05	07 07 08 10 11 10 08 06 05 05 04 04 03 03 03 03 03 02 02 02 02 01 01 01 01 01 01 01 00																	
000.02	-1.06	08 07 07 09 12 14 10 06 04 03 03 02 02 02 02 02 02 01 01 01 01 01 00																	
000.27	-1.05	08 08 08 08 08 07 05 03 02 01 01 01 01 01 01 01 01 01 01 01 01 01 01 01 01 01 00																	
000.52	-1.05	08 08 07 07 06 04 04 03 02 01 01 01 01 01 01 01 01 01 01 01 01 01 01 01 01 01 01 01 01 01 01 00																	
000.77	-1.04	05 05 05 05 04 03 03 02 01 01 01 01 01 01 01 01 01 01 01 01 01 01 01 01 01 01 01 01 01 00																	
001.02	-1.06	04 03 02 02 02 02 01 01 01 01 01 01 01 01 01 01 00																	
001.26	-1.03	02 01 01 01 01 01 01 01 01 01 01 01 01 01 00																	
l^{II}	b^{II}	- 90	-100	-110	-120	-130	-140	-150	-160	-170	-180	-190	-200	-210	-220	-230	-240	-250	km/sec

TABLE 16 *(continued)*

l^{II}	b^{II}	+50	+60	+70	+80	+90	+100	+110	+120	+130	+140	+150	+160	+170	+180	+190	+200	+210	+220	+230	+240	+250	km/sec
359.24	+0.93	20 14 08	05 05 09	13 18 20	19 18 17	14 11 08	-- -- --	--															
359.51	+0.92	18 11 07	07 08 09	11 12 13	14 14 13	10 07 05	-- -- --	--															
359.75	+0.94	17 10 07	07 07 08	09 11 12	12 12 11	09 08 05	-- -- --	--															
000.00	+0.93	17 10 06	05 05 06	08 09 10	10 10 10	08 06 04	03 02 01	00															
000.25	+0.95	12 07 06	06 06 06	07 09 10	12 14 14	13 09 06	03 01 00																
000.51	+0.94	12 07 04	03 03 05	07 08 09	10 10 10	09 07 05	04 04 03	03 02	02 01 01	00													
000.75	+0.95	13 08 06	05 05 05	07 11 13	14 14 13	12 11 10	09 08 07	06 05	04 04 03	03 03	02 02 02	02 01 00											
001.00	+0.93	12 07 05	04 04 04	05 08 11	12 12 12	11 09 07	05 03 02	01 00	00 01 01	01 02	02 02 01	01 01 01	00										
001.24	+0.96	16 09 04	04 04 06	08 10 13	14 15 15	14 10 07	06 05 05	04 04	03 03 03	03 03 03	03 03 02	02 02 02	02 02 02	01 01 00									
001.50	+0.93	11 05 03	03 03 05	07 09 12	16 16 14	12 08 06	05 03 03	02 02 02	02 03 03	03 03 03	03 03 03	03 02 02	01 00										
001.72	+0.97	07 05 03	04 05 07	08 10 12	13 13 12	09 06 04	03 03 02	02 02 02	02 02 02	02 02 01	01 00												
002.01	+0.94	06 04 03	05 07 08	08 09 09	09 09 08	08 07 05	03 01 00																
358.50	+0.68	21 11 06	06 06 06	08 12 18	21 22 22	23 22 22	22 21 20	16 11 06	04 03 02	01 00													
358.75	+0.68	08 06 07	09 11 12	13 16 20	21 21 20	20 19 17	15 13 11	10 09 07	05 03 01	00													
359.01	+0.66	09 07 08	10 12 13	13 15 17	19 19 17	16 15 12	10 08 06	04 03 02	01 00														
359.25	+0.68	08 08 10	12 14 15	16 16 17	17 16 15	13 12 10	09 08 06	04 03 02	01 00														
359.52	+0.66	13 10 10	11 11 11	10 10 10	10 10 10	10 09 09	09 09 09	09 07 06	05 03 02	01 01 00													
359.75	+0.70	10 09 09	09 09 09	09 10 10	10 10 10	08 07 07	07 08 08	08 08 07	06 06 05	04 03 03	02 02 01	01 00											
000.01	+0.69	06 04 05	07 09 10	10 09 10	10 11 11	10 08 08	08 08 08	08 08 07	05 03 02	01 00													
000.25	+0.69	08 06 06	06 07 08	09 11 12	13 13 12	11 10 09	08 07 07	08 09 09	07 05 04	03 02 01	00												
000.51	+0.69	07 06 05	05 06 07	08 11 13	13 13 13	12 11 09	08 08 08	09 09 08	07 06 05	04 03 03	03 02 02	01 01 00											
000.75	+0.70	05 04 05	06 08 09	10 12 13	13 13 13	12 12 12	12 12 12	12 11 11	10 10 09	08 08 07	06 04 03	02 01 00											
001.01	+0.68	17 13 09	06 04 05	07 10 12	15 17 17	15 14 12	12 10 09	08 07 06	06 06 07	09 10 10	09 07 06	04 03 02	02 01 00										
001.23	+0.71	08 07 07	07 08 09	12 15 18	19 18 16	13 11 10	10 10 10	10 09 09	09 08 08	08 08 08	08 08 07	07 06 06	05 04 03	02 02 01	01 00								
001.51	+0.68	13 08 07	08 09 10	11 12 13	17 18 17	13 11 09	07 07 06	06 05 05	05 06 07	07 07 07	07 06 05	04 04 03	03 03 02	01 00									
001.75	+0.70	06 04 04	06 08 10	11 12 12	12 11 10	08 06 05	04 03 03	03 03 04	04 05 05	05 05 05	05 04 03	03 02 --	-- -- --										
002.01	+0.69	04 01 01	03 06 06	06 06 06	06 06 05	05 05 04	03 03 03	03 03 03	04 05 06	06 06 06	05 05 04	03 02 01	01 01 00										
358.50	+0.41	20 11 07	08 12 13	14 15 16	18 19 22	24 26 29	29 29 27	23 18 13	10 07 04	02 01 00													
358.75	+0.42	21 12 10	12 16 18	19 19 19	19 19 19	20 21 22	22 22 21	18 15 11	08 06 04	02 01 00													
359.01	+0.42	19 13 13	16 19 22	21 20 19	19 19 19	19 19 19	19 19 18	16 13 08	05 02 01	00													
359.25	+0.43	18 16 18	19 19 19	19 19 19	19 19 19	19 19 19	19 19 19	18 16 13	10 07 05	03 02 01	00												
359.52	+0.42	19 18 17	16 15 15	15 15 16	16 16 17	17 18 19	20 20 20	18 16 13	10 07 05	03 02 01	01 01 00												
359.76	+0.45	24 16 13	11 12 13	14 14 14	14 15 15	16 17 18	20 22 23	21 18 16	13 11 09	07 05 03	02 02 01	01 01 01	00										
000.01	+0.44	18 11 08	09 11 14	14 14 14	14 14 14	15 16 17	19 23 24	23 22 19	16 14 12	10 08 06	05 03 02	02 01 00											
000.25	+0.44	17 10 09	09 10 11	11 12 13	13 15 16	17 19 21	23 25 27	27 26 24	21 18 16	13 11 09	07 05 03	02 00											
000.51	+0.44	15 09 09	09 11 12	14 15 17	17 18 19	19 19 20	23 25 28	29 28 25	23 21 19	17 14 12	10 08 05	03 02 00											
000.76	+0.45	16 10 09	09 10 12	15 17 19	20 21 22	22 21 21	21 22 23	24 26 26	25 23 21	19 17 15	13 10 08	06 03 02	00										
001.01	+0.43	16 12 11	13 16 18	19 20 21	22 23 24	23 22 20	19 19 20	22 23 24	24 23 22	20 18 17	15 13 11	08 06 04	03 01 00										
001.24	+0.46	18 13 14	15 17 20	22 23 24	25 26 26	25 22 20	18 18 18	19 21 22	23 22 21	20 19 17	16 14 13	11 09 08	05 04 02	01 00									
001.51	+0.43	15 13 13	13 15 17	19 21 22	23 23 23	23 21 19	17 16 16	17 18 19	20 22 22	21 19 17	16 14 13	13 12 10	08 07 05	03 02 00									
001.74	+0.46	15 10 10	11 12 13	14 15 16	17 17 17	16 14 12	11 11 12	13 15 17	19 20 20	18 16 14	12 10 08	07 07 07	06 05 03	02 01 00									
001.98	+0.47	16 10 08	09 11 13	13 13 13	11 10 08	07 06 06	06 07 08	09 10 11	13 15 15	14 12 09	07 06 07	08 09 08	06 04 03	02 01 00									
358.50	+0.18	17 13 09	09 11 15	17 17 16	15 14 14	14 16 18	20 20 17	14 10 06	05 04 03	02 01 00													
358.75	+0.17	19 17 16	16 18 21	23 22 21	17 15 14	15 17 19	20 20 17	14 11 07	05 03 02	01 00													
359.02	+0.16	22 22 22	22 22 21	21 21 20	17 14 14	16 17 18	18 17 16	15 12 09	05 03 01	01 00													
359.26	+0.17	24 24 23	21 20 19	18 17 16	15 15 16	17 19 21	24 25 25	23 20 17	13 08 05	03 01 00													
359.52	+0.16	26 23 20	18 18 17	16 16 16	15 15 15	15 16 19	22 24 29	28 24 18	15 12 10	08 07 05	03 02 01	00											
359.77	+0.19	18 11 10	10 10 11	13 15 15	15 14 13	13 13 15	18 21 25	28 30 29	26 22 19	16 14 10	06 03 02	01 00											
000.02	+0.18	10 03 04	09 13 16	18 20 22	21 19 19	21 25 28	32 32 31	30 29 26	24 21 18	17 15 13	10 06 04	03 02 01	01 00										
000.26	+0.20	16 11 09	10 12 13	15 17 17	16 15 17	20 24 28	32 34 35	35 33 31	29 26 24	21 18 15	12 10 07	05 03 01	00										
000.52	+0.18	20 15 13	14 15 17	18 19 20	20 19 19	21 25 29	32 34 35	35 33 32	30 28 27	24 21 17	13 10 07	05 03 02	01 00										
000.76	+0.20	22 18 16	17 19 20	21 22 22	21 20 19	20 21 22	24 26 28	30 32 34	32 28 24	22 20 18	16 14 13	11 08 04	02 00										
001.01	+0.18	22 18 18	21 25 26	27 28 27	24 21 20	20 21 22	23 24 26	27 29 30	29 25 22	20 19 16	14 13 13	12 11 07	04 03 02	01 00									
001.25	+0.21	24 19 19	23 27 29	31 32 32	28 23 20	20 20 20	22 23 24	25 27 28	30 30 28	25 22 19	19 18 17	16 15 13	10 06 04	03 01 00									
001.51	+0.18	23 18 16	18 21 24	27 27 26	24 21 19	19 19 20	20 21 23	25 27 30	32 32 30	26 21 18	16 15 15	16 16 15	13 10 08	06 05 04	02 01 00								
001.74	+0.21	22 18 14	13 14 16	18 20 20	20 19 17	14 12 12	12 14 17	19 22 23	23 23 21	18 15 13	11 12 12	13 13 13	13 11 10	08 06 05	03 02 00								
002.00	+0.19	23 16 11	09 09 09	10 12 12	09 05 03	04 06 07	10 11 13	15 17 20	22 23 22	19 15 12	10 09 08	08 08 08	10 10 10	10 10 09	08 06 04	02 01 00							
l^{II}	b^{II}	+50	+60	+70	+80	+90	+100	+110	+120	+130	+140	+150	+160	+170	+180	+190	+200	+210	+220	+230	+240	+250	km/sec

TABLE 16 *(continued)*

l^{II}	b^{II}	+ 50	+ 60	+ 70	+ 80	+ 90	+100	+110	+120	+130	+140	+150	+160	+170	+180	+190	+200	+210	+220	+230	+240	+250	km/sec
358.51	-0.06	19 13 09 09 11 16 16 15 14 13 13 13 12 11 09 08 06 05 04 03 02 01 00																					
358.76	-0.07	23 18 16 17 18 18 16 14 12 11 10 10 10 11 12 12 11 10 10 09 08 06 05 03 02 02 01 01 00																					
359.02	-0.07	26 23 23 23 22 20 17 15 13 13 12 12 12 12 12 12 12 10 07 04 03 03 02 02 01 00																					
359.25	-0.06	26 25 27 27 22 18 15 14 15 15 15 16 16 16 16 16 16 16 16 14 11 08 05 02 01 01 00																					
359.52	-0.07	29 26 25 27 25 19 14 12 16 16 16 16 16 17 18 19 20 21 21 20 19 16 10 07 05 06 05 03 01 00																					
359.76	-0.05	10 08 12 16 16 16 16 16 15 15 16 16 18 20 21 23 24 24 23 21 17 15 15 15 13 10 07 03 02 00																					
000.01	-0.06	03 01 05 12 15 17 17 17 17 17 18 18 19 20 21 23 25 28 28 27 25 23 19 16 15 16 15 11 08 06 05 03 02 01 01 00																					
000.25	-0.04	18 11 11 16 19 20 20 20 20 21 21 22 23 23 24 25 26 27 28 27 26 23 21 19 19 21 23 22 15 08 05 03 02 00																					
000.52	-0.04	27 21 17 20 23 23 23 23 23 23 23 24 24 24 24 25 26 28 29 29 28 26 23 21 19 19 20 20 16 12 09 06 03 01 00																					
000.76	-0.04	28 23 20 23 27 28 27 26 26 26 27 27 27 27 27 27 27 28 30 30 30 28 25 23 22 21 21 20 18 16 13 10 06 03 02 01 00																					
001.01	-0.05	30 23 22 24 27 32 34 35 31 28 27 27 28 29 28 27 26 27 29 31 31 30 25 21 19 21 23 22 20 17 14 11 09 06 03 02 00																					
001.25	-0.04	31 24 22 24 28 35 38 38 33 28 28 27 26 25 25 25 25 26 28 32 33 32 31 29 28 26 25 23 21 19 17 15 13 10 08 06 04 03 02 01 01 00																					
001.51	-0.05	29 23 22 23 25 29 33 36 31 24 21 20 19 19 19 21 23 26 29 32 32 32 31 30 28 27 24 23 21 19 18 17 15 14 13 12 10 07 04 02 01 01 00																					
001.74	-0.06	28 22 18 15 15 19 23 26 23 18 14 13 13 13 15 17 20 25 30 32 33 32 30 28 26 23 21 19 17 16 16 15 15 14 13 12 11 10 09 08 06 04 02 01 00																					
002.00	-0.05	24 20 16 12 09 09 12 15 14 09 07 06 07 10 12 16 20 23 26 28 28 28 26 23 20 18 15 13 11 11 11 11 11 10 11 12 13 13 13 13 12 11 08 06 03																					
358.52	-0.33	17 10 07 06 05 05 05 04 04 04 04 05 05 05 04 03 02 02 01 00																					
358.76	-0.32	18 13 11 10 09 09 08 06 04 05 07 07 07 06 05 04 03 03 02 01 01 00																					
359.02	-0.33	24 19 16 14 12 10 08 07 07 08 08 08 07 07 06 05 04 04 03 03 02 02 01 00																					
359.26	-0.30	28 23 19 16 13 11 09 09 08 08 08 07 07 06 06 06 06 05 05 05 04 03 02 01 00																					
359.53	-0.33	26 19 16 14 12 11 10 09 08 07 07 06 06 07 07 07 07 06 06 05 04 03 02 01 00																					
359.75	-0.30	19 15 12 11 10 09 08 08 07 06 06 06 07 08 09 09 09 08 07 06 05 04 03 02 01 00																					
000.03	-0.32	10 09 08 10 13 13 12 10 09 08 09 11 12 13 13 12 12 11 11 10 08 07 06 05 04 03 03 02 02 01 01 01 00																					
000.26	-0.30	16 12 12 14 13 11 10 09 09 09 09 10 10 10 11 12 12 12 11 10 08 07 05 05 05 05 05 04 03 03 02 01 01 00																					
000.52	-0.31	24 18 16 16 15 15 14 13 13 13 13 13 13 14 15 15 15 15 14 12 11 09 07 06 06 06 06 06 06 05 04 02 01 01 01 01 00																					
000.76	-0.29	30 22 17 17 18 19 19 19 19 19 19 19 19 19 18 18 18 18 17 16 14 11 09 07 07 07 07 07 07 08 07 06 04 02 02 02 02 01 01 01 01 01 00																					
001.02	-0.31	30 24 18 19 21 25 26 24 22 21 22 23 24 23 22 22 21 21 20 19 17 14 12 11 10 10 10 10 10 10 10 10 08 07 04 03 03 02 02 02 02 01 01 01 00																					
001.25	-0.28	29 22 20 22 25 30 30 27 24 22 22 22 23 23 23 23 23 23 23 23 22 21 20 19 18 17 16 14 13 12 15 16 14 12 10 08 06 05 04 03 03 02 01 01 00																					
001.51	-0.32	25 21 18 16 16 18 21 21 21 19 18 18 18 18 18 19 20 22 24 24 23 22 20 19 18 17 16 16 15 13 12 11 11 10 10 09 08 07 06 05 03 02 01 00																					
001.77	-0.30	23 14 10 09 11 14 16 17 15 12 10 10 10 11 13 15 17 20 23 24 22 20 17 16 15 13 12 11 11 10 10 10 -- -- -- -- -- -- -- -- -- -- -- --																					
002.00	-0.29	25 19 13 08 05 05 07 09 08 05 03 04 06 09 11 15 18 22 26 26 25 24 22 20 18 16 14 11 09 08 09 11 12 12 12 12 13 14 14 13 12 11 09 07 05																					
358.52	-0.57	11 08 05 03 03 03 03 03 03 03 02 02 01 01 00																					
358.74	-0.57	11 09 08 07 06 05 04 03 03 03 03 03 02 02 01 01 00																					
359.00	-0.58	17 11 10 09 08 06 05 04 03 03 03 03 02 02 01 00																					
359.27	-0.57	19 14 12 11 09 07 05 04 04 04 04 04 04 03 02 01 00																					
359.52	-0.58	21 16 14 12 10 07 05 04 04 04 04 05 04 03 02 01 00																					
359.76	-0.55	18 15 13 12 10 07 06 05 05 05 05 06 06 04 03 02 01 00																					
000.01	-0.55	14 09 08 09 10 08 06 05 05 05 05 05 05 05 06 06 06 06 05 04 04 03 03 02 02 02 01 01 01 00																					
000.26	-0.56	18 15 12 10 08 07 06 06 06 07 07 07 07 06 05 05 04 03 03 02 02 01 01 01 01 01 01 01 01 01 00																					
000.52	-0.55	16 12 11 11 10 10 10 09 09 08 08 08 08 08 07 07 06 05 04 03 02 01 01 01 01 01 01 01 01 01 00																					
000.76	-0.54	20 17 15 14 13 12 12 12 12 12 12 12 11 11 11 10 09 09 08 07 07 06 05 05 04 04 03 03 02 02 01 01 01 00																					
001.02	-0.55	20 16 13 14 16 17 17 15 13 12 15 16 16 16 16 16 14 12 10 08 06 05 05 04 04 03 03 03 02 02 02 01 01 00																					
001.26	-0.54	19 17 17 18 18 19 20 20 20 20 20 20 19 19 19 18 18 17 16 14 12 10 09 08 08 09 09 09 07 05 04 03 03 02 02 01 01 00																					
001.52	-0.55	18 16 15 14 15 17 19 21 22 23 21 19 18 17 20 21 20 18 16 14 13 12 11 10 09 08 08 07 07 07 07 07 07 07 07 06 06 05 04 03 02 01 00																					
001.76	-0.55	14 12 11 11 13 16 17 17 16 16 15 14 14 15 16 19 19 19 19 18 16 15 14 13 11 11 10 09 08 08 07 07 06 06 06 07 07 07 05 03 02 01 01 00																					
002.01	-0.55	13 10 08 06 07 09 12 12 11 10 10 11 13 15 15 16 16 18 19 19 18 15 13 12 11 10 09 08 08 07 07 07 07 06 07 07 08 09 08 06 05 03 02 01 00																					
358.51	-0.82	08 05 05 04 04 04 03 04 04 04 04 03 02 02 01 01 00																					
358.76	-0.82	08 04 02 01 01 01 01 01 01 01 01 02 02 02 02 02 02 02 02 02 02 01 01 00																					
359.03	-0.82	11 06 03 03 04 05 05 05 04 03 02 02 02 02 03 03 03 03 03 02 02 01 00																					
359.27	-0.80	13 09 06 05 05 05 05 04 03 03 02 02 02 02 02 02 02 02 02 02 02 02 01 01 01 00																					
359.53	-0.82	14 10 07 05 05 05 04 04 03 03 02 02 02 02 02 02 02 02 02 02 02 01 01 01 01 00																					
359.76	-0.81	12 09 06 05 04 03 03 03 02 02 02 02 02 02 02 02 02 02 02 02 02 02 02 01 01 01 00																					
000.02	-0.82	11 08 05 04 03 03 02 02 02 02 02 02 02 02 02 02 02 02 01 01 01 01 01 01 00																					
000.26	-0.78	11 08 05 04 03 03 02 02 02 02 02 02 02 02 02 02 02 02 01 01 01 00																					
000.53	-0.80	12 08 05 04 04 04 04 04 03 03 03 02 02 02 01 01 00																					
000.76	-0.79	12 08 06 05 06 06 06 06 06 05 05 05 05 05 05 06 06 05 05 04 04 03 02 02 01 00																					
001.02	-0.80	13 10 08 08 08 09 09 09 09 09 09 09 08 08 08 08 08 07 06 05 03 02 02 01 00																					
l^{II}	b^{II}	+ 50	+ 60	+ 70	+ 80	+ 90	+100	+110	+120	+130	+140	+150	+160	+170	+180	+190	+200	+210	+220	+230	+240	+250	km/sec

TABLE 16 (*continued*)

l^{II}	b^{II}	+50	+60	+70	+80	+90	+100	+110	+120	+130	+140	+150	+160	+170	+180	+190	+200	+210	+220	+230	+240	+250	km/sec
001.25	-0.79	14	10	11	14	14	14	12	12	11	10	08	05	01	01	00							
001.53	-0.79	08	05	06	10	12	13	10	08	10	09	07	05	04	03	02							
001.76	-0.80	10	07	08	15	15	15	15	15	13	11	09	06	05	05	04	03	02	01	00			
002.01	-0.78	11	09	11	12	13	13	13	13	12	10	09	09	09	08	06	04	03	02	01	01	00	
358.51	-1.07	06	03	01	01	02	02	02	01	00													
358.76	-1.07	04	03	02	02	02	01	01	00														
359.02	-1.06	06	05	02	02	01	00																
359.27	-1.06	07	05	04	03	03	02	01	01	00													
359.53	-1.06	08	07	05	04	03	03	03	02	01	01	00											
359.77	-1.06	05	04	03	02	01	00																
000.02	-1.06	07	05	03	02	02	01	00															
000.26	-1.04	05	04	02	01	00																	
000.52	-1.04	09	05	04	02	01	00																
000.78	-1.04	08	07	05	04	02	01	00															
001.02	-1.05	10	08	06	05	04	03	03	02	02	01	01	01	00									
001.26	-1.03	11	11	10	07	05	05	04	03	03	02	02	02	01	01	00							
001.76	-1.03	12	11	10	10	10	12	10	08	08	07	06	05	04	03	02	01	01	00				
002.02	-1.05	07	06	06	07	08	10	08	07	07	06	05	04	03	03	02	02	01	01	00			
l^{II}	b^{II}	+50	+60	+70	+80	+90	+100	+110	+120	+130	+140	+150	+160	+170	+180	+190	+200	+210	+220	+230	+240	+250	km/sec

positions of the measurements at negative and positive velocities. The added lines are the integration limits which will be described in the next chapter. The positions in parentheses refer to measurements for which the velocity range is not complete. In table 16 this is indicated by dashes. The values for l^{II} and b^{II} were computed with the electronic computer Electrologica X1 from the α and δ values read off, together with the sidereal time, from the analogue computer in Dwingeloo. This gave l^{II} and b^{II} with an accuracy of $\pm 0°.01$. In table 16, l^{II} and b^{II} have been given with the same accuracy.

In order to avoid decimals in the table the unit used is half that used throughout this article, or about 0.5 °K. The numbers should therefore be divided by 2 to obtain intensities in the normal scale of about 1 °K.

The contour diagrams (figure 31) are in the form of b–V charts. For $b^{II} = -0°.06$ a l–V chart is given as an example (figure 32). In this figure the main maximum and the 3-kpc arm have also been drawn.

Between $l^{II} = -2°$ and $-6°$ the disk was measured in 1962 and 1963 with a new parametric amplifier. These measurements will be described in a second article. Our present analysis of this part of the disk will be based on the measurements of the general survey.

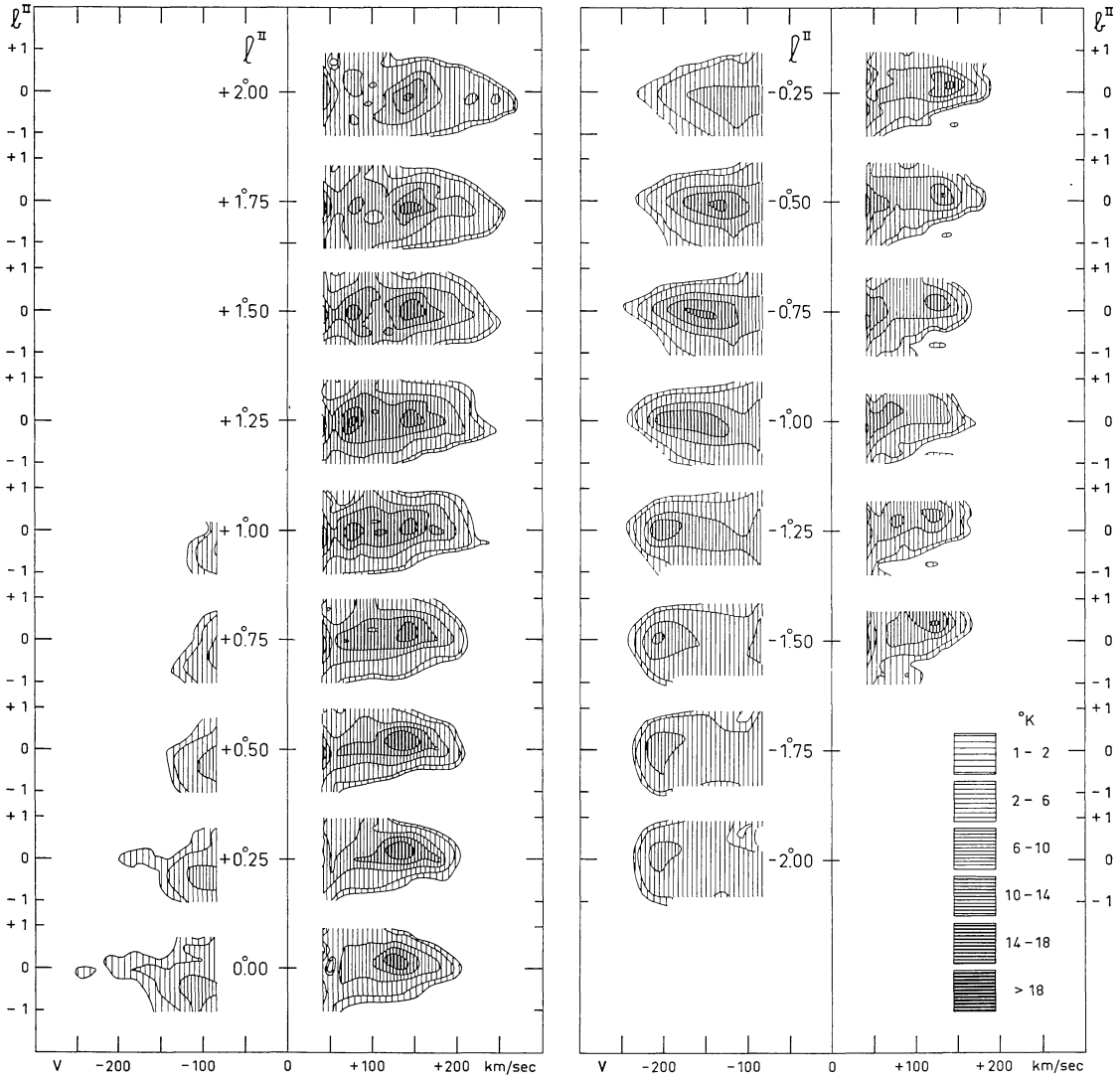

Figure 31. b–V charts of the inner part of the nuclear disk derived from the C measurements.

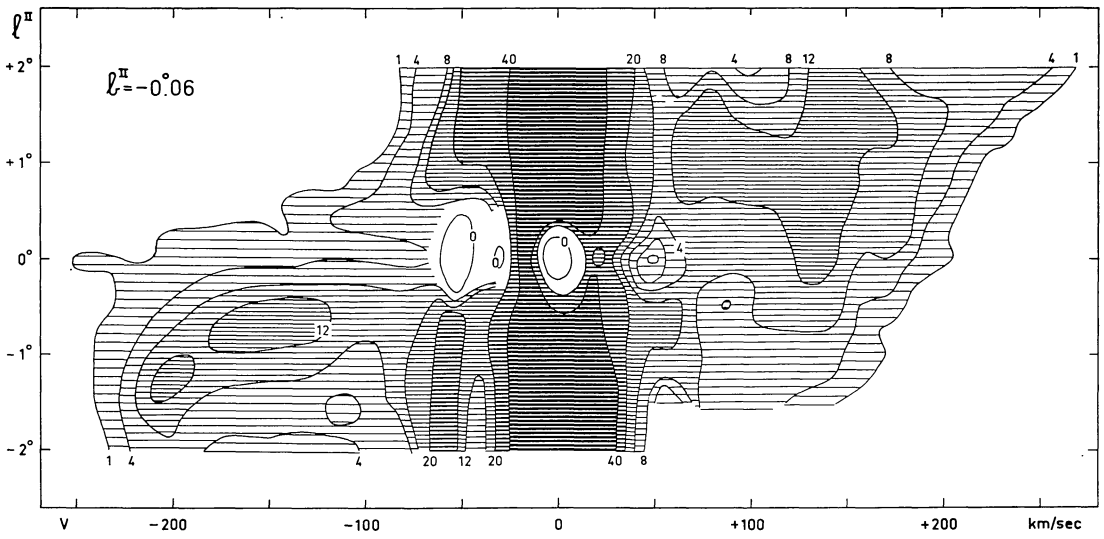

Figure 32. l–V chart at $b^{II}=-0°.06$. The numbers indicate brightness temperatures.

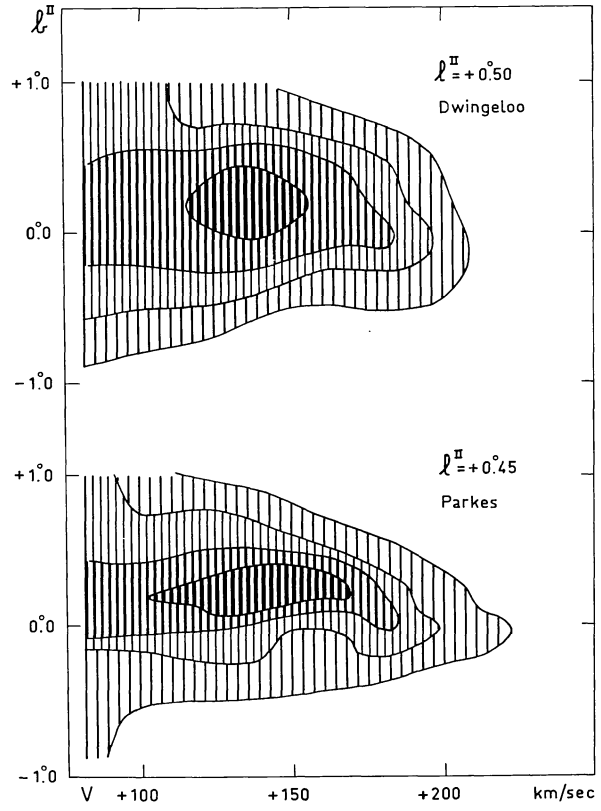

Figure 33. Comparison between Parkes and Dwingeloo, indicating the effect of the beamwidth.

In April 1963, Dr Kerr and Professor Oort observed the nuclear disk with the 210-ft telescope in Parkes. They kindly offered their observations for comparison with the Dwingeloo results. Figure 33 shows a comparison of the b–V diagrams for $l^{II}\approx+0°.50$ at positive velocities. The upper one has been taken from figure 31, the lower one gives the measurements at Parkes. The intensity scale is rather uncertain, because the final reduction of the Parkes observations has not yet been finished. Nevertheless the agreement is excellent. Dr Kerr has meanwhile made observations with a dense grid, the results of which will soon be published.

10. Analysis

10.1. *Expanding and rotating hydrogen for longitudes between $-2°$ and $+2°$*

We have already discussed the fact that the expansion velocity at positive velocities is high (135 km/sec) and may extend over a considerable range, whereas at negative velocities the 3-kpc arm seems to be the only expanding material (expansion velocity 53 km/sec). We have provisionally attempted to separate in the following way the non-expanding gas in the nuclear disk from the expanding gas at the same longitude. Both the po-

sitive-velocity and the negative-velocity parts of the line profile were averaged over four regions of about two square degrees each. These regions are indicated in figure 30 by rectangles. All four regions extend from $b^{II} = -0°.9$ to $+0°.8$. The larger regions extend in l^{II} from 359°.6 ($-0°.4$) to 358°.2 ($-1°.8$) at negative velocities, while at positive velocities the longitude interval is symmetrically reversed and extends from $l^{II} = +0°.4$ to $+1°.8$. The smaller regions cover the longitudes between $\pm 0°.4$ and $\mp 0°.9$. The two larger and the two smaller regions may be compared. If we assume that there is no emission from outside the disk at negative velocities, the mean profile for negative velocities at positive longitudes (the smaller region) has to be very low, which is indeed the case (cf. the left-hand side of figure 34, where also the positive-velocity part of the line profile for the corresponding region is given). For a very rough comparison we have taken the difference between positive- and negative-velocity emission as an estimate of the amount of expanding hydrogen outside the disk. On the assumption that the amount and velocity of the expanding hydrogen does not vary much with longitude over the very small longitude intervals considered, we can use this difference to "correct" the positive-velocity emission at positive longitudes (the larger region), so as to obtain a pure picture of the non-expanding disk. The thin line in figure 34 gives this "corrected" profile. This, then, should represent the line profile for the part of the disk which lies at positive longitudes. We can now compare

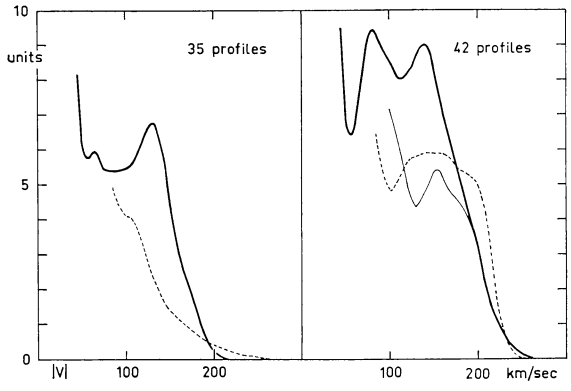

Figure 34. Mean of the smaller (35) and larger (42) regions (see figure 30). The heavy full-drawn line is the mean profile at positive velocities. The dashed line gives the mean negative-velocity profile. The thin line is the contribution at the positive-velocity side due to the disk (see section 10.1).

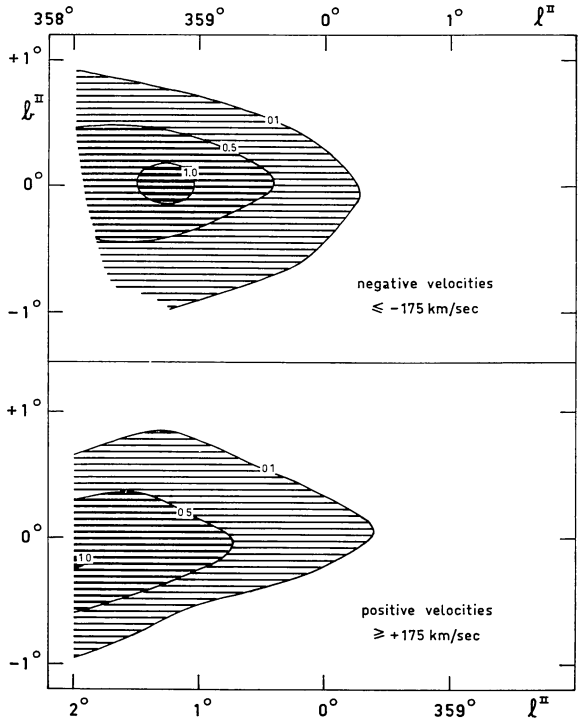

Figure 35. Contours of equal N_H for high velocities. Contour-lines are for 0.1×10^{21}, 0.5×10^{21} and 1.0×10^{21} atoms/cm². The longitude scale for the negative velocities is shown at the top, for positive velocities at the bottom; the latter has been reversed for the purpose of comparison.

this with the part of the disk at the corresponding negative longitudes and negative velocities (again for the larger region). As shown in the right hand side of figure 34, the line profiles for the two parts of the disk at opposite sides of the centre are very nearly the same. We have taken this as an indication that we are indeed dealing with a rather complete rotating disk, equally visible on both sides of the centre.

Another approach to this problem is to assume that the emission of the highest absolute velocities comes only from the disk. For absolute velocities higher than 175 km/sec the two averaged profiles for positive and negative velocities as shown in figure 34, do not differ too much.

An l–b contour map of N_H for this velocity range (figure 35) shows that the density drops steeply at a distance of about 1° from the centre, where the rotation velocity is about 175 km/sec. This figure again clearly shows the general symmetry between the high positive and negative velocities.

For each longitude we have averaged the values of N_H for $|V| > 175$ km/sec for the latitudes $b^{II} = +0°.69$, $+0°.19$, $-0°.56$ and $-0°.81$. The other three latitudes, around $b^{II} = -0°.06$ have been left out in order to avoid possible absorption effects. The variation of this $\bar{N}_H$ with longitude is given in figure 36 as a full-drawn line for the positive and as a dashed line for the negative velocities. The longitude scale is from left to right for the positive velocities, and from right to left for negative velocities. It may be noted that the two curves are nearly parallel, at a distance of 0°.2 from each other. One might explain this difference by a displacement of $+0°.1$ of the disk's axis of rotation relative to $l^{II} = 0°.0$. Another possible explanation is that the shift is due to a slight asymmetry in the rotation. Only a very small difference is needed. If the lower limit for the velocities at the positive longitudes is set at + 170 km/sec instead of + 175 km/sec, the values of N_H have already increased sufficiently to make the two curves coincide (cf. the thin curve in figure 36). A small difference like this might even be caused by a small radial motion of the local standard of rest, which would then have to approach the centre with a velocity of a few km/sec.

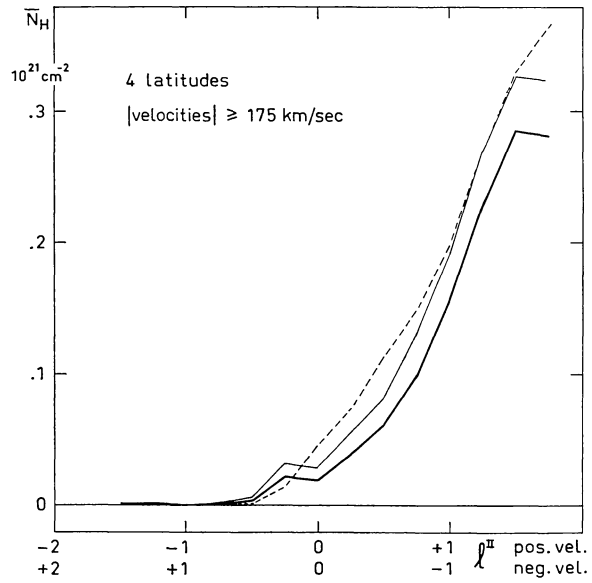

Figure 36. Variation with longitude of the number of hydrogen atoms with velocities above 175 km/sec. N_H has been averaged over latitudes $b^{II} = +0°.69$, $+0°.44$, $-0°.56$ and $-0°.81$. The heavy line is for the positive velocities above +175 km/sec, the thin line is for the positive velocities above +170 km/sec. This latter line coincides fairly well with the dashed curve for negative velocities. The longitude scale for the positive velocities has been reversed.

10.2. *Distribution of the emission in latitude for longitudes between* $-2°$ *and* $+2°$

In the same manner we can get the density distribu-

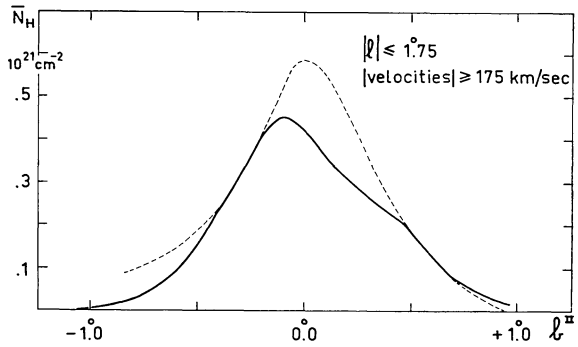

Figure 37. Distribution of high-velocity hydrogen in latitude ($|V| \geq 175$ km/sec). $\bar{N}_H$ is the average for eleven longitudes (the smaller and the larger region of figure 30). The heavy line corresponds to positive velocities, the dashed curve to negative velocities. The maximum of the former is at $b^{II} = -0°.1$; the latter is symmetrical around $b^{II} = 0°.0$.

TABLE 17

	Figure 37		Figure 38	
	$-1° < l^{II} < +1°.75$	$-1°.75 < l^{II} < +1°$	$+1° > l^{II} > -2°$	$-5° < l^{II} < -2°$
	$V > +175$ km/sec	$V < -175$ km/sec	$V < -80$ km/sec	
$(\bar{N}_H)_{max}$ (10^{21} atoms/cm^2)	0.45	0.59	1.54	0.84
Median latitude	0°.00	+0°.02	+0°.11	+0°.18
Halfwidth in latitude	0°.80	0°.69	1°.12	1°.53
Corrected half-thickness	0°.57	0°.40	0°.97	1°.42
Half-thickness (pc) ($R_0 = 10$ kpc)	100	70	170	250

tion of the disk in latitude, by considering the gas with $|V| > 175$ km/sec. For this purpose we have averaged N_H for the eleven longitudes considered, combining, therefore, the larger *and* the smaller regions of the last section. The heavy line in figure 37 shows the result for the positive velocities. The negative velocities are indicated by a dashed line. The contribution from the negative velocities is fairly symmetrical. The peak of the emission at positive velocities is shifted by about $-0°.07$ relative to that for the negative velocities. Table 17 summarizes the results. The last two lines in table 17 give the halfwidths in latitude corrected for the beamwidth of the instrument, and the corresponding thickness of the gas layer in parsecs. They are evidently rather inaccurate.

10.3. *The whole disk feature*

So far we have only discussed a rather small portion of the disk, as we have limited ourselves to velocities above + 175 km/sec and below − 175 km/sec and to the longitude interval $-2°$ to $+2°$. In this section we shall consider velocities below − 80 km/sec in the longitude ranges $-5°$ to $-2°$ and $-2°$ to about $+1°$. The smaller positive velocities are not very well suited for a discussion of the disk, because of the superposition of the component with a high velocity of expansion. Table 17 gives some pertinent data for these two longitude intervals. It should be remembered that the data for the interval $l^{II} = -5°$ to $-2°$ are from the somewhat scarce observations of the general survey. Figure 38 shows the distribution in latitude. The distribution for velocities below − 175 km/sec, which is also given in figure 37, has been added for comparison. The thickness of the layer has a tendency to decrease for higher velocities and for smaller distances to the nucleus. In the longitude interval $-5° < l^{II} < -2°$ the thickness of the layer is practically the same as that found everywhere else in the Galactic System. Only in the outermost regions, beyond $R = 10$ kpc, the thickness increases to rather larger values.

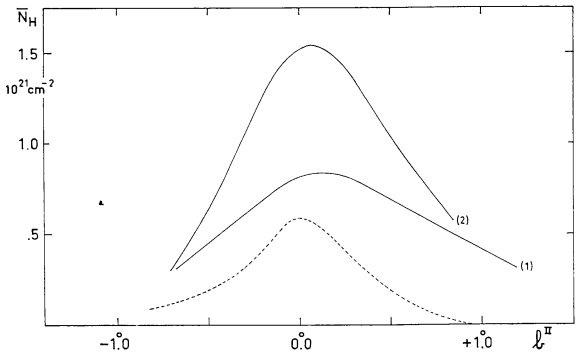

Figure 38. Distribution in latitude ($V < -80$ km/sec). Curve (1) is the average for longitudes $l^{II} = -5°$ to $-2°$, curve (2) for $l^{II} = -2°$ to $+1°$. The H I masses computed in the text have been derived from these curves. The wings have been estimated. The distribution for $V < -175$ km/sec (dashed curve) has been added for comparison; this is the same as the dashed curve in figure 37.

In the longitude interval $-5°$ to $-2°$ a second maximum of N_H occurs around $l^{II} = -3°.3$ (figure 14). This has been ascribed earlier to a ring at 600 pc from the centre (ROUGOOR and OORT, 1960). The latitude of the ring is higher than the average for the whole longitude interval, which is $b^{II} = +0°.18$. At $l^{II} = -5°$ the maximum N_H occurs at $b^{II} = +0°.7$. This supports the idea that the ring, or at least the maximum at $l^{II} = -3°.3$, is connected with the positive-velocity feature described in section 4.4, which also had its maximum density near $b^{II} = +0°.7$.

The disk has a remarkably sharp cut-off at $l^{II} = -4°.5$ (except for the higher latitudes as just described). This corresponds to a distance of 800 pc from the centre.

The mass of the portion of the disk lying between $l^{II} = -2°$ and $-5°$ can be found easily from the maximum N_H and the thickness of the layer, because all the emission from it is in the velocity interval we have used. For the longitudes above $l^{II} = -2°$ the velocity interval used is not large enough, because part of the emission will be at the same velocities as the 3-kpc arm or the main maximum. Another part of the emission is invisible, due to the absorption of Sgr A. Close to the nucleus N_H might become very high, as is already indicated by the Australian measurements at Parkes. In table 18 the H I masses are given, together with the total masses, derived from the rotation velocities (see below).

If the feature at negative velocities is correctly interpreted as a disk in which, at least for distances beyond 200 pc from the centre, the rotation is far larger than the expansion component, we may assume that the velocities of the maxima of the profiles correspond to the rotation velocities. In figure 39 we have plotted these velocities as a function of l^{II}. We have also plotted some points obtained from a l–V chart at $b^{II} = 0°.0$

TABLE 18

l^{II}	R (pc)	H I mass (solar masses) In longitude range indicated	H I mass (solar masses) Between R limits indicated	Total mass (solar masses) Between R limits indicated
$-5°$ to $-2°$	870 to 350	0.6×10^6	2.1×10^6	7×10^9
$-2°$ to $+1°$	350 to (0)	$> 0.6 \times 10^6$	—	3×10^9

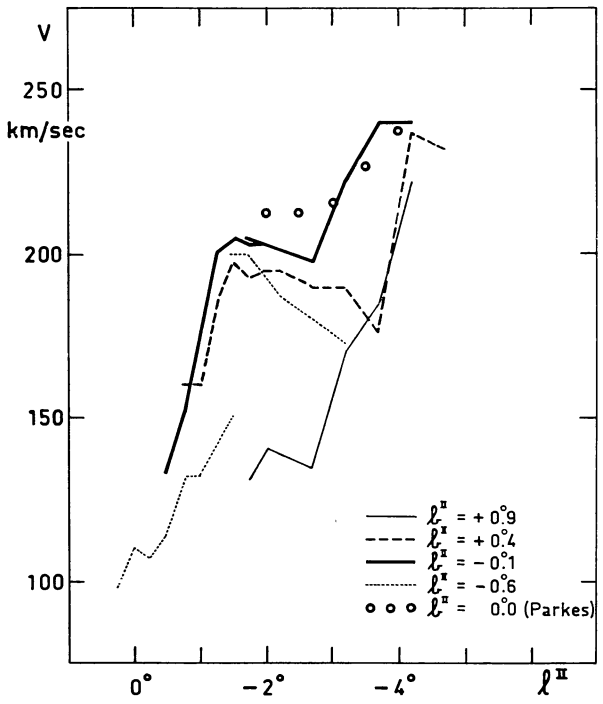

Figure 39. Velocities of the maxima of the features found at various longitudes and latitudes. The circles represent velocities from a chart of Dr Kerr. The dotted line in the lower left represents the velocities of the expanding or contracting arm at −110 km/sec (section 4.1).

constructed by Dr Kerr from measurements with the Parkes telescope, which he kindly sent us. The agreement with the Dwingeloo results is quite good, considering the rather low intensities and the difference in beamwidth.

The velocities at $b^{II} = +0°.9$ fall off more rapidly with decreasing distance to the centre than at other latitudes. However, in view of the low intensities one can hardly conclude anything from this. The values at latitudes $b^{II} = +0°.4$ and $-0°.1$ are in reasonable agreement with each other.

No values could be obtained for longitudes less than 0°.50 from the nucleus, because there is either no emission, or the emission is masked by absorption. From about $l^{II} = -3°$ to $-1°.5$ the velocities at $b^{II} = -0°.6$ are nearly the same as those for $b^{II} = +0°.4$ and $-0°.1$. At the latter longitude a second maximum occurs which can be followed up to $l^{II} = +1°$ (cf. figure 11). This is the contracting or expanding arm at −110 km/sec already described in section 4.1 as the fifth feature.

The steep decrease in the overall intensity of the disk inward from $l^{II} = -1°.5$ is the explanation of the remarkably sharp edges we have found in figure 35. In reality, the slope indicated in this figure might be due entirely to the finite beamwidth of the telescope (0°.56), and the cut-off might be abrupt. The relatively large beamwidth is the reason that the points below $l^{II} = -1°.5$ cannot represent the rotation velocities at the corresponding distances from the nucleus. We can only say that the rotation curve might be steeper than shown in figure 39.

If we take a rotation velocity of 240 km/sec at the edge of the disk at $l^{II} = -5°$, and a rotation velocity of 200 km/sec at $l^{II} = -2°$, we can compute the *total* masses, between 870 and 350 pc and between 350 and 0 pc (table 18). A more detailed distribution has been

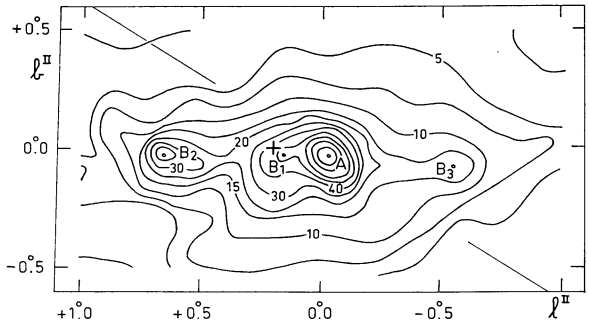

Figure 40. Part of the isophote chart of Cooper and Price (cf. KERR, 1962). The components A, B1, B2 and B3 are indicated. Numbers are °K. The oblique lines show the track along which the scans of ROBINSON *et al.* (1964) have been made. The cross refers to the centre of the disk derived from figures 36 and 37.

given by ROUGOOR and OORT (1960), who computed the rotation curve and the mass density in the parts within 100 pc from the centre through a comparison with M 31. This method gives rotation velocities which are somewhat higher than we have determined here.

10.4. *The absorption at + 50 km/sec*

In figure 32 a small absorption patch can be seen at the position of Sgr A at +50 km/sec. The profile at that position is shown in figure 41. We looked first for a small arm-like emission at the adjacent longitudes. Although there is some emission, it is at a slightly higher velocity (+ 70 km/sec). The analysis of the source Sgr A (section 7.1) provided another explanation: The absorption dip might be caused by the rapidly rotating disk in front of source B 1 (figure 40). If we assume that the rotation axis is at $l^{II} = 0°.0$, the component of the rotation at B1 might very well be of the order of + 50 km/sec. That the feature is not connected with an arm-like structure outside the disk is confirmed by the observations of Dr Kerr, who found no absorption at this velocity at the position of source B2. The absorption dip which he measured at the centre with the Parkes telescope (beam 0°.2) is much deeper than ours, and it is slightly displaced in velocity (+ 40 km/sec). The displacement may well be due to the small beamwidth and to the small angular size of the source.

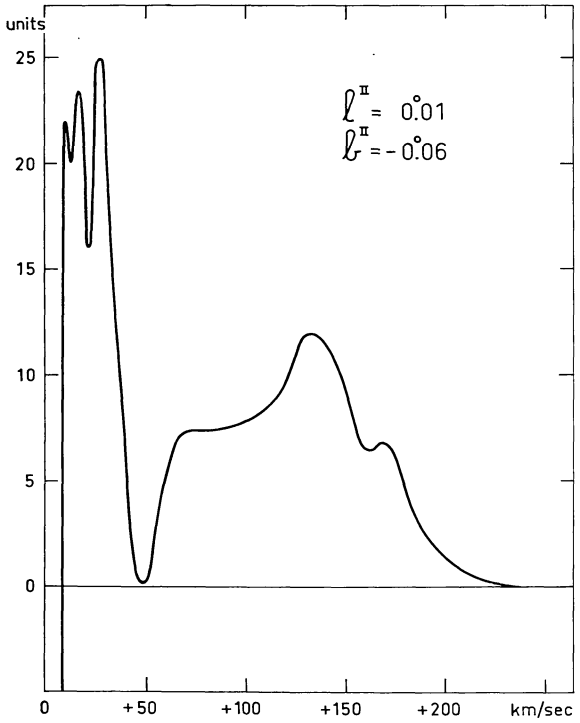

Figure 41. The profile on Sgr A at the positive-velocity side. The absorption at + 50 km/sec is striking, but less deep than the H I absorption dip observed in Parkes, which is, moreover shifted to +40 km/sec. The OH absorption at this velocity as recently observed by the Australian group is still very much more intense and very much wider (ROBINSON *et al.*, 1964).

A most startling discovery was made by ROBINSON *et al.* (1964) observing the 18-cm line of the hydroxyl radical (OH). They measured an absorption dip of − 80 °K instead of the expected absorption of the order of − 1 °K. (In Cas A the absorption at 0 km/sec is only − 2 °K.) A second surprising fact was the enormous velocity dispersion of the absorption feature, amounting to about 60 km/sec. The 18-cm line profile of Sgr A is mainly governed by this absorption.

Scans in right-ascension made by the Australian observers (along the oblique line in figure 40) show convincingly that the absorption at + 40 km/sec is centred on component A. The centre of rotation of the disk was found in section 10.1 to lie at a slightly higher longitude than A. Although this result was not very precise, it is somewhat improbable that the true centre of rotation would lie at a *lower* longitude than A, such as would be required if the velocity of the displaced absorption band would be a component in the line of sight of pure rotation in the disk.

A private communication by Bolton indicates that extremely strong OH absorption occurs also in front of component B2, up to about $l^{II} = + 0°.7$, at a velocity of + 90 km/sec, and with characteristics that fit in quite well with absorption in the nuclear disk. Therefore, whatever is the nature of the absorption in front of component A, the disk must also have a high density of OH. It is, of course, quite possible that the OH/H ratio is much larger in this very peculiar region than elsewhere in the Galactic System, and that the bulk of the hydrogen is in molecular form.

These new H I and OH high-resolution observations show that it is impossible, at the moment, to derive the nuclear gasstreams with any precision. In order to decide about expansion for features like the 3-kpc arm it is sufficient to know that the centre of rotation lies within a few tenths of a degree from $l^{II} = 0°.0$. For the nuclear disk the centre of rotation should be known

with higher accuracy. So far, the absorption due to the nuclear disk has only been found at positive velocities. The fact that towards higher longitudes the band of OH absorption shifts so rapidly to higher velocities, shows that the rotation component must be rather high. We cannot decide how high, because the actual position of B2 in the galactic plane (it might even be the projection of a ring) is not known.

Only a complete survey around the Sgr A complex both in the H I and OH line with a high resolution might reveal if

a) The nuclear gas streams are contracting, expanding or purely rotating.

b) The centre of rotation is at the position of component A. This centre of rotation should be derived from the observed gas streams.

Acknowledgements

The author is greatly indebted to Professor J. H. Oort, whose support has been invaluable in bringing this investigation to a good end.

Professor H. C. van de Hulst has read the manuscript critically, which resulted in several desirable alterations.

The 21-cm line receiver was designed by Professor C. A. Muller. Without his perseverance in improving it to the present excellent state this article would never have been written.

The assistance of all staff members and personnel of the Leiden and Dwingeloo Observatories was greatly appreciated.

Many thanks are due to Drs F. J. Kerr, J. G. Bolton and B. J. Robinson of the Radiophysics Laboratory, C.S.I.R.O., Sydney. They kindly put their results obtained with the 210-ft Parkes telescope at our disposal before publication.

Dr B. F. Burke of the Department of Terrestrial Magnetism of the Carnegie Institution of Washington kindly provided information on that part of the central region which cannot be observed from Dwingeloo.

The Dwingeloo Observatory, where the observations were made, is financed by the Netherlands Organization for Pure Research (Z.W.O.).

References

W. A. Baade, 1951, *Pub. Obs. Univ. Michigan* **10** 7
W. A. Baade, 1955, *Mitt. Hamburger Sternw.* **23** 127
W. A. Baade, 1963, *Evolution of Stars and Galaxies*, ed. C. Payne-Gaposchkin (Harvard Univ. Press, Cambridge, Mass.)
W. A. Baade and N. U. Mayall, 1951, *Problems of Cosmical Aerodynamics* 165 (Proc. of the Symposium on the Motion of Gaseous Masses of Cosmical Dimensions, Paris, 1949)
B. F. Burke and M. A. Tuve, 1962, *Year Book of the Carnegie Institution of Washington* No. 61 214
B. G. Clark, V. Radhakrishnan and R. W. Wilson, 1962, *Ap. J.* **135** 151
G. Courtès and P. Cruvellier, 1960a, *Ann. d'Ap.* **23** 419
G. Courtès and P. Cruvellier, 1960b, *C.R.* **251** 2470
F. D. Drake, 1959a, *Sky Tel.* **18** 428
F. D. Drake, 1959b, *A.J.* **64** 329
F. D. Drake, 1959c, *Annual Rep. Nat. Radio Astr. Obs.* No. 2
J. D. Fernie, 1962, *A.J.* **67** 769
H. Gursky, R. Giacconi, F. R. Paolini and B. B. Rossi, 1963, *Phys. Rev. Letters* (in press)
H. C. van de Hulst, C. A. Muller and J. H. Oort, 1954, *B.A.N.* **12** 117 (No. 452)
H. C. van de Hulst, E. Raimond and H. van Woerden, 1957, *B.A.N.* **14** 1 (No. 480)
Hugh M. Johnson, 1961, *Ap. J.* **133** 309
F. J. Kerr, 1962, *Sky Tel.* **24** 254
F. J. Kerr, J. V. Hindman and C. S. Gum, 1959, *Austr. J. Phys.* **12** 270
K. K. Kwee, C. A. Muller and G. Westerhout, 1954, *B.A.N.* **12** 211 (No. 458)
A. Lallemand, M. Duchesne and M. F. Walker, 1960, *P.A.S.P.* **72** 76
J. Lequeux, 1962, *Ann. d'Ap.* **25** 221
D. S. Mathewson, J. R. Healey and J. M. Rome, 1962, *Austr. J. Phys.* **15** 354 and 369
E. F. McClain, 1955, *Ap. J.* **122** 376
B. Y. Mills, A. G. Little, K. V. Sheridan and O. B. Slee, 1958, *Proc. I.R.E.* **46** 67
R. Minkowski, 1951, *Pub. Obs. Univ. Michigan* **10** 25
C. A. Muller, 1956. *Philips Techn. Rev.* **74** 305 and 351
C. A. Muller and G. Westerhout, 1957, *B.A.N.* **13** 151 (No. 475)
G. Münch, 1960, *Ap. J.* **131** 250
J. H. Oort, 1952, *Ap. J.* **116** 233
Yu. N. Pariiskii, 1961, *Astr. Zhur.* **38** 242 (*Soviet Astr.* **5** 182)
E. Raimond, 1962/63, *Sitzber. Akad. Heidelberg* **2** 91
B. J. Robinson, F. F. Gardner, K. J. van Damme and J. G. Bolton, 1964, *Nature* (in press)
G. W. Rougoor and J. H. Oort, 1960, *Proc. Nat. Acad. Sci.* **46** 1
M. Schmidt, 1957, *B.A.N.* **13** 247 (No. 475)
M. F. Walker, 1962, *Ap. J.* **136** 695
G. Westerhout, 1957, *B.A.N.* **13** 201 (No. 475)
G. Westerhout, 1958, *B.A.N.* **14** 215 (No. 488)
H. van Woerden, G. W. Rougoor and J. H. Oort, 1957, *C.R.* **244** 1691
H. van Woerden, K. Takakubo and L. L. E. Braes, 1962, *B.A.N.* **16** 321 (No. 524)